



universität
wien

DISSERTATION

Titel der Dissertation

Role of plectin in microtubule dynamics

Verfasserin

Mag. Rocío García de la Cruz Valencia

angestrebter akademischer Grad

Doktorin der Naturwissenschaften (Dr. rer. nat.)

Wien, im Mai 2012

Studienkennzahl (It. Studienblatt):

A 091 490

Dissertationsgebiet (It. Studienblatt):

Molekulare Biologie

Betreuer:

Univ.-Prof. Dr. Gerhard Wiche

*“Caminante, son tu huellas
el camino, y nada más;
caminante, no hay camino,
se hace camino al andar. ”*

*“Wanderer, your footsteps are
the path, and nothing more;
wanderer, there is no path,
the path is made by walking.”*

- Antonio Machado

Acknowledgements

First and foremost, I would like to thank my supervisor, Prof. Gerhard Wiche, for giving me the opportunity to work on this project, and especially for all the scientific discussions. I am also grateful to all the lab members and the people in the department for their help and support. In particular, I would like to thank Ewa Krupa, Eva Mihailovska, and Gernot Walko for their help with experiments and their contributions to this thesis. Last but not least, I would like to thank my partner and my family for their constant support.

TABLE OF CONTENTS

TABLE OF CONTENTS.....	8
SUMMARY	13
ZUSAMMENFASSUNG	15
1 INTRODUCTION	17
THE CYTOSKELETON	17
1.1.1 <i>Actin</i>	18
1.1.2 <i>Intermediate filaments</i>	18
1.1.3 <i>Microtubules</i>	20
1.1.4 <i>Microtubule associated proteins (MAPs)</i>	22
1.1.5 <i>Cytoskeletal linker proteins</i>	24
1.1.1 <i>MT regulation</i>	26
Post-translational modification (PTMs)	26
MT-stabilizing proteins	28
MT-destabilizing proteins	31
Actin-MT crosstalk.....	32
IF-MT crosstalk.....	33
1.1.2 <i>Plectin</i>	34
Molecular properties.....	34
Isoform diversity	35
Plectin in connective tissue	36
Plectin in muscle	37
Epithelial plectin.....	39
Plectin in the nervous system	40
Plectin and disease.....	41

Plectin and MTs.....	42
2 AIMS OF THE THESIS.....	47
3 RESULTS	48
PART I - PLECTIN 1C IN KERATINOCYTES	48
3.1.1 <i>Lack of P1c in keratinocytes leads to increased stability of MTs</i>	48
3.1.2 <i>Reversal of MT stabilization in P1c^{-/-} keratinocytes requires full-length P1c</i>	50
3.1.3 <i>P1c deficiency affects MT dynamics</i>	52
3.1.4 <i>Glucose uptake is increased in P1c-deficient keratinocytes</i>	55
3.1.5 <i>Lack of P1c leads to aberrant mitotic spindles and diminished growth rate.....</i>	58
3.1.6 <i>P1c-deficiency affects shape and directional migration of cells.....</i>	60
3.1.7 <i>Lack of P1c causes alterations in FA dynamics.....</i>	61
3.1.8 <i>MTs in P1c-deficient keratinocytes show increased decoration by MAPs</i>	63
PART II - PLECTIN 1C IN NEURONS	69
3.1.9 <i>P1c-deficient neurons exhibit increased MT stability and altered MT dynamics.....</i>	69
3.1.10 <i>P1c-deficiency affects growth cone extension and neuritogenesis</i>	73
3.1.11 <i>Lack of P1c leads to abnormal vesicle transport in DRG neurons.....</i>	79
3.1.12 <i>P1c deficiency causes abnormalities in membrane excitability of DRG neurons.....</i>	82
3.1.13 <i>Differential extractability of tau from hippocampal wt and P1c^{-/-} lysates</i>	84
4 DISCUSSION.....	87
PLECTIN 1C ACTS AS A MT DESTABILIZER IN A SPATIALLY-CONTROLLED MANNER.....	87
P1C DESTABILIZES MTs BY ANTAGONIZING MAP-MEDIATED MT STABILIZATION	88
IS MT DESTABILIZATION P1C-SPECIFIC?.....	90
P1C DEFICIENCY IMPAIRS NEURITE OUTGROWTH AND BRANCHING.....	90
IS AXONAL TRANSPORT ALTERED IN P1C-DEFICIENT DRG NEURONS?	92
IS MEMBRANE EXCITABILITY AFFECTED IN P1C-DEFICIENT NEURONS?	93

ARE THERE ANY SIMILARITIES BETWEEN P1C DEFICIENCY AND TAUOPATHY OR NEURODEGENERATIVE DISORDER PHENOTYPES?	93
CLOSING REMARKS.....	95
5 MATERIAL AND METHODS	96
PLASMIDS	96
ANTIBODIES, ANTISERA AND DYES	96
DNA METHODS	99
5.1.1 Preparation of plasmid DNA.....	99
5.1.2 Determination of DNA concentration.....	100
PROTEIN METHODS	100
5.1.3 Determination of concentration.....	100
5.1.4 SDS-Polyacrilamide gel electrophoresis (PAGE).....	100
5.1.5 Coomassie staining.....	101
5.1.6 Immunoblotting.....	101
5.1.7 Quantification of protein bands on immunoblots	102
5.1.8 Preparation of total cell and tissue lysates	103
5.1.9 Endogenous MT-binding assay	103
5.1.10 RhoA pull down assay	103
pGEX-2T-RBD culture	103
pGEX-2T-RBD: Growth and Induction	104
pGEX-2T-RBD: Cell lysis	104
Purification of GST-Rhotekin-BD (GST-RBD).....	105
RhoA pull down assay.....	105
5.1.11 Extraction of sarcosyl-insoluble tau.....	106
MAMMALIAN CELL CULTURE	107
5.1.12 Cultivation of p53 ^{-/-} keratinocytes	107

5.1.13 Isolation of primary keratinocytes	108
5.1.14 Isolation and cultivation of DRG neurons	109
5.1.15 Freezing and thawing of cells	110
5.1.16 Transient transfection	110
FuGene6 (Roche)	110
Nanofectin (PAA)	111
Nucleofector™ Technology (Lonza)	111
Amaxa® human keratinocyte Nucleofector® kit	111
Amaxa® basic neuron SCN Nucleofector® kit	112
5.1.17 Nocodazole and colchicine treatment	112
5.1.18 Oxidative stress	112
5.1.19 DRG explants	112
5.1.202-NBDG uptake	113
5.1.21 Na ⁺ uptake	113
5.1.22 Synaptic vesicle exocytosis and endocytosis with FM dyes	113
5.1.23 Current clamp electrophysiology	114
MICROSCOPY	114
5.1.24 Immunolabeling for immunofluorescence microscopy	114
5.1.25 Confocal microscopy	115
5.1.26 Wide-field microscopy	115
5.1.27 Deconvolution	115
5.1.28 Time-lapse video microscopy	116
Visualization of MT dynamics	116
Visualization of FA dynamics	116
Single cell migration	116
Visualization of synaptic vesicles	117

Growth cone extension	117
5.1.29 <i>Image processing and semiquantification</i>	117
STATISTICAL ANALYSES	118
LIST OF FIGURES AND TABLES	119
ABBREVIATIONS	122
REFERENCES	127
CURRICULUM VITAE	152

SUMMARY

Plectin, a polypeptide of very large size (>500 kDa) and member of the plakin cytolinker protein family, is one of the most abundant and versatile cytolinkers expressed in mammalian cells. One of its outstanding features is its functional diversity that is mainly based on the alternative splicing of a series of different first coding exons resulting in different isoforms.

A number of observations made in previous studies, including the targeting of overexpressed plectin isoform 1c (P1c) to microtubules (MTs), the partial colocalization of P1c with MTs in cultured cells, and the *in vitro* binding of neural plectin to MT-associated proteins (MAPs), pointed towards a potential interaction of plectin with MTs. Moreover, ACF7 and BPAG1, other members of the plakin cytolinker protein family, have been shown to be involved in the regulation of MT dynamics, both acting as MT stabilizers. Based on these previous observations and additional unpublished data from this laboratory one of the major goals of my thesis was to identify the role of plectin in MT dynamics. Of particular interest in this context was the question whether plectin isoform P1c antagonizes MAP-mediated MT stabilization, and if so, what was the underlying molecular mechanism. I report here that contrary to other cytolinker proteins, P1c acts as a destabilizer of MTs and that this destabilization relies on IF-dependent P1c localization.

Since P1c is a major isoform in keratinocytes and neurons, I searched for a mechanistic link between plectin-related changes in MT dynamics and alterations in MT-dependent processes of physiological significance in keratinocytes and neurons isolated from P1c-deficient mice. Functioning as a promoter of MT dynamics, I found plectin to affect vital MT-dependent functions and properties of keratinocytes, including glucose uptake, cell division and growth, focal adhesion turnover, shape and polarized migration of cells. P1c-deficient primary DRG neuronal cultures were found to be a suitable system to study the consequences

of altered MT dynamics in neurons. The data revealed alterations in the processes of neuritogenesis, such as outgrowth and branching of neurites, distorted synaptic vesicle transport along neurites, and ability of neuronal membrane to depolarize.

Finally, I describe a model where P1c destabilizes MTs by antagonizing MAP-mediated MT stabilization. The reported findings unmask P1c as a MT destabilizer and show that cytolinker-mediated destabilization is required for the correct performance of multiple physiological processes. These findings point towards a fascinating new feature of cytoskeletal filament cross-talk, namely the potential of IFs to destabilize MTs via an associated cytolinker protein, thereby stimulating MT dynamics.

ZUSAMMENFASSUNG

Plectin ist ein Protein des Zytoskeletts und ein Mitglied der Plakin Zytolinker Proteinfamilie. Plectin ist ein sehr großes Protein (> 500kDa), welches in einer Vielzahl von Säugetier-Geweben und Zelltypen exprimiert. Die aussergewöhnlichste Eigenschaft von Plectin ist seine funktionelle Vielfalt, welche auf alternativem Spleissen einer großen Vielzahl von ersten kodierenden Exons beruht, wodurch verschiedene Isoformen entstehen. Zahlreiche Beobachtungen in früheren Studien wiesen bereits auf eine mögliche Interaktion von Plectin Isoform 1c (P1c) mit Mikrotubuli (MTi) hin. Dazu gehörte die gezielte Anlagerung von überexprimiertem P1c an MTi, die partielle Koloalisation von P1c mit MTi in kultivierten Zellen, sowie die Bindung von neuronalem Plectin an MTi-assoziierte Proteine (MAPe) in vitro. Darüber hinaus ist bereits gezeigt worden, dass andere Plakin Zytolinker Proteine, wie zum Beispiel ACF7 oder BAPG1, an der Regulation von Dynamik von MTi beteiligt sind, indem sie MTi stabilisieren. Aufgrund dieser früheren Ergebnisse und anderer unpublizierter Daten aus diesem Labor war es daher das Hauptziel meiner Doktorarbeit, die Rolle von Plectin in der Dynamik von MTi aufzuklären. In diesem Zusammenhang war es von besonderem Interesse, die Frage zu beantworten, ob P1c antagonistisch auf die MAP-vermittelte Stabilisierung von MTi wirkt, und, falls dies tatsächlich der Fall sein sollte, den zu Grunde liegenden molekularen Mechanismus aufzuklären. Ich zeige in meiner Arbeit, dass im Gegensatz zu anderen Plakin Zytolinker Proteinen P1c als Destabilisator von MTi agiert, und dass diese Destabilisierung davon abhängt, ob P1c an Intermediärfilamente (IFe) gebunden ist. Da P1c die Hauptisoform in Keratinozyten und Neuronen ist, suchte ich in diesen Zellen nach einer mechanistischen Verbindung zwischen Veränderungen der Dynamik von MTi, welche durch Plectin verursacht werden, und Änderungen von MTi-abhängigen physiologischen Prozessen. Ich konnte herausfinden, dass P1c in seiner Rolle als positiver Regulator von MTi-Dynamik verschiedene

MTi-abhängige Funktionen und Eigenschaften von Keratinozyten beeinflusst. Dazu gehören die Aufnahme von Glucose in die Zelle, Zellteilung und Wachstum, der Umsatz von fokalen Adhäsionskontakten, Zellform und polarisierte Zellmigration. Mit primären neuronalen Zellkulturen, welche aus Ganglien der dorsalen Wurzel von P1c knockout Mäusen isoliert worden waren, erhielt ich ein ideales Kulturmodell zur Untersuchung der Funktion von P1c in der Dynamik von MTi in Neuronen. Untersuchungen von solchen Zellen zeigten Veränderungen im Prozess der Neuritogenese, veränderten Transport von synaptischen Vesikeln entlang von MTi, und eine gestörte Fähigkeit von knockout Neuronen zu depolarisieren. Abschliessend beschreibe ich in meiner Doktorarbeit ein Modell, welches zeigt, wie P1c durch antagonistische Wirkung auf MAPe MTi destabilisieren könnte. Meine Resultate zeigen, dass P1c MTi destabilisiert und dass Zytolinker wichtig für den korrekten Ablauf einer Vielzahl von physiologischen Prozessen sind. Diese Ergebnisse zeigen eine neue faszinierende Eigenschaft von zytoskeletärem „crosstalk“ auf, nämlich das Potential von IFn, mittels assoziierter Zytolinker MTi zu destabilisieren und deren Dynamik zu beeinflussen.

1 INTRODUCTION

The Cytoskeleton

The cytoskeleton is a system of intracellular filaments responsible for organizing the cell shape and the cell interaction with the environment. It provides mechanical strength as well as enables the cells to rearrange their components to grow, migrate, divide and adapt to changing environmental conditions. Although long time considered as a unique feature of eukaryote cells, prokaryotes also present an active and dynamic cytoskeleton. Prokaryotes show a surprisingly complex cytoskeletal composition that share with the eukaryotic cytoskeleton the main functions and properties, providing resistance to external forces, acting as scaffold or enabling cell division (Wickstead & Gull, 2011).

The cytoskeleton of eukaryotic cells is composed of three major types of filaments. Actin filaments provide protrusive and contractile forces. Microtubules (MTs) form a polarized network allowing vesicle and organelle movement along the cell. Finally, intermediate filaments (IFs) endow cells with mechanical strength and resistance to shear stress. All of them are essential to the spatial organization of the cells, are dynamic and adaptable. Each type of filament is constructed from smaller protein subunits that can be repetitively assembled and disassembled, facilitating rapid structural reorganization. Despite these common features, each cytoskeletal filament type has unique mechanical properties and stability that result in their individual roles. In addition, there are a large number of cytoskeleton-associated proteins that regulate the dynamics of the filaments and coordinate their functions, by regulating their polymerization, providing energy, or anchoring them to cellular structures. Among these proteins we find the MT- and actin-associated proteins and proteins belonging to the cytolinker family.

1.1.1 Actin

Actin filaments or microfilaments are long filamentous polymers of ~7 nm diameter formed by globular actin subunits. They are composed by two parallel protofilaments that twist around each other in a right-handed helix. As a result of the regular and parallel orientation of actin subunits, the ends of the polymer are different presenting distinct kinetic rate constants for association and dissociation. The plus end or barbed end of actin filaments polymerizes and depolymerizes faster than the minus end or pointed end. During this process known as treadmilling, actin subunits are recruited at the plus end and shed from the minus end. When the subunits change rapidly from the free to the polymerized state, but keeping the length of the filament unchanged, the process is known as “steady-state treadmilling”. Actin dynamics can be altered by drugs like phalloidin (that binds to and stabilizes filaments, causing net polymerization), or latrunculin (that binds to and stabilizes actin monomers, causing net depolymerization).

Actin filaments determine the cell shape and are necessary for cell movement. There are many types of actin-based superstructures (Chhabra & Higgs, 2007; Doherty & McMahon, 2008). Actin filaments can be organized as a mesh underlying and tightly in contact with the plasma membrane. They can also form a dense network of highly branched (lamellipodia and ruffles) or long unbranched (filopodia) actin filaments at the leading edge of migratory cells. Long bundles of actin cables (stress fibers) are usually anchored at adhesion sites, and actin-rich structures can be associated with invaginations in endocytic and phagocytic structures.

1.1.2 Intermediate filaments

IFs are a superfamily of 10 nm-fibers. They are named after their diameter, between thin actin filaments (~7 nm) and myosin filaments (~15 nm) (Ishikawa *et al*, 1968). There is a large

variety of IFs that are differentially expressed in different tissues and were originally classified into five categories (Fuchs & Weber, 1994). (i) Type I IFs correspond to acid keratins and include eleven epithelial keratins, K9-K20, and four hair keratins, Ha1-Ha4. (ii) Type II keratins are basic or neutral, and include eight epithelial keratins, K1-K8, and four hair keratins, Hb1-Hb4. Both types of keratins assemble as obligatory heteropolymers and are expressed differentially at various stages of development and differentiation. (iii) Type III IF proteins encompass vimentin (mesenchymal cell types and transformed cell lines), desmin (smooth, skeletal, and cardiac muscle), glial fibrillary acidic protein (GFAP) (glial cells and astrocytes) and peripherin (peripheral nervous system). Type III IFs form homopolymers, but they can also assemble as a heteropolymers with other type III IF proteins or with neurofilaments (NFs). (iv) The type IV group comprehends NF proteins and α -internexin. NFs are divided into NF-L (light, 62 kDa), NF-M (medium, 102 kDa), and NF-H (heavy, 110 kDa). NF proteins are expressed in axons, dendrites, and perikarya, while α -internexin is also expressed in neurons, but playing a more important role during embryonic development. (v) Type V group contains the proteins composing the nuclear lamina, lamins. Lamins form a meshwork on the inner surface of the nuclear membrane, providing a framework for the nucleus and participating in chromatin organization. There are three types of lamins, lamins A, B, and C, presented in different combinations depending on the cell type and differing in their functions. (vi) There are also a so-called type VI group of IFs that can not be included in any of the previous groups, but they are considered part of the IF superfamily according to their sequence and structure. Within this group we can find nestin and filensin, proteins expressed in the developing central nervous system and during differentiation of the vertebrate lens epithelia, respectively.

All IF proteins share a common structure. Unlike actin and tubulin, they form non-polarized filaments. IFs have a central α -helical domain, the rod, flanked by nonhelical head (N terminus) and tail (C terminus) domains. The assembly takes places after a first formation of

parallel and in-register dimers, followed by their association into stable tetramers. Contrary to other cytoskeletal filaments, IFs do not require auxiliary proteins or factors to assemble. However, their function and reorganization can be regulated by phosphorylation. Different kinases, like protein kinase A, protein kinase B, cAMP-dependent kinase, and cdc2 kinase phosphorylate vimentin (Chou *et al*, 1990; Eriksson *et al*, 2004), desmin (Huang *et al*, 2002), NFs (Shea & Lee, 2011; Sunil *et al*, 2012), and lamins (Fields & Thompson, 1995).

IFs provide cells with resistance to mechanical stress. Up to date, 93 distinct diseases related to IFs have been identified. Among them we find Alexander disease, Charcot-Marie-Tooth disease and amyotrophic lateral sclerosis, caused by mutations in IF of glial and neural cells (Liem & Messing, 2009). Mutations in desmin cause skeletal muscle dystrophies and cardiopathies (Carlsson & Thornell, 2001). Keratin mutations lead to diseases classified as epidermolysis bullosa simplex (EBS), a heterogeneous group of skin blistering disorders (Intong & Murrell, 2012).

1.1.3 Microtubules

MTs are hollow polarized cylinders. They are cytoskeletal polymers composed of α - and β -tubulin monomers. Tubulin monomers assemble linearly into protofilaments that associate laterally to form ~24 nm-wide cylindrical structures. The initial structures forming are small sheets of protofilaments that later close to form MTs containing 13 protofilaments. MT polymerization occurs in three steps. First, MT nucleation requires γ -tubulin that acts as a scaffold for α - and β -tubulin aggregation. The nucleation rate depends on the initial concentration of soluble tubulin. Second, during aggregation or elongation, tubulin dimers are incorporated as a complex with GTP. Finally at steady state, MT length remains constant but the two polymer ends behave different. The plus end incorporates new tubulin dimers, while the minus end loses them. As occurs in actin filaments, this process is named treadmilling.

However, it is very rare that MT length remains constant. Usually individual MTs present long phases of assembly (rescue) and rapid phases of disassembly (catastrophe) (Figure 1). Rapid transitions from one state to the other are known as dynamic instability (Mitchison & Kirschner, 1984; Schulze & Kirschner, 1986). MT polymerization can be altered using drugs.

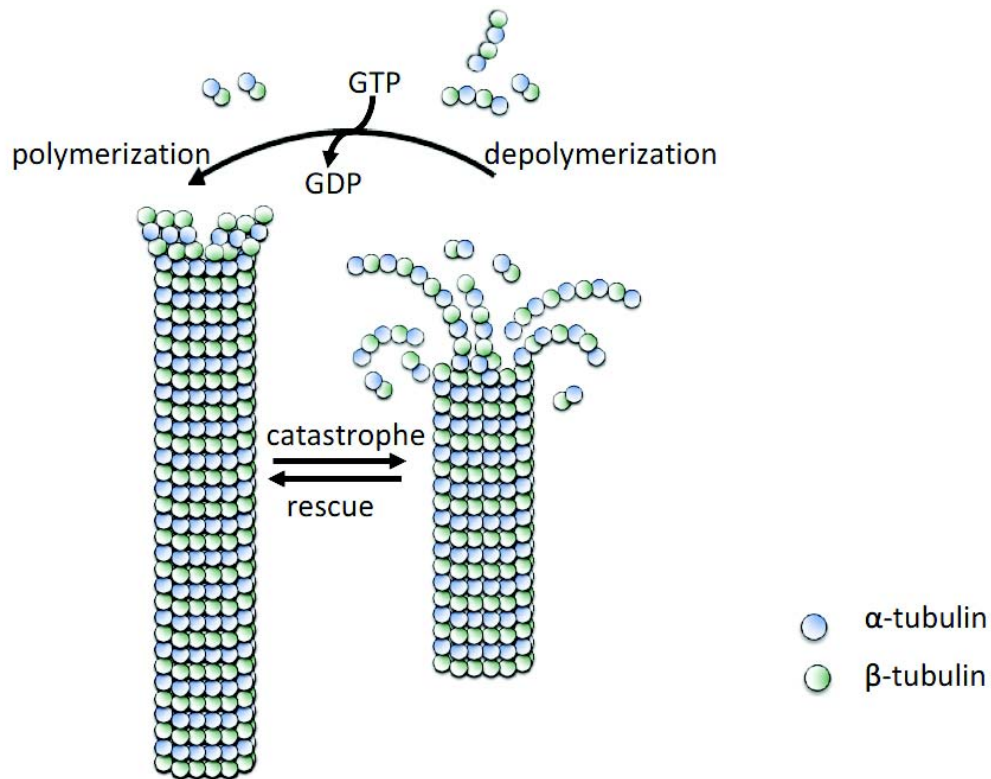


Figure 1. Schematic representation of MT dynamics. Tubulin dimers are incorporated as a complex with GTP at the plus end of the MT. At the minus end, tubulin dimers are bound to GDP. Dynamic MTs undergo length fluctuations due to spontaneous phases of catastrophe and rescue (Adapted from Conde & Cáceres, 2009).

Colchicine and vinblastine bind to MTs and induce their depolymerization. By sequestering tubulin dimers, also nocodazole induces MT depolymerization. In contrast, taxol binds to MTs and stabilizes them, inhibiting their dynamics. MTs are required for maintaining cell shape and polarization, cell division, intracellular transport and they participate together with actin

filaments in cell locomotion. In addition, MTs have been shown to play an essential role in organization and dynamics of axons and dendrites. Their dynamics and functions are fine-tuned and regulated by other proteins binding to them. There are proteins that facilitate MT stabilization, like MT-associated proteins (MAPs), and cytolinkers like ACF7/MACF or BPAG1. Proteins leading to MT destabilization are Op18/stathmin, SCG10 (Conde & Cáceres, 2009). MT or MT-related protein dysfunction have been identified in a variety of neurological disorders such as Alzheimer and Parkinson's disease (Tischfield *et al*, 2011; Lee *et al*, 2001).

1.1.4 Microtubule associated proteins (MAPs)

MAPs form a diverse protein family characterized by their interaction with MTs (Olmsted, 1986; Wiche, 1989). In most of the cases MAP-tubulin interaction is responsible for MT stabilization and promotion of polymerization. Although the first attempts to isolate MAPs were done by purifying them from brain due to the high content in MTs of this tissue, MAPs are expressed ubiquitously. MAP proteins have been divided in different categories according to their structure and expression pattern. Among them, tau presents a highly complex variety of isoforms as a result of distinct splicing of transcripts. These isoforms differ in the number of MT-binding repeats and in the presence of exons 2 and 3 (Figure 2). MAP1, MAP2, and tau are expressed primarily in neurons, however MAP2 has been found also in keratinocytes and in other non-neuronal tissues (Wiche *et al*, 1984; Liu *et al*, 2007). Tau was identified in other non-neuronal cells like muscle as well (Gu *et al*, 1996; Janué *et al*, 2010). E-MAP-115 is another MAP restricted to epithelia (Masson & Kreis, 1993). In contrast, MAP4 is expressed ubiquitously (Parysek *et al*, 1984). XMAP215 shows also a MT-polymerizing activity in addition to its MAP-stabilizing activity (Brouhard *et al*, 2008).

Particularly noteworthy is the MAP2/tau family of MAPs (Dehmelt & Halpain, 2004).

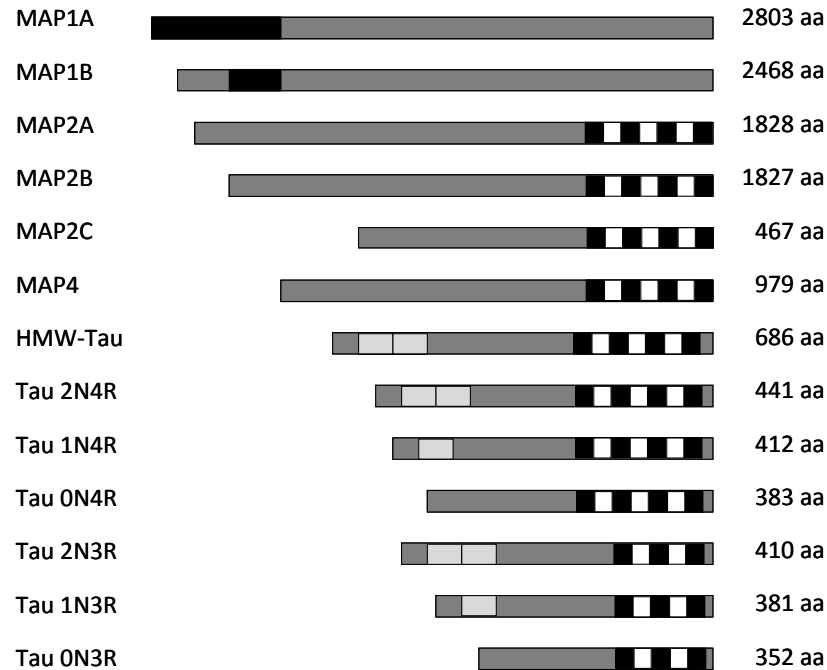


Figure 2. Schematic representation of MAPs. MT-binding domains are black colored. Similar domains sharing 18-amino acids repeats are depicted in white. Light grey boxes represent alternatively spliced exons 2 and 3 of tau protein.

The MAP2/tau family includes MAP2, MAP4 and tau. All of them share a C-terminal domain harboring MT-binding repeats and have alternative splice isoforms (Figure 2). MAP2 and tau increase MT stability and rigidity (Felgner *et al*, 1997) and are responsible for MT-bundling (Lewis *et al*, 1989). MAP2 is mainly found in dendrites of differentiated neurons (Sanchez *et al*, 2000) and MAP2c has been related to Alzheimer's disease due to its specific interaction with apolipoprotein E (Huang *et al*, 1994). Tau is normally described as an axonal protein but an additional dendritic function of tau has been identified (Ittner *et al*, 2010). In addition, tau has been shown to inhibit kinesin-dependent traffic of organelles (Stamer *et al*, 2002; Dixit *et al*, 2008) and to participate in axonal branching by protecting MTs against severing proteins like katanin (Qiang *et al*, 2006). Tau has also been implicated in neurofibrillary tangle formation and amyloid- β toxicity in Alzheimer's disease (Kampers *et al*, 1999; Ballatore *et al*, 2007; Ittner

et al, 2010) and in frontotemporal dementias like parkinsonism, frontotemporal lobar degeneration and motor neuron disease (Fu *et al*, 2010).

1.1.5 Cytoskeletal linker proteins

The plakin family of proteins (also known as cytolinkers) are responsible for strengthening cells against mechanical stress and regulating cytomatrix plasticity by networking and anchoring cytoskeletal filament systems to organelles and junctional complexes (Wiche, 1998; Fuchs & Karakesisoglou, 2001; Leung *et al*, 2002; Sonnenberg & Liem, 2007). They are a family of large, multi-domain proteins that link cytoskeletal networks to each other, to organelles and to membranes (Figure 3). They are built up by a combination of modular domains, but not all of

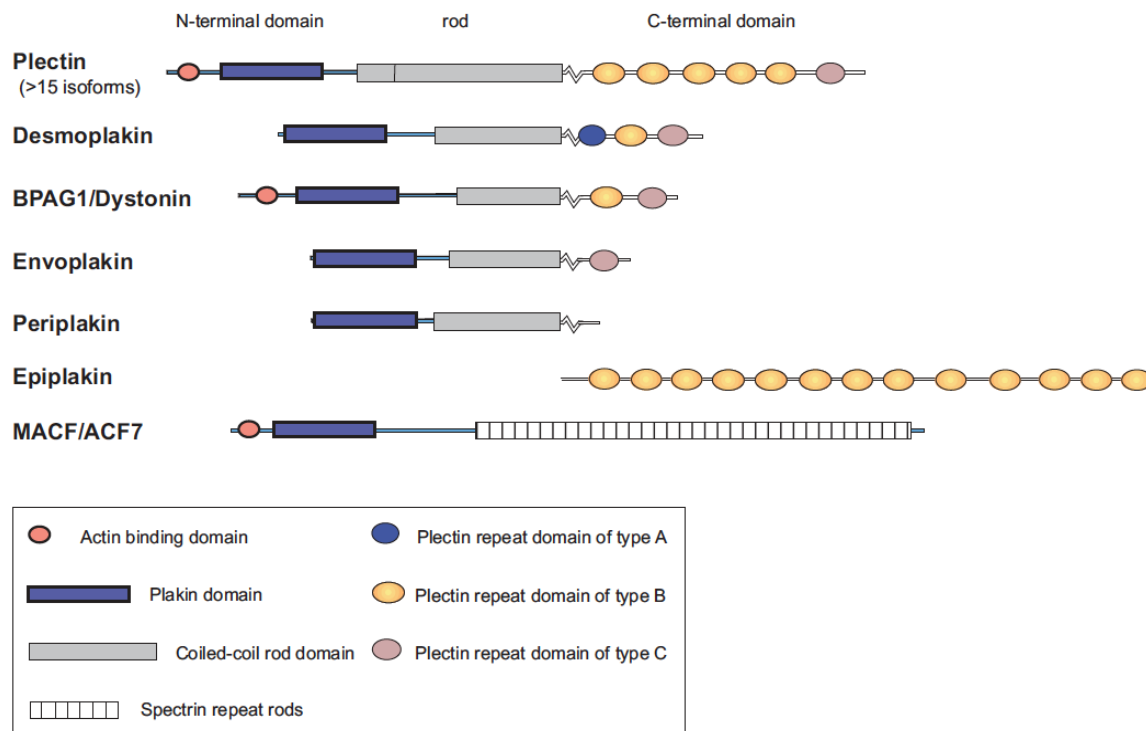


Figure 3. Mammalian cytolinker proteins. Functional domains of mammalian plakins including actin-binding domain, plakin domain, coiled-coil rod domain, spectrin repeat rod, plectin repeat domains are specified. (R. Spurny, PhD thesis).

them are shared by all cytolinkers: (i) a calponin-type actin-binding domain (ABD) consisting of two calponin-homology (CH) domains presented in alternatively spliced forms; (ii) a plakin domain, containing six α -helical segments, that is important for interaction with different proteins; (iii) a coiled-coil α -helical rod domain (with 10.4 residue charge periodicity) that mediates the dimerization of molecules, as it occurs in plectin (Wiche *et al*, 1991); (iv) a plectin repeat domain (PRD) composed by four complete and one partial 38-residue motif. PRDs can be categorized in A, B, and C repeats; the IF-binding domain is located in the PRD domain; (v) a spectrin repeat (SR) domain characteristic of the spectrin family made up of three α -helices connected by two loop regions; (vi) EF-hand calcium-binding motifs; (vii) Gas2-homology region named GAR domain or a GSR domain functioning as MT-binding sites in some of the cytolinker proteins (Leung *et al*, 2002).

Seven plakin protein family members have been identified up to date: desmoplakin, bullous pemphigoid antigen 1 (BPAG1), MT-actin cross-linking factor (ACF7), periplakin, envoplakin, epiplakin, and plectin; they are expressed in a large variety of tissues. Desmoplakin is responsible for anchoring IFs to desmosomes, structures that mediate intercellular adhesion in tissues subjected to mechanical stress (for review see Getsios *et al*, 2004). As a result of alternative splicing in the central rod domain, there are two isoforms of desmoplakin, DPI (322 kDa) and DPII (259 kDa) (Virata *et al*, 1992). Both isoforms are expressed in all types of epithelia, but DPI is also found in cardiac cells and in follicular dendritic cells associated with desmin and vimentin, respectively (Angst *et al*, 1990; Franke & Moll, 1987). Desmoplakin is involved in autoimmune diseases such as paraneoplastic pemphigus and genetic disease like striate palmoplantar keratoderma. In mice, desmoplakin deletion leads to embryonic death (Leung *et al*, 2002). The autoimmune skin blistering disease bullous pemphigoid (Moll & Moll, 1998) is associated with autoantibodies against BPAG1 and BPAG2. In addition, mutations in the *Bpag1* gene lead to sensory neuron degeneration

observed in mice with dystonia musculorum (Brown *et al*, 1995). Dystonia musculorum is a recessive neuropathy affecting sensory neurons and including disorganization of the cytoskeleton, accumulation of neuronal IFs and muscle weakness (Dalpe *et al*, 1998; Dalpe *et al*, 1999). ACF7 also known as MACF1, trabeculin or macrophin, is a cytolinker protein that is highly expressed in epidermis, and responsible for interconnecting MTs and actin filaments (Leung *et al*, 1999). Albeit no disease involving ACF7 has been reported yet, ACF7-deficient mice die at the gastrulation stage of the embryogenesis (Kodama *et al*, 2003). Periplakin and envoplakin are closely related and represent the smallest proteins of the plakin family (~200 kDa) (Ruhrberg & Watt, 1997; Ruhrberg *et al*, 1996). Both proteins are components of the cornified envelope and localized at desmosomes and IFs in differentiated keratinocytes. They are involved in paraneoplastic pemphigus and pemphigus foliaceus autoimmune diseases. Epiplakin is a very large protein (725 kDa) composed solely of PRDs, 13 in humans and 16 in mice. It was originally isolated as an autoantigen in a serum obtained from a patient with subepidermal blistering disease and its expression is restricted to epithelial tissues (Fujiwara *et al*, 1992; Fujiwara *et al*, 1996; Spazierer *et al*, 2003).

1.1.1 MT regulation

MT dynamics and functions are fine-tuned and regulated by other proteins binding to the polymer. Some MT-binding proteins are MT stabilizers or growth promoters, while others promote MT depolymerization (Figure 4). Post-translational modifications (PTMs) of MTs seem to be crucial to spatially and temporally control the activity of MT regulatory proteins.

Post-translational modification (PTMs)

PTMs are chemical modifications that occur to the proteins after their translation. Many PTMs, such as phosphorylation or ubiquitinylation, directly affect the function and activity of the

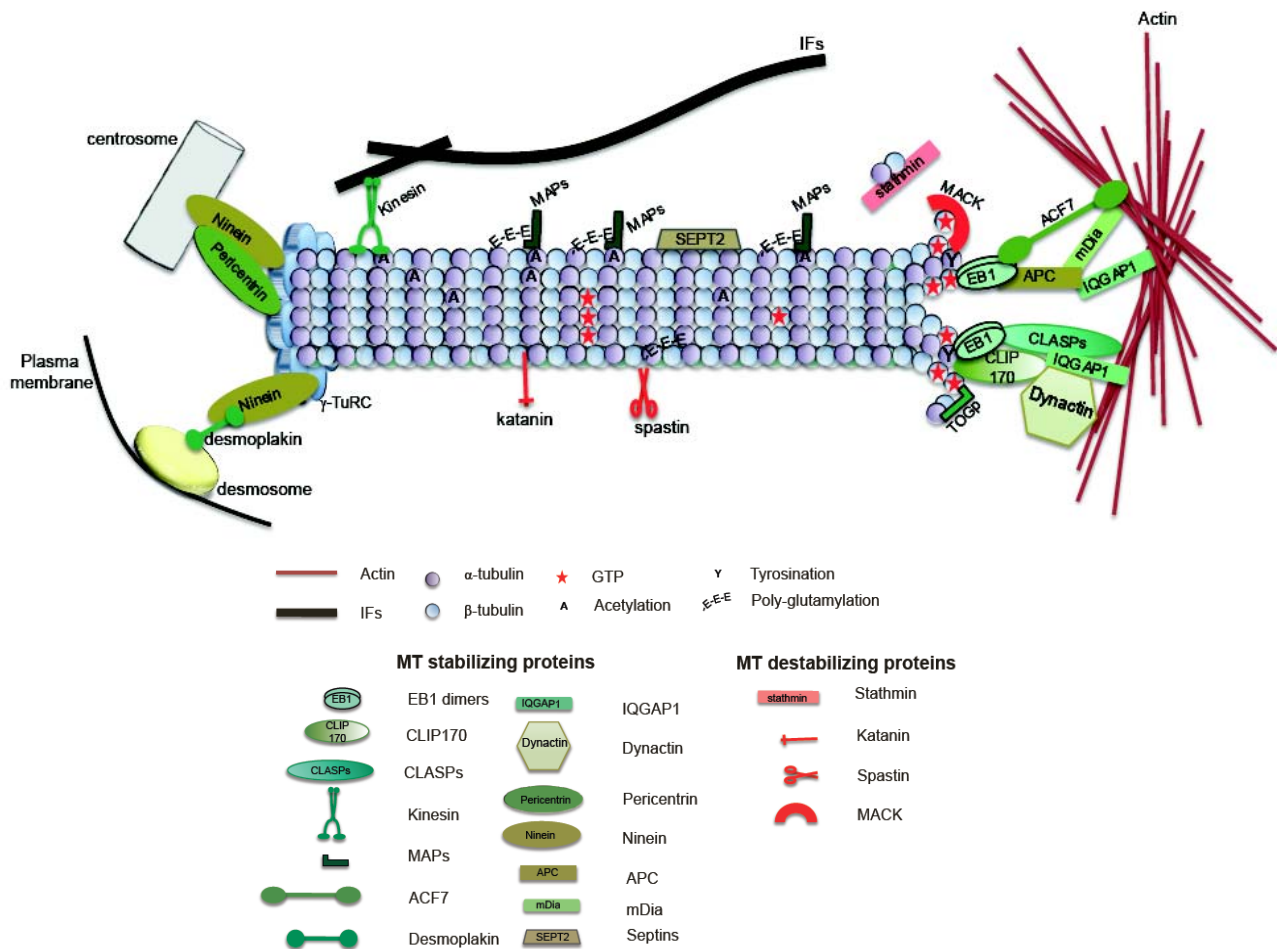


Figure 4. Model of MT-regulating proteins and PTMs. MT dynamics are regulated by proteins that bind along the MTs. MT-stabilizing proteins are depicted in green and destabilizing proteins in red.

proteins. Albeit, there is no apparent direct effect of PTMs on MTs, PTMs are emerging as control elements in the regulation of the interaction of tubulin with MT-binding proteins (for a review see Janke & Bulinski, 2011). The best studied PTMs of MTs are acetylation, detyrosination, $\Delta 2$ -tubulin generation (see below), polyglutamylation, and polyglycylation.

Acetylation of Lys40 on α -tubulin takes place once the MT is polymerized, functioning as a marker of relatively old and stable MTs (Piperno *et al*, 1987; Bulinski *et al*, 1988). Acetylated MTs increase the MT-binding affinity of molecular motors like KIF5A, KIF5B/kinesin

and dynein (Reed *et al*, 2006), stimulating vesicle and membrane bound organelle transport (Friedman *et al*, 2010). Acetylation of tubulin has also been proposed to induce enzymatic MT severing (Sudo & Baas, 2010).

Tyrosination occurs on dimerized α -tubulin (Raybin & Flavin, 1977) while detyrosination is mediated by a cytosolic carboxipeptidase that is active only on polymerized MTs, leaving a Glu residue exposed at the C terminus. Detyrosinated tubulin can be further converted to $\Delta 2$ -tubulin (by removal of the Glu residue exposed at the C terminus after tubulin detyrosination) that irreversibly locks MTs in a stable state, since tubulin tyrosin ligase is unable to again tyrosinate $\Delta 2$ -tubulin (Paturle-Lafanechère *et al*, 1991). Similar to acetylated MTs, detyrosination increases the binding of kinesin and IFs to MT (Liao & Gundersen, 1998; Kreitzer *et al*, 1999).

Polyglutamylation consists in the progressive addition of one or more glutamate residues near the C terminus of polymerized α - or β -tubulin (Edde *et al*, 1990). MT-stabilizing proteins like MAPs or MT-severing proteins such as katanin or spastin might be attracted to MTs by long poly-glutamate tails (Bonnet *et al*, 2001; Lacroix *et al*, 2010).

The extension of glycine side chains from glutamate residues near the accessible C terminus of α - or β -tubulin is known as polyglycylation, and in contrast to other PTMs, it is confined to cilia and flagella (Redeker *et al*, 1994).

MT-stabilizing proteins

Among the MT-stabilizing proteins, there is a complex and diverse set of MT-interacting proteins that can be classified according to their localization on MTs. According to this, there are MT-stabilizing proteins that bind all along the MT surfaces, plus end- (+TIP), and minus end-binding proteins.

The best known MT-stabilizing proteins are those that belong to the MAP2/tau family. They bind along the sides of acetylated MTs and contribute to their stabilization by crosslinking adjacent MTs (Felgner *et al*, 1997). However, MAPs are not the only MT-stabilizing proteins that bind along MTs. Septins form a novel family of filamentous GTPases that have been shown to inhibit MT catastrophes and participate in MT guidance during polymerization (Spiliotis, 2010; Bowen *et al*, 2011). The septin family consists of multiple genes and protein isoforms that can associate with cell membranes or the cytoskeleton. They decorate fragments of the MTs near the nuclear envelope and the cell periphery. Septins have been suggested to function as spatial localizers within the MTs, interacting with MAPs, motors and tubulin. Indeed, SEPT2 was found to compete with MAP4 for MT-binding at poly-glutamylated sites (Spiliotis *et al*, 2008). In addition, motor proteins, such as kinesins, participate in transporting tubulin heterodimers and oligomers promoting the assembly of tubulin (Kimura *et al*, 2005).

MT plus ends are subjected to a highly complex regulation. A delay between polymerization and GTP hydrolysis of GTP- β -tubulin creates a GTP-cap. The loss of this cap induces rapid depolymerization of the MTs, however some GTP remnants have been identified in older parts of MTs (Dimitrov *et al*, 2008). Nevertheless, the GTP-cap is not the only way how the plus end is regulated. The +TIP protein family has been extensively studied. It is composed of structurally unrelated proteins that often colocalize and share common functions (Lansbergen & Akhmanova, 2006; Akhmanova & Steinmetz, 2008; Jiang & Akhmanova, 2011). Albeit there are some +TIP proteins with a MT-destabilizing role, most of them are involved in promoting MT growth and stabilization. Although proteins within the +TIP family can be quite different from each other in structure, they contain serine-rich sequences that have been shown to interact with EB1, and have autoinhibitory domains. The end-binding (EB) protein family consists of proteins of very similar structure and sequence. The members of this family are expressed depending on the differentiation stage of different cell types. EB1 is a

ubiquitously expressed EB protein that dimerizes and promotes MT polymerization by increasing the rescue frequencies and decreasing the rate of depolymerization and the time of MTs spend in pausing. It has also been shown that EB1 promotes persistent growth by suppressing catastrophes in vitro (Komarova *et al*, 2009). EB3 promotes MT growth and it is important during neurite formation by coordinating filamentous actin-MT interaction (Geraldo *et al*, 2008) and for the organization of MTs during myotube differentiation (Straube & Merdes, 2007). EB3 binding to MTs is regulated via aurora A-mediated phosphorylation that leads to EB3-SIAH1 binding. SIAH1 is ubiquitin E3-ligase that targets EB3 for degradation (Ban *et al*, 2009).

Another essential component of the +TIP family is cytoplasmic linker protein 170 (CLIP170). Deletion of CLIP170 results in very low MT rescue frequency (Komarova *et al*, 2002). It is part of a subgroup of +TIP proteins named CAP-Gly proteins (cytoskeleton-associated protein Gly-rich) that interacts with the EEY/F domain of EB1 and tyrosinated α -tubulin (Peris *et al*, 2006; Mishima *et al*, 2007). CLIP170 was described as a phospho-sensitive MAP (Rickard & Kreis, 1991), and indeed, its binding to MTs is regulated by mTOR and AMP kinase PKA (Choi *et al*, 2002; Nakano *et al*, 2010; Lee *et al*, 2010). CLASPs are CLIP-associated proteins that contribute to promote rescue events by recruiting tubulin dimers at the tips of MTs and by their interaction with EB1 (Akhmanova *et al*, 2001; Al-Bassam *et al*, 2010). The binding affinity of CLASPs to EB1 is decreased by GSK3 β phosphorylation (Kumar *et al*, 2009).

Another +TIP protein recruiting tubulin dimers at the plus-end and promoting MT growth is TOG protein, a MAP with MT-polymerizing activity (Brouhard *et al*, 2008). There are some +TIP proteins specifically expressed in a cell-type dependent manner, such as Lis1 and its binding partner doublecortin in neurons. Absence of any of them leads to type I lissencephaly, a disease characterized by a smooth cerebral surface. Lis1 is responsible for targeting

CLIP170, dynein and dynactin (Tai *et al*, 2002) and reduces the catastrophe events of MTs (Sapir *et al*, 1997). Among the +TIP protein family, other tissue specific proteins have been described, such as neuron-navigator 1 in neurons (Martínez-López *et al*, 2005) or melanophilin in melanocytes (Wu *et al*, 2005).

Finally, there are proteins responsible for MT stabilization at the minus end of MTs. In interphase cells, MTs are organized in a MT-organizing center like centrosomes (MTOC), or loosely organized with a large number of free minus ends generated by release from MTOC, cytoplasmic assembly, or severing of pre-existing MTs (Dammerman *et al*, 2003). MT minus ends are stabilized due to the association of γ -tubulin with other proteins to form the γ -tubulin ring complex (γ -TuRC) that functions as a nucleation seed for MTs but also as stabilizing cap to avoid depolymerization. Pericentrin and ninein are γ -TuRC proteins that are localized at the centriole and anchor MTs to the centrosome (Abal *et al*, 2002; Lin *et al*, 2006). Pericentrin and ninein, relocate γ -TuRCs from the centrosome to the nuclear envelope during skeletal muscle differentiation (Bugnard *et al*, 2009). Ninein also anchors MT at epithelial cell junctions through an interaction with desmoplakin (Lechler & Fuchs, 2007). Nehzah is another MT stabilizing protein that anchors MT minus ends at junctions in epithelia cells independently of the γ -TuRC (Meng *et al*, 2008).

MT-destabilizing proteins

Several types of MT-binding proteins have been identified as MT destabilizers and are crucial for mitotic spindle organization. The MT-severing proteins katanin, spastin and fidgetin form a family of closely related enzymes that regulate the number and length of MTs through their severing activity. PTMs and other MT-binding proteins regulate MT activity and function (Zhang *et al*, 2007; Roll-Mecak & McNally, 2010). Members of the kinesin-13 family, such as KIF2A and MACK, have been shown to induce a conformational change of tubulin dimers that

triggers catastrophe events. They are thought to function by bending and peeling off individual protofilaments to generate rings (Ems-McClung & Walczak, 2010). Removal of Y from α -tubulin leads to decreased binding of MCAK and KIF2A to MTs (Peris *et al*, 2009). In addition, +TIP protein EB1 recruits MCAK to the plus end of MTs and this interaction is regulated by aurora B-mediated phosphorylation (Andrews *et al*, 2004; Lan *et al*, 2004). Stathmin is a MT-destabilizing protein that, distinctly to MACK, binds to tubulin heterodimers, and curves them into a complex that cannot be incorporated into polymerized MTs (Belmont *et al*, 1996).

Actin-MT crosstalk

Cell motility, growth cone guidance, cell division, and wound healing require coordination between MT and actin filament dynamics (Rodríguez *et al*, 2003; de Forges *et al*, 2012). Different MT- and actin-binding proteins, cytolinkers and signaling cascades mediate the coordination between the two systems. Different +TIP proteins are responsible for anchoring MTs to the actin cell cortex. Adenomatous polyposis coli (APC) protein is transported by kinesin to the MT plus end where it stimulates their polymerization by binding to EB1 and anchors them at the cell cortex via mDia (a RhoA effector) and IQGAP1 (an Rac/Cdc42 effector) (Wen *et al*, 2004; Reilein & Nelson, 2005). CLASP proteins attach distal MTs ends to cortical sites and act independently of APC (Mimori-Kiyosue *et al*, 2004). Dynein and p150^{glued} are the biggest subunits of the dynactin complex that is recruited by EB1 and CLIP170. Dynactin participates not only in centering the centrosome in interphase cells or positioning the mitotic spindle, but also pulls the ends of MTs to the cell cortex (Dujardin & Vallee, 2002; Gomes *et al*, 2005). Cytolinkers are also involved in crosslinking actin and MTs. ACF7 is a spectraplaklin that accumulates at the tips of MTs through a direct interaction with EB1. Thereby it contributes to the control of cell polarity and migration, and stabilizes MTs (Kodama *et al*, 2003).

There are several non-exclusive hypotheses to describe actin-MT crosstalk, involving MT- and actin-binding proteins and signaling proteins. One possible mechanism to explain it might be a model where structural interaction of MTs and actin would be coupled with signaling cascades (Figure 5). MT breakage and depolymerization occurs as a result of actin retrograde flow (Waterman-Storer & Salmon, 1997). Depolymerizing MTs are thought to release the MT-bound Rho guanine nucleotide exchange factor (GEF)-H1 that is responsible for RhoA activation (Krendel *et al*, 2002). RhoA activation results in myosin phosphorylation leading to actin contraction and promoting the local stabilization and polymerization of MTs (Cook *et al*, 1998; Ren *et al*, 1999). MT polymerization activates Rac and Cdc42 leading to actin polymerization and protrusion formation (Waterman-Storer *et al*, 1999).

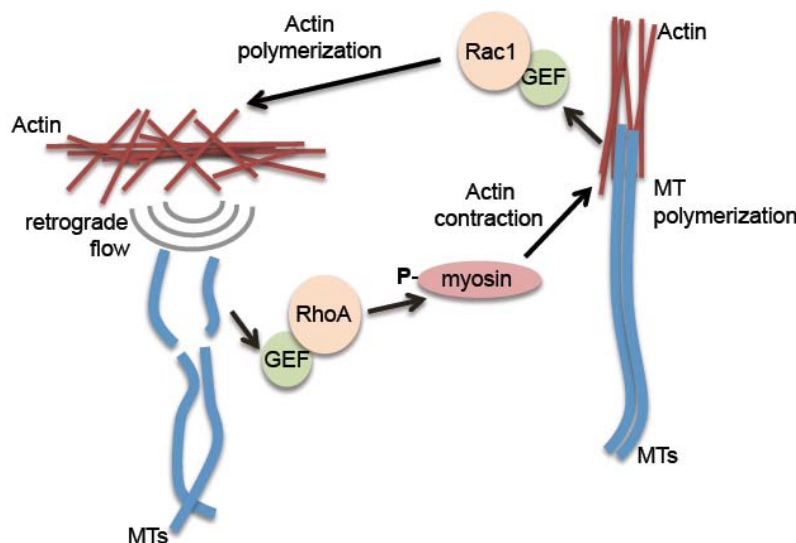


Figure 5. Scheme representing actin-MT crosstalk. Upon actin retrograde flow, MT breakage frees GEFs activating RhoA signaling pathway. This leads to actin contraction, MT polymerization and activation of Rac1, promoting new actin polymerization.

IF-MT crosstalk

In contrast to actin, there is no direct evidence of IF-MT crosstalk. Although the cytolinker proteins plectin and BPAG1 have been identified as crosslinker between IFs and MTs (Svitkina

et al, 1996; Yang *et al*, 1999), no clear effects of IFs on MTs have been described yet. BPAG1 deficiency leads to MT destabilization independently of whether IFs are present or not.

1.1.2 Plectin

Plectin is one of the best characterized cytolinkers and the most versatile one (Wiche & Winter, 2011). Plectin was first purified in association with IFs (Pytela & Wiche, 1980). The discovery of plectin's widespread expression in tissues and cells, especially at junctional sites, suggested a possible role of plectin in the formation of cell junctions and anchorage of cytoplasmic filaments (Wiche & Baker, 1982; Wiche *et al*, 1983). The crosslinking activity of plectin was first elucidated in studies on plectin's molecular properties (Foisner & Wiche, 1987) and plectin-binding to IFs (Foisner *et al*, 1988). The plectin gene was first cloned and sequenced from rat (Wiche *et al*, 1991), and then from human (Liu *et al*, 1996). A detailed analysis of exon-intron organization of the rat gene locus was described in the following year by Elliott *et al* (1997), but it was not until 1999 that a detailed analysis of the murine plectin gene locus was published (Fuchs *et al*, 1999). A better understanding of plectin's exact role came with the generation of plectin-deficient mice (Andrä *et al*, 1997), and the discovery that defects in the plectin gene cause epidermolysis bullosa simplex associated with muscular dystrophy (EBS-MD) (Gache *et al*, 1996; Smith *et al*, 1996), a severe skin blistering disease.

Molecular properties

Plectin is a large cytolinker protein of ~500 kDa that is composed of a central rod domain flanked by globular N-terminal head and C-terminal tail domains (Foisner & Wiche, 1987) (Figure 6). The central ~200 nm long α -helical coiled-coil rod structure is encoded by a single exon. It contains five subregions, each ~200 residues long, with a strict period of charged amino acids at 10.4 residues that might be involved in association between plectin molecules (Wiche *et al*, 1991). Indeed, it has recently been shown that dimeric rod domains can

associate laterally, forming stable polymers (Walko *et al*, 2011). The C-terminal globular domain (also encoded by a single exon) contains five PRD of the B type and one PRD of the C

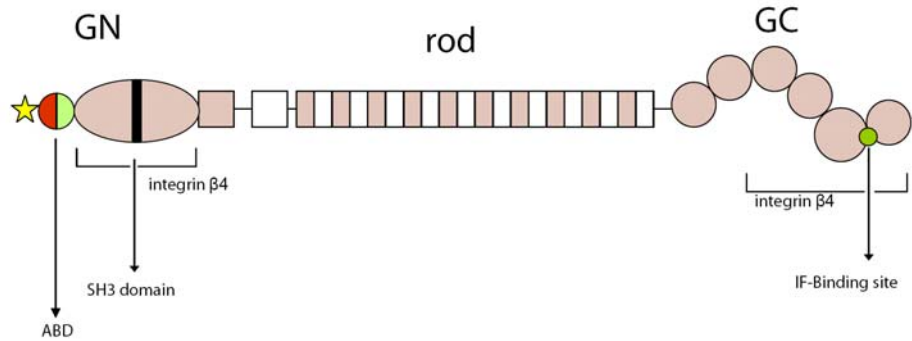


Figure 6. Domain map of plectin. The plectin molecule comprises a central rod flanked by globular N-terminal (GN) and C-terminal domains (GC). Subdomains binding to actin (ABD), MAPs (SH3 domain), IFs, and integrin $\beta 4$ are indicated.

type. The IF-binding region of plectin consists of ~50 amino acid residues linking PRDs 5 and 6 (Nikolic *et al*, 1996). The globular C-terminal domain contains an additional binding site for integrin $\beta 4$ (Reznicek *et al*, 1998) and a unique phosphorylation site for cdk1 kinase (Malecz *et al*, 1996).

Isoform diversity

Plectin is the most versatile cytolinker protein mainly due to its unique and complex exon-intron organization. Alternative splicing of the 5'-end of plectin's gene gives rise to at least 16 different transcripts (Figure 7): Eleven alternative first exons are spliced into a common exon 2. Eight of them are first coding exons (1-1g), and three of them are non-coding (1h, 1i, 1j). Three additional non-coding exons (E0, E0a and E-1) splice into exon 1c, and another two (2 α and 3 α) are optionally spliced within the exons encoding the ABD (Fuchs *et al*, 1999). This broad variety of sequences determines the cellular targeting of the different isoforms (Reznicek *et*

et al., 2003). Plectin isoforms show preferential binding to an assortment of cellular structures, including hemidesmosomes (HDs), focal adhesions (FAs), costameres, mitochondria, MTs, nuclear/endoplasmic reticulum membranes, and Z-disks. Being expressed in the various cell types and tissue in different combinations and proportions, plectin isoforms connect the cellular structures targeted with the corresponding cell-type-specific IF network. By anchoring IFs at distinct cellular structures plectin isoforms control IF cytoarchitecture and thereby basic and other cell type-specific features of cells (Wiche & Winter, 2011).

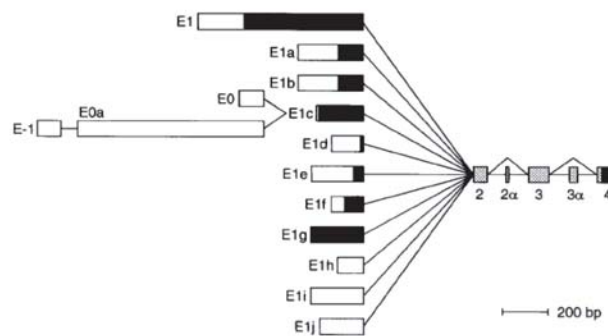


Figure 7. Transcripts generated by alternative splicing at the 5'-end of the plectin gene. Eleven alternative exons splice into exon 2. Eight of them are first coding exons (1-1g), three of them are non-coding (1h-1j). In addition, there are three non-coding exons that splice into exon 1c (E0, E0a and E-1). Two optionally spliced exons (2 α and 3 α) are indicated. Black boxes indicate coding regions and white boxes designate non-coding sequences (Fuchs *et al.*, 1999).

Plectin in connective tissue

First immunolocalization studies revealed plectin throughout the cytoplasm of immortalized fibroblast cell cultures (Wiche & Baker, 1982), and in cells of mesenchymal origin in various rat tissues examined (stomach, kidney, small intestine, liver, uterus and urinary bladder) (Wiche *et al.*, 1983). However, most of the features known about connective tissue plectin came from studies of plectin-deficient fibroblasts. One of plectin's major isoforms in fibroblasts is plectin 1

(P1). P1^{-/-} fibroblasts show impaired migration and alterations of the actin cytoskeleton (Abrahamsberg *et al*, 2005), reminiscent of plectin-null (P0) fibroblasts (Andrä *et al*, 1998). Another isoform of plectin prominently expressed in fibroblasts is plectin 1b (P1b). P1b targets mitochondria via its N-terminal part and anchors them to IF networks via its C terminus. P1b-deficient fibroblasts show abnormal mitochondrial shape and distribution (Winter *et al*, 2008). Plectin has also been shown to have an influence on vimentin IF cytoarchitecture of fibroblasts. Plectin is associated with vimentin from the early stages of filament assembly, is required for the formation of IFs and their directional growth towards the cell periphery, and plectin-deficient fibroblasts undergo faster mitosis than their wild-type (wt) counterparts (Spurny *et al*, 2008). Moreover, plectin participates in the regulation of the de novo IF formation (Burgstaller *et al*, 2010). Plectin 1f (P1f), one of the major isoforms expressed in fibroblasts is a component of FA-evolved fibrillar adhesions (FbAs) that are centrally located. P1f recruits vimentin intermediates (squiggles) to these sites and stabilizes FbAs, thus acting as a nucleation center for filament formation. As a result, vimentin filaments form a cage around the nucleus of the cell that in plectin-deficient fibroblast is distorted (Figure 8). Plectin deficiency in fibroblasts results also in increased stability of actin filaments, compromised signaling (decreased Src and FAK activities) and decreased migration potential (Andrä *et al*, 1998; Osmanagic-Myers *et al*, 2004; Osmanagic-Myers *et al*, 2006; Gregor *et al*, 2006).

Plectin in muscle

Plectin is expressed in the three major types of muscle, localizing along the sarcolemma in smooth muscle cells (Wiche *et al*, 1983; Tanaka *et al*, 2001), at intercalated disks and Z-disks of cardiac muscle (Wiche *et al*, 1983; Zernig & Wiche, 1985; Konieczny *et al*, 2008), and at the sarcolemma and Z-disks in skeletal muscle (Wiche *et al*, 1983; Konieczny *et al*, 2008). However, the influence of plectin on IF network organization becomes most noticeable in

skeletal muscle. In this type of muscle four major isoforms of plectin are expressed, namely P1, P1b, P1d, and P1f. P1d is associated with Z-disks, P1f with the dystrophin-glycoprotein complex at the sarcolemma, P1b with mitochondria, and P1 with the outer nuclear/sarcoplas-

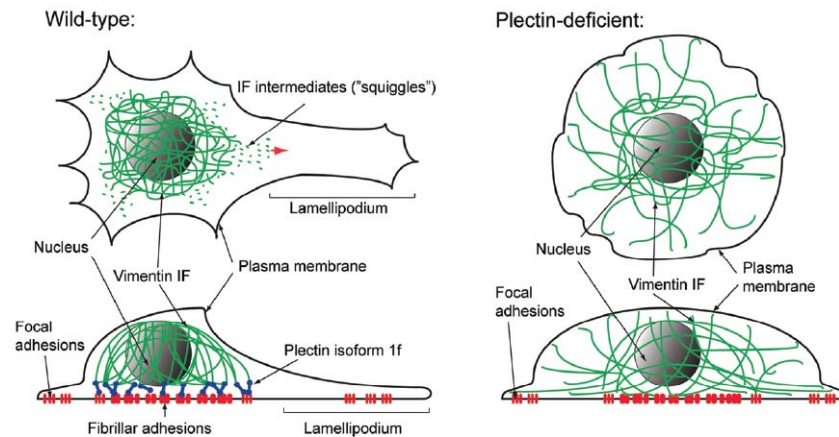


Figure 8. Simplified representation of plectin's function as organizer of fibroblast cytoarchitecture. Vimentin filaments form a cage around the nucleus through their P1f-mediated attachment to FbAs and centrally located FAs in polarized fibroblasts. Anterogradely transported (red arrow) vimentin filament intermediates ("squiggles") are "captured" by FA-associated P1f and by tandem-fusion will extend the filaments forming the centrally located cage-like network. Plectin-deficient cells are rounded, not polarized and their vimentin network extends to the outermost boundary of the cell (Burgstaller *et al*, 2010).

mic reticular membrane system (Reznicek *et al*, 2007; Konieczny *et al*, 2008) (Figure 9). P1d and P1f are crucial for linking the contractile apparatus via desmin IFs to the sarcolemmal costameric protein skeleton. Disruption of either P1f or P1d leads to the loss of muscle fiber integrity (Konieczny *et al*, 2008). Albeit already newborn plectin-deficient (null) mice revealed abnormalities in skeletal and cardiac muscle, they were unusable for more detailed studies because they die within 2-3 days after birth (Andrä *et al*, 1997). Hence, the phenotypic analysis of plectin-deficient muscle had to be carried out with conditional (MCK-Cre) striated muscle restricted knock out and isoform-specific knock out mice (Konieczny *et al*, 2008).

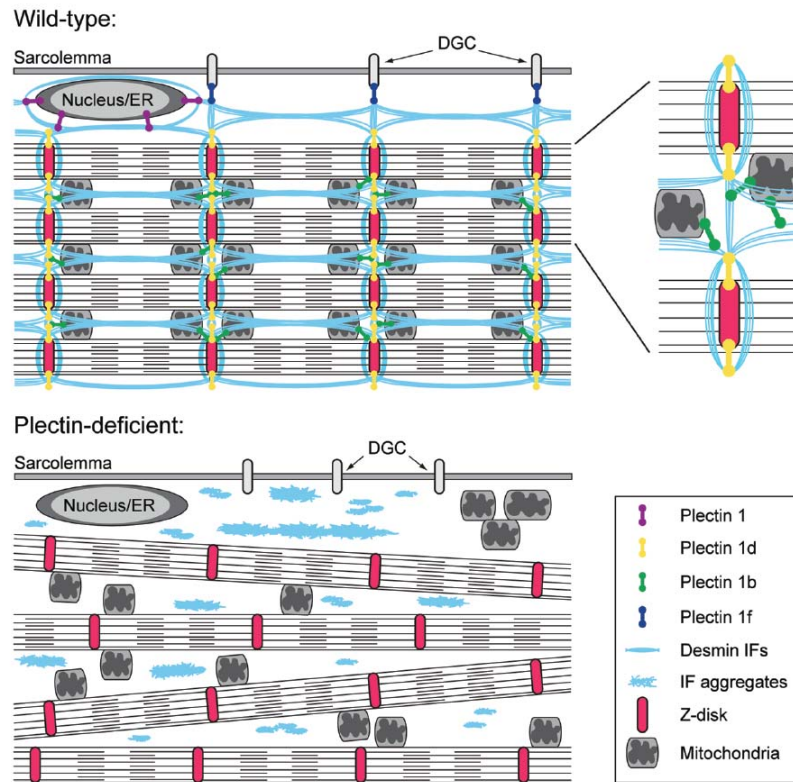


Figure 9. Model depicting the role of plectin in skeletal muscle fibers. The four major plectin isoforms expressed in muscle, P1, P1b, P1d, and P1f anchor desmin IFs to the outer nuclear/SR membrane system, mitochondria, Z-disks, and the sarcolemmal dystrophin-glycoprotein complex, respectively. Plectin-deficiency causes aggregation of desmin IFs and misalignment of Z-disks (Wiche & Winter, 2011).

Epithelial plectin

Early studies on plectin distribution revealed plectin expression in practically all mammalian tissues. Antibodies to plectin were found to prominently decorate the basal surface membrane of stratified and simple epithelial cell layers (Wiche *et al*, 1983). In basal keratinocytes, keratin IFs are linked to hemidesmosomal integrin $\beta 4$ via plectin isoform 1a (P1a) (Andrä *et al*, 2003; Kostan *et al*, 2009). Plectin-null (P0) and conditional (K5-Cre) plectin knockout mice, both dying early after birth, show blistering on their extremities and on the oral epithelium after initial nursing (Andrä *et al*, 1997; Ackerl *et al*, 2007). Although HDs are not structurally affected in P0

keratinocytes, they are reduced in number and their mechanical stability is compromised. More recently it was shown that the selective degradation of HD-associated P1a, by proteases activated specifically in keratinocytes, results in reduced numbers and dysfunction of HDs (Walko *et al*, 2011). Selective proteolytic degradation of P1a might be required also for epithelial differentiation (Kostan *et al*, 2009).

A second major isoform of keratinocytes, P1c has been shown to partially colocalize with MTs and cosediment with pre-assembled MTs (see below). Reminiscent of IF network alterations observed in plectin-deficient fibroblasts, keratinocytes lacking plectin display keratin networks where filaments appear to be bundled and extending to the periphery. In contrast, wt cells exhibit keratin networks that are more delicate and juxtapositioned to the nucleus, leaving a filament-free ring-shaped zone at the cell margins (Osmanagic-Myers *et al*, 2006). However, contrary to plectin-null fibroblasts, plectin-deficient keratinocytes show increased migration rates, corresponding to elevated basal activities of mitogen-activated protein (MAP) kinase Erk1/2 and of the membrane-associated upstream protein kinases c-Src and PKC δ (Osmanagic-Myers *et al*, 2006). Plectin deficiency leads to the skin blistering disease EBS (Gache *et al*, 1996; Smith *et al*, 1996) and EBS-Ogna (see chapter below).

Plectin in the nervous system

Little is known about the role of plectin in the nervous system. As shown by analyses of plectin transcripts, P1c is a major isoform not only of epidermal cells but also of neural cells (Figure 10). This is not unexpected considering that epidermal and neural cells share a common developmental origin, the ectoderm.

Thanks to P1c-specific antibodies and the availability of P1c-deficient (P1c^{-/-}) mice to be used as optimal negative control, P1c was found to be expressed late in development and

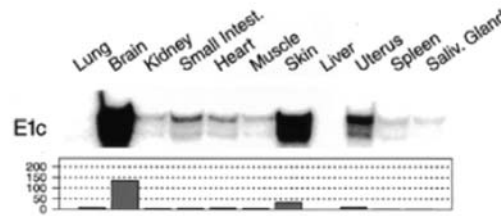


Figure 10. Tissue distribution of murine exon 1c. Autoradiography (upper panel) and quantification (lower panel) of RNase-protected RNA bands obtained using exon 1c-specific probes. (Fuchs *et al*, 1999).

associated with postsynaptic dendrites of central nervous system neurons, spinal cord motor neurons, sciatic nerve axons, and Schwann cells. In central nervous system, P1c was preponderantly expressed in the hippocampus. P1c deficiency affects the behavior of mice as shown by their reduced exploratory activity and voluntary wheel running (Michael Zörer, PhD thesis). In addition, lack of P1c leads to reduced nerve conduction velocity in motor neurons combined with a reduction in motor neuron calibers (Fuchs *et al*, 2009).

Plectin and disease

Most of the plectin mutations reported lead to epidermolysis bullosa simplex associated with muscular dystrophy (EBS-MD) (Gache *et al*, 1996; Smith *et al*, 1996). EBS-MD patients suffer from severe skin and mucous membranes blistering and late-onset muscular dystrophy. In addition, other plectin mutations were reported to cause EBS-MD with myasthenic syndrome (EBS-MD-MyS) (Banwell *et al*, 1999; Forrest *et al*, 2010; Selcen *et al*, 2011), limb-girdle muscular dystrophy type 2Q (LGMD2Q) (Gundesli *et al*, 2010), and EBS with pyloric atresia (EBS-PA) (Rezniczek *et al*, 2010; Natsuga *et al* 2010). Moreover, a dominant mutation in plectin has been reported to cause the rare skin blistering disease EBS-Ogna, which was originally identified in a Norwegian kindred and in an unrelated German family (Koss-Harnes *et*

vimentin IFs (Svitkina *et al*, 1996). Additionally, unpublished data from our group show P1c immunofluorescence microscopy to partially colocalize with MTs (Figure 12A), and to cosediment with pre-assembled MTs (Figure 12B) (G. Walko, unpublished; Andrä *et al*, 2003). Albeit the C-terminal tail contains GSR repeats that were reported to be a MT-binding site, it was shown by G. Walko (PhD thesis) that the C-terminal domain of plectin is not able to associate with MTs.

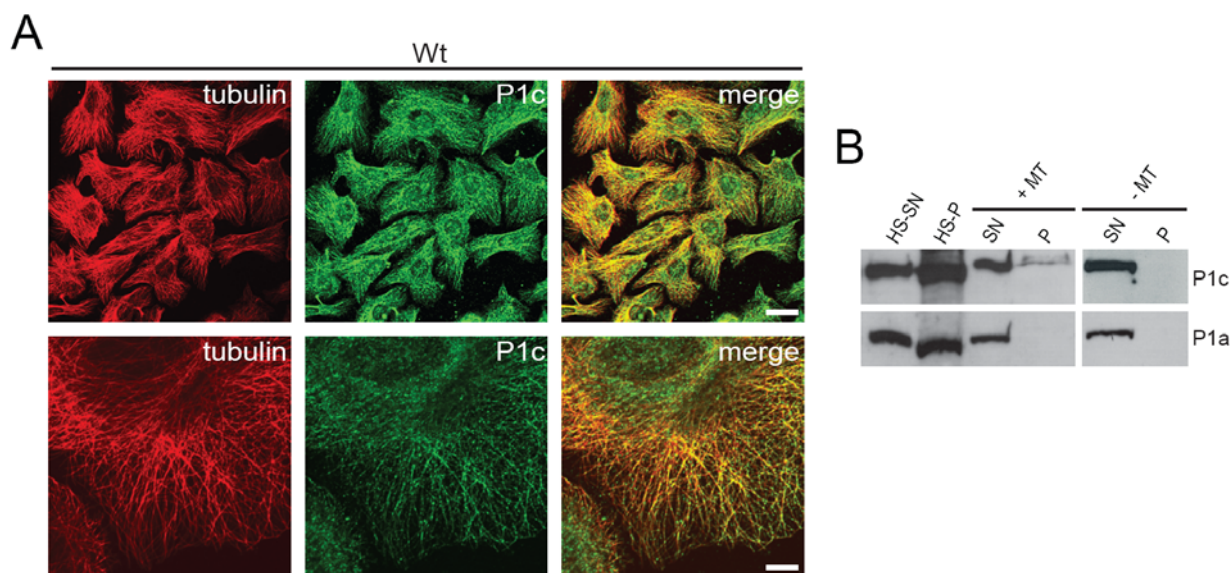


Figure 12. P1c interacts with MTs. **A)** Immortalized wt and P0 keratinocytes were immunolabeled using anti- α -tubulin and anti-P1c isoform-specific antibodies. Note even distribution of P1c (upper panels), and speckled decoration of MTs (lower panels). Scale bars, 50 μ m (upper row); 10 μ m (lower row). **B)** Wt keratinocyte cell homogenates were separated into high-speed supernatant (HS-SN) and pellet (HS-P) fractions, and the HS-SN fraction was incubated with (+MT) or without (-MT) taxol-stabilized MTs and centrifuged. Pellet (P) and supernatant (SN) fractions were analyzed by immunoblotting using isoform-specific antibodies. Note a fraction (~30%) of endogenous P1c cosedimented with pre-assembled MTs (G. Walko, unpublished).

The ABD of plectin is followed by a plakin domain containing spectrin repeats and a SH3 domain. Interestingly, preliminary data from our laboratory demonstrated that the SH3 domain present within the plakin domain is able to bind to high molecular weight (HMW)-MAPs and antagonize their MT-stabilizing effect (unpublished). At the molecular level, previous solid-phase binding studies had revealed binding of full-length plectin isolated from rat glioma C6

cells to HMW-MAPs purified from brain (Herrmann & Wiche, 1987). Afterwards, the laboratory strategy was to identify which molecular domain(s) of plectin were involved in MAP-binding. Using various fragments of P1c, expressed as fusion proteins with N-terminal GST tags, it was found that those containing the central part of plectin's N-terminal plakin domain preceding the rod, showed binding to at least one of the HMW-MAPs. The minimal fragment showing MAP-binding, p20-21, corresponded to plectin's putative SH3 domain (Ortega *et al*, 2011), raising the possibility that plectin bound to MAPs via this domain. A similar type of interaction has previously been shown for tau, another major MAP, which binds to the SH3 domain of the non-receptor tyrosine kinases Fyn and Src (Lee *et al*, 1998). P1c-MAP binding has further been demonstrated by co-sedimentation of HMW-MAPs with P1c immunoprecipitated from mouse brain lysates using anti-P1c isoform-specific antibodies (Figure 13C; E. Mihailovska, unpublished data).

To better understand the molecular mechanism involved in MT destabilization through plectin, the effects of plectin's SH3 domain on MAP-promoted *in vitro* assembly of tubulin into MTs has previously been studied in this laboratory (L. Janda, unpublished data). For these assays MAP-free tubulin was used, along with fragment p20-21, and recombinant MAP2c. Upon incubation of MAP-free tubulin with MAP2c, under conditions where tubulin itself polymerized only poorly (if at all), ~65% of the tubulin was found to form polymers in the absence of fragment p20-21 (Figure 13A, lane 4). When fragment p20-21 at increasing concentrations was mixed with MAP2c prior to induction of MT formation, increasing amounts of MAP2c were found in the soluble fractions, indicating reduced MT-binding of MAP2c in the presence of fragment p20-21. Ultimately, reduced MAP2c-binding to MTs led to a shift of tubulin from the insoluble to the soluble fraction, indicating an inhibition of MAP2c-promoted MT assembly. Also previous results of the group showed that fragment p20-21 could compete with MTs for tau-binding under conditions where the polymeric state of MTs was maintained

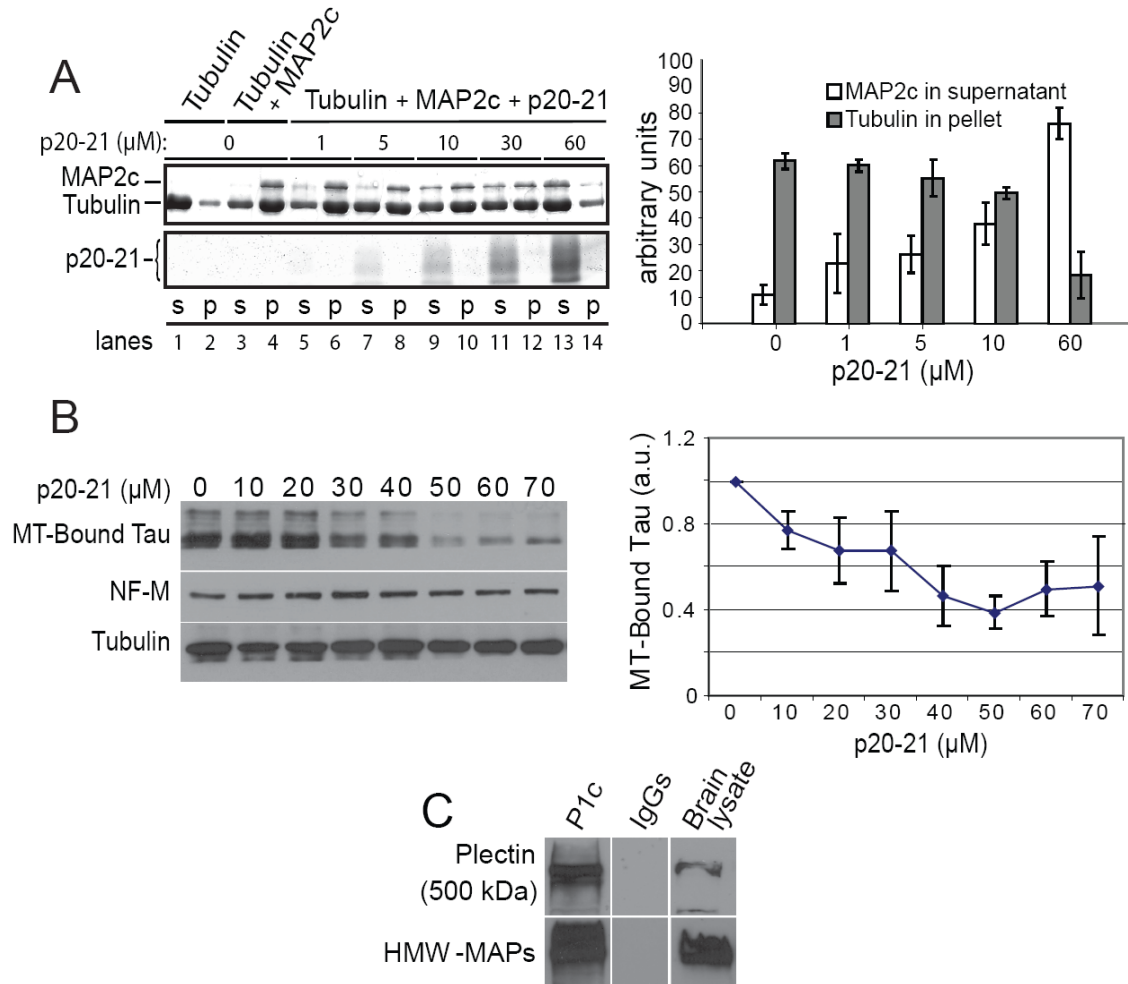


Figure 13. Plectin's SH3 domain (fragment p20-21) compromises recombinant MAP-MT interaction. **A)** MTs were assembled in vitro from purified samples of tubulin and MAP2c in the presence of fragment p20-21 (at concentrations indicated) and sedimented by centrifugation. Resulting pellets (p, containing polymerized MTs and MT-bound MAP2c), and supernatants (s, containing soluble tubulin and unbound MAP2c), and p20-21 were analyzed by SDS-PAGE. Coomassie-stained gel bands corresponding to MAP2c in supernatant (white bars in bar diagram) and tubulin in pellet fractions (grey bars) were quantified. Error bars, \pm SD (n=5). (L. Janda, unpublished data) **B)** The detachment of endogenous tau from MTs contained in brain lysates was measured by SDS-PAGE of the sedimented MT fractions after incubation of lysates with p20-21 at concentrations indicated. Protein bands corresponding to MT-bound tau, tubulin (representative of MT polymers), and NF protein M (NF-M, loading control) are shown. Quantitation (graph) as in (A). Error bars, \pm SEM (n=5). (E. Mihailovska, unpublished data). **C)** Co-immunoprecipitation of P1c and HMW-MAPs from brain lysates. Note MAPs-P1c coprecipitation when anti-P1c antibodies, but not IgGs alone, were used (n=3) (E. Mihailovska, unpublished data).

(without disassembly of the polymer) (E. Mihailovska, unpublished data). For this, increasing concentrations of fragment p20-21 were incubated with MTs contained in brain lysates under conditions that were favorable for their polymerized state even after removal of MAPs. The analysis of polymeric MTs (i.e. sedimentable by high-speed centrifugation) and their co-assembling (bound) proteins by immunoblotting clearly revealed a decrease in MT-bound tau protein with increasing concentrations of fragment p20-21 (Figure 13B). These data suggested that plectin's SH3 domain could detach MAPs from MTs.

2 AIMS OF THE THESIS

A number of observations made in previous studies, including the targeting of overexpressed P1c to MTs, the partial colocalization of P1c with MTs in cultured cells, and the *in vitro* binding of neural plectin to MAPs, pointed towards a potential interaction of plectin with MTs. Moreover, ACF7 and BPAG1, other members of the plakin cytolinker protein family, have been shown to be involved in the regulation of MT dynamics, both acting as MT stabilizers. Based on these previous observations and additional unpublished data from this laboratory, one of the major goals of my thesis was to analyze whether plectin plays a role in regulating MT dynamics. Of particular interest in this context was the question whether plectin isoform P1c antagonizes MAP-mediated MT stabilization, and if so, what was the underlying molecular mechanism.

A second major goal of my thesis was to search for a mechanistic link between plectin-related changes in MT dynamics and alterations in MT-dependent processes of physiological significance. Since P1c is a major isoform in keratinocytes and neurons, and the preliminary data obtained in the laboratory showed that P1c colocalizes with MTs, the most convenient system for this investigation was to use keratinocytes and neurons isolated from P1c-deficient mice. To analyze whether P1c-dependent MT organization could alter basic cellular functions in keratinocytes, processes including glucose uptake, cell division and growth, FA turnover, shape and polarized migration of cells were to be studied. P1c-deficient primary dorsal root ganglia (DRG) neurons should be assessed as a system in which to study the consequences of altered MT-dynamics for neurite cell functions, such as neurite outgrowth and branching, synaptic and other vesicle transport along neurites, and neuronal membrane depolarization.

3 RESULTS

This section is subdivided into two parts. Both address plectin isoform P1c's potential role as a regulator of MT dynamics and the consequences such regulation might have for MT-dependent cellular functions. While part I addresses the keratinocyte cell system, part II is focused on neuronal cells.

Part I - Plectin 1c in keratinocytes

Preliminary results obtained in previous studies of this group showed partial colocalization of P1c with MTs in cultured keratinocytes (see Introduction). However, the biological significance of P1c's presumptive interaction with MTs or its effects on the dynamic behavior of MTs had not been investigated.

3.1.1 Lack of P1c in keratinocytes leads to increased stability of MTs

Proteins that bind along MTs often alter the mechanical properties of the polymer, either by stabilizing (e.g. MAPs, ACF7/MACF) or destabilizing (e.g. Op18/stathmin, SCG10) (Conde & Cáceres, 2009). To investigate whether P1c shares such properties and to analyze its specific role in MT network organization, I chose to study primary P1c-deficient keratinocytes (derived from P1c isoform-specific knockout mice, Fuchs *et al*, 2009) in comparison to P0 keratinocytes and wt keratinocytes. This combination of cell types represents an optimal system to distinguish between isoform P1c-specific and other plectin isoform deficiency-related phenotypes. First, I investigated whether the absence of P1c affected the stability of MTs by tracing and quantifying MTs that remained polymerized after treatment of P1c^{-/-} and wt primary keratinocytes with low doses of the MT-depolymerizing drug nocodazole (for details see chapter 5, Material and methods). Unexpectedly, I found MTs in P1c^{-/-} keratinocytes to be

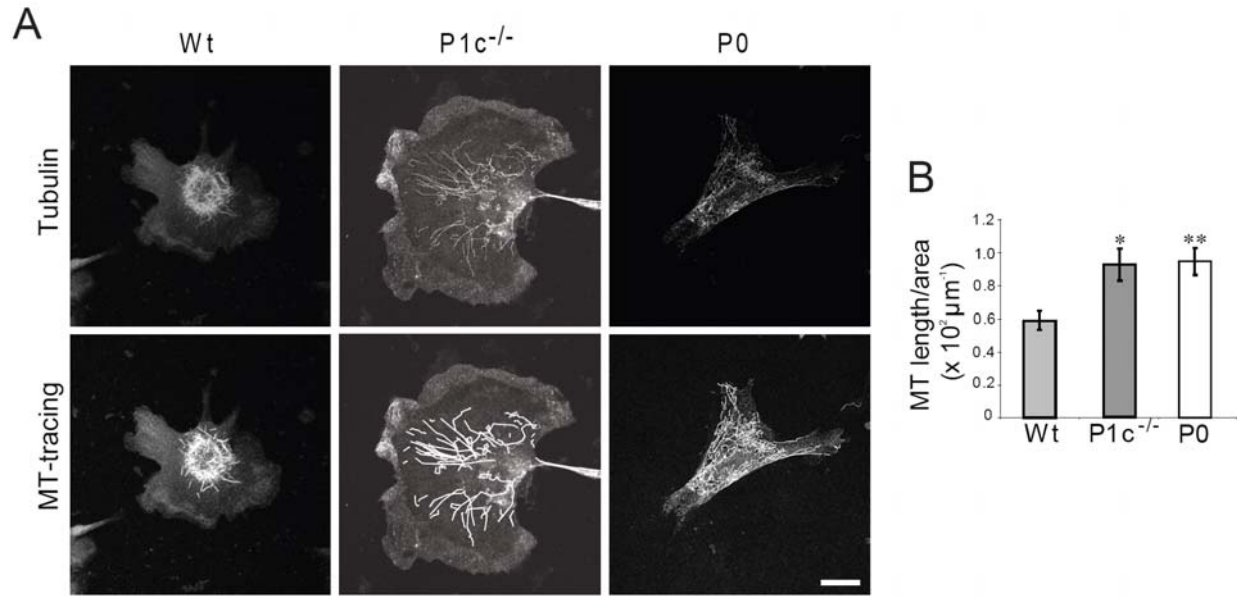


Figure 14. P1c deficiency affects drug resistance of keratinocyte MTs. **A)** Nocodazole-treated primary keratinocytes (wt, P1c^{-/-}, and P0) were immunolabeled using antibodies to α -tubulin. Intact MTs remaining after nocodazole treatment were traced (MT tracing). Note the abundant presence of intact MTs in nocodazole-treated P1c^{-/-} and P0 cells (MT tracing, lower row) in contrast to wt keratinocytes. Scale bar, 20 μ m. **B)** Statistical evaluation of data shown in **A** by one-way ANOVA-test and post-hoc Tukey correction compared to wt values (n=5; ~20 cells/experiment) *P<0.05; **P<0.01; ***P<0.001. Error bars, \pm 95% CI.

more, rather than less stable compared to those in wt cells (Figure 14), and a similar phenomenon was observed in P0 keratinocytes (Figure 14).

As stable populations of MTs are usually enriched in post-translationally acetylated α -tubulin (Piperno *et al*, 1987; Bulinski *et al*, 1988), I investigated the distribution and quantified the levels of acetylated tubulin present in MTs of primary P1c^{-/-} keratinocytes and compared them to those of wt and P0 cells. Subjecting cells to double immunofluorescence microscopy, using anti-tubulin antibodies not discriminating between the modified (acetylated) and unmodified forms of the protein and antibodies that were specific for the acetylated version, I found that in wt keratinocytes only the central part of the cells was stained for acetylated tubulin, whereas in both mutant cell types (P1c^{-/-} and P0) acetylated MTs were present at the cell center as well as at the periphery. A quantification of acetylated tubulin-positive areas (in

pixels) versus unmodified (total) tubulin-positive areas (for details see Material and methods) showed the acetylated form to be ~3-fold increased in plectin-deficient ($P1c^{-/-}$ and P0) keratinocytes compared to wt cells (Figure 15A). Increased acetylation of MTs in plectin-deficient keratinocytes was confirmed by immunoblotting analysis of tubulin present in extracts from proliferating cells (Figure 15B). Overall, these data were fully consistent with the observed higher nocodazole-resistance of MTs from mutant cells (see Figure 14).

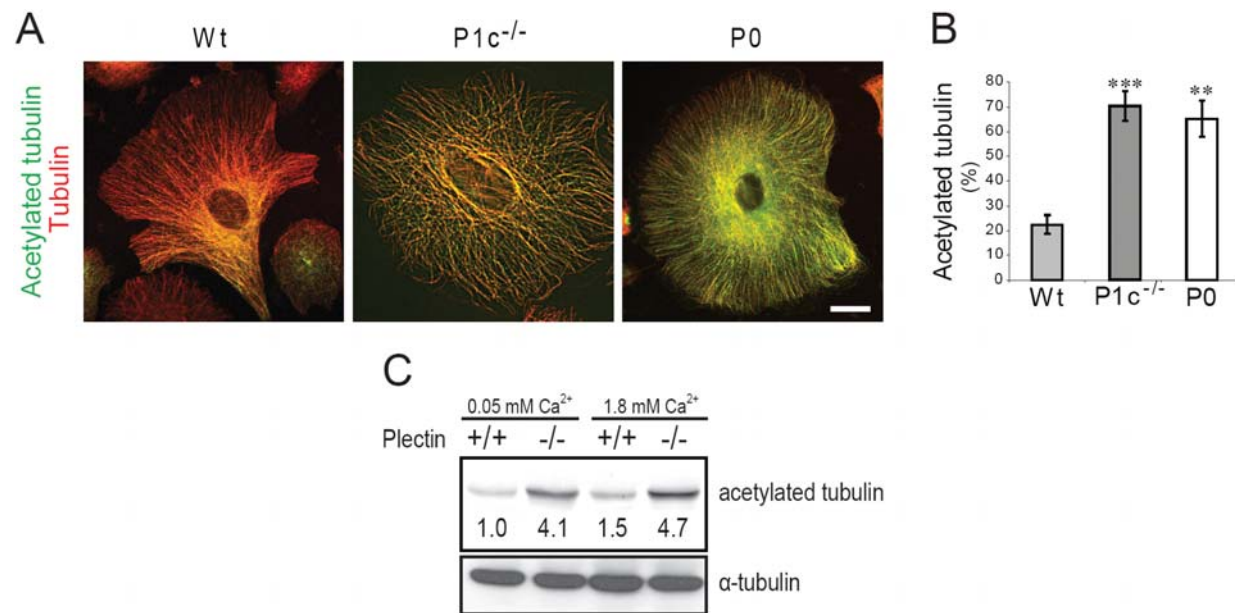


Figure 15. P1c deficiency affects acetylation of keratinocyte MTs. **A)** Indicated cells types were analyzed by immunofluorescence microscopy using rat monoclonal anti-tubulin (red) and mouse monoclonal anti-acetylated tubulin (green) antibodies. Note more prominent signal to acetylated tubulin antibodies in $P1c^{-/-}$ and P0 keratinocytes compared to wt cells. Scale bar, 20 μ m. **B)** Statistical evaluations were done by a one-way ANOVA-test and post-hoc Tukey correction compared to wt values ($n=5$; ~20 cells/experiment). * $P<0.05$; ** $P<0.01$; *** $P<0.001$. Error bars, \pm 95% CI. **C)** Quantitation (immunoblotting) of acetylated tubulin present in cell lysates from immortalized wt and P0 keratinocytes prior to (0.05 mM Ca^{2+}) and after exposure (3h) to 1.8 mM Ca^{2+} . Numbers, quantified relative levels of acetylated tubulin.

3.1.2 Reversal of MT stabilization in $P1c^{-/-}$ keratinocytes requires full-length P1c

To assess whether MT stabilization in mutant cells was directly linked to P1c deficiency, we performed rescue experiments where primary $P1c^{-/-}$ keratinocytes were transiently transfected

with cDNA expression plasmids encoding EGFP fusion proteins with either full-length P1c-EGFP (P1c-EGFP), or one of two N-terminal fragments of P1c; a shorter one (P1c-8-EGFP) comprising the N-terminal ABD preceded by the isoform-specific exon 1c-encoded sequence, and a similar longer one (P1c-30-EGFP) extending to plectin's central α helical coiled-coil rod domain. Upon forced expression, P1c-EGFP was found accumulated at filamentous structures around the nucleus but was visualized also in a dotted pattern throughout the cytoplasm (Figure 16 A, upper panels). In contrast, P1c-8-EGFP colocalized with stress fibers (Figure 16A, middle panels) as has previously been described (Rezniczek *et al*, 2003). P1c-30-EGFP

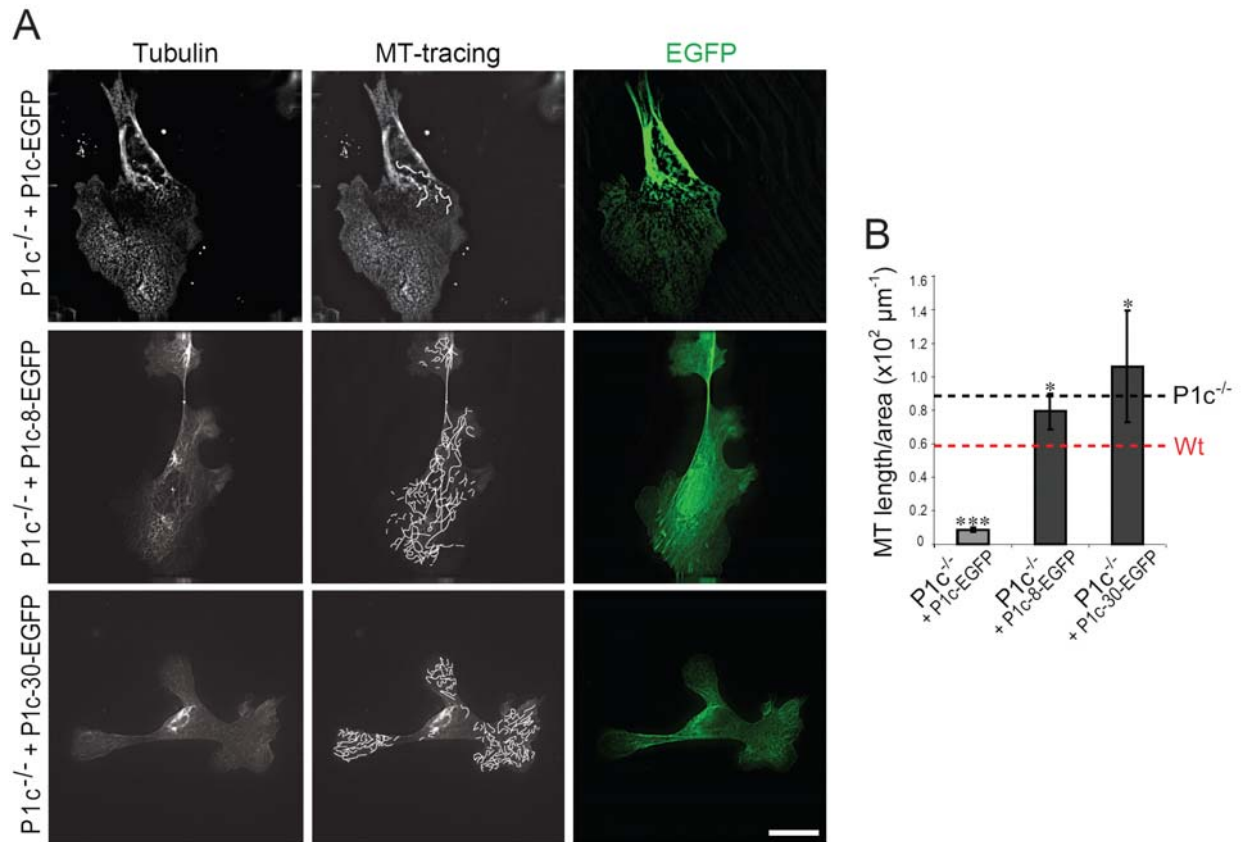


Figure 16. P1c variants lacking the IF-binding domain fail to rescue nocodazole sensitivity in P1c-deficient keratinocytes. **A)** Nocodazole-treated primary P1c^{-/-} keratinocytes transfected with full-length P1c-EGFP (upper row), P1c8-EGFP (middle row), and P1c-30-EGFP (lower row) were immunolabeled using antibodies to α -tubulin (tubulin). Drug-resistant MTs remaining in cells were traced (MT tracing). Scale bar, 15 μm . **B)** Bar graph shows quantification of MT length normalized to total cell area; red and black broken lines indicate corresponding values measured for wt and P1c^{-/-} cells, respectively (see Fig. 14) (n=3; 6 cells/experiment). *P<0.05; **P<0.01; ***P<0.001. Error bars, \pm 95% CI.

was found associated with filamentous structures throughout the cytoplasm (Figure 16A, lower panels). When MTs in transfected cells were exposed to nocodazole to assess their resistance towards drug-induced disassembly, we found that full-length P1c expression not only led to a reversal of the phenotype but even to an overshooting effect (Figure 16B, bar graph), i.e. destabilization of MTs to levels below that of wt cells, probably due to overexpression of P1c to levels higher than normal. Contrary to full-length P1c, expression of the truncated versions P1c-8 and P1c-30 did not effect a statistically significant reduction of MT stability, as revealed by the abundant presence of MTs remaining after nocodazole treatment (Figure 16A, middle and lower panels). Similarly, when MT acetylation was measured upon transfection of cells, only full-length P1c led to a reduction of acetylated MT signals, corresponding to a partial restoration of the phenotype (Figure 17A).

These data strongly suggested that P1c indeed was destabilizing rather than stabilizing MTs, contrary to what had been observed with other cytolinker protein family members, such as ACF7/MACF and BPAG1 (Kodama et al., 2003; Yang et al., 1999). Moreover, the results obtained with truncated forms of P1c suggested that the full-length protein, or at least a version of it containing the IF-binding site, was required in order to reset MT stability to the less stable state of wt cells.

3.1.3 P1c deficiency affects MT dynamics

To explore whether the increased stability of MTs observed in plectin-deficient cells was reflected in their dynamic behavior, we transfected keratinocytes with EGFP-tagged tubulin (Krylyshkina et al., 2002), enabling the visualization of rapidly shortening (catastrophe) and regrowing (rescue) MTs at the cell margins. Because of limited transfection rates obtained with primary keratinocytes, for these experiments immortalized wt and P0 keratinocytes were used. In addition to measuring catastrophe

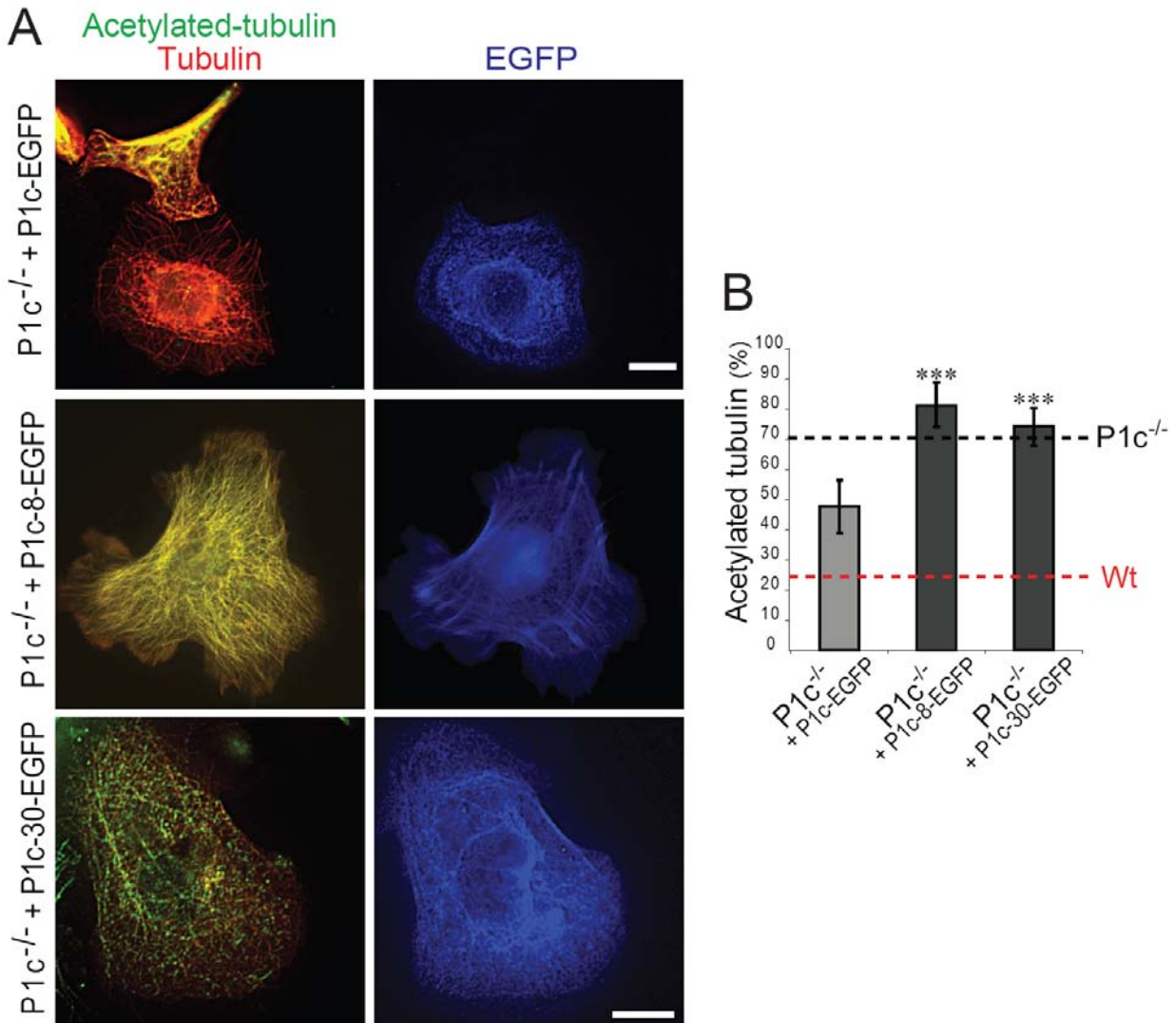


Figure 17. P1c variants lacking the IF-binding domain fail to reverse increased MT acetylation in P1c-deficient keratinocytes. **A)** The proportion of acetylated tubulin present in primary P1c^{-/-} keratinocytes expressing full-length or truncated versions of P1c was determined by immunofluorescence microscopy. **B)** Channels: red, tubulin; green, acetylated tubulin; blue, EGFP. Bar graph represents statistical evaluations as in Figure 16 B. Scale bars, 15 μ m (upper row); 10 μ m, middle and lower rows.

and rescue frequencies of MTs, we quantified the proportions of MTs that were growing perpendicular towards the membrane versus those bending or sliding along the membrane (compare to Kodama et al., 2003). The results revealed a nearly identical rescue frequency in wt and P0 cells, but a ~2.5 fold decrease of catastrophe frequency in P0 compared to wt cells

(Figure 18 A and B); this was consistent with the higher stability of MTs towards nocodazole, as observed in mutant cells (see Figure 14). Interestingly, while in wt cells most of the MTs were growing perpendicularly towards the membrane and upon reaching it underwent rapid disassembly (catastrophe) (Figure 18A), P0 cells showed a higher percentage of MTs that upon reaching the membrane were bending or sliding along it instead of disassembling (Figure 18C).

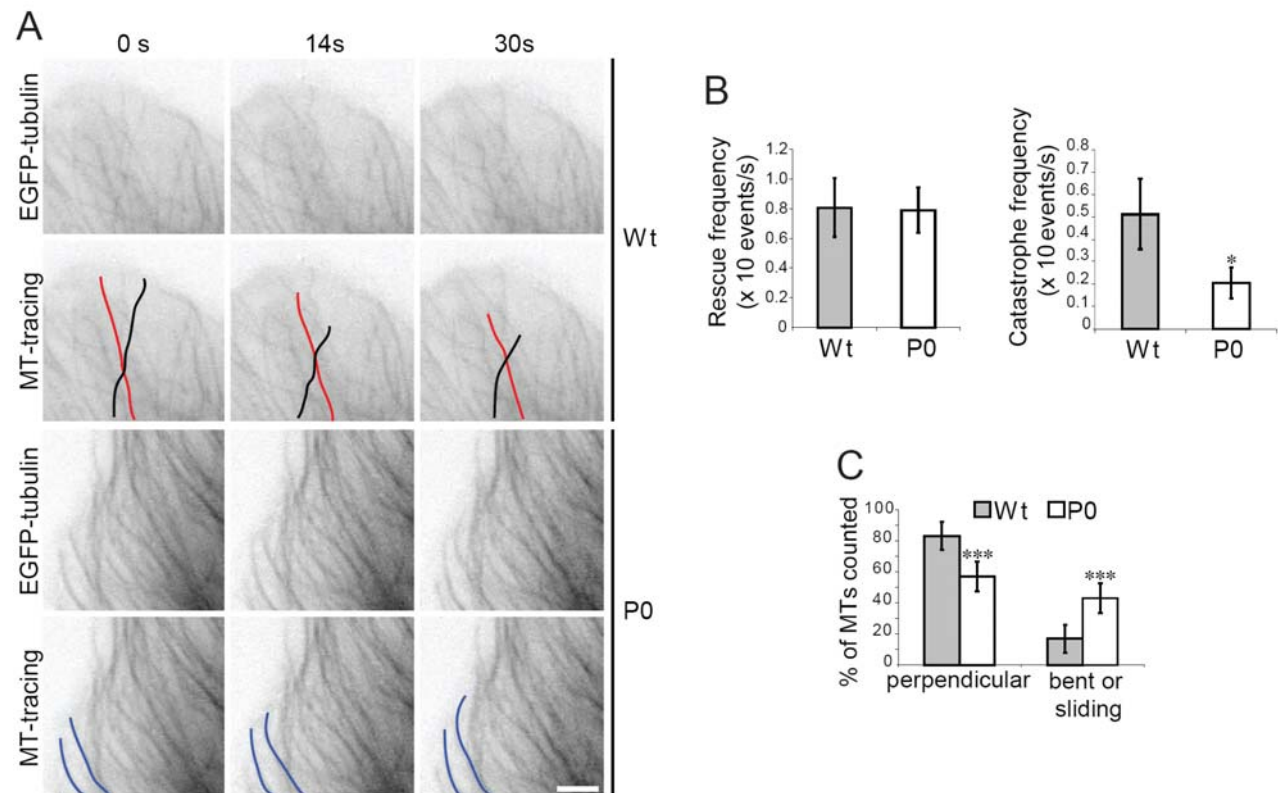


Figure 18. P1c affects dynamic properties of MTs. **A)** Images taken from a time-lapse recording of immortalized wt and P0 keratinocytes transfected with EGFP-tubulin and outlining (MT-tracing) of representative MTs. MTs outlined in red and black denote two examples of shrinking MTs in a wt cell, while lines in blue represent MTs in a P0 cell that failed to undergo catastrophe after reaching the membrane. Scale bar, 5 μ m. **B)** Bar graphs showing analyses of rescue and catastrophe frequencies (n=3; >10 cells/experiment). *P<0.05. Error bars, \pm 95% CI. **C)** Graph represents proportions (%) of MTs in wt versus P0 cells that were growing perpendicularly towards the plasma membrane (without bending), or bending and/or sliding along the membrane (n=3; 10 cells/experiment). ***P<0.001. Error bars, \pm 95% CI.

To investigate the growth parameters of MTs in more detail, we performed time-lapse microscopy of MTs labeled with GFP-tagged +TIP protein EB1 (Stepanova *et al*, 2003). In

accordance with the lower MT catastrophe frequency of P0 cells (Figure 18B), the number of EB1 comets quantified in GFP-EB1-transfected P0 keratinocytes was ~2.7 times higher than in wt cells (Figure 19).

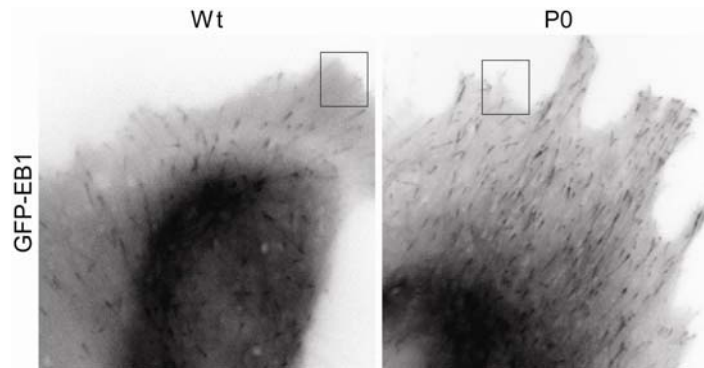


Figure 19. Time-lapse images of GFP-EB1 comets in wt and P0 keratinocytes. Note higher numbers of GFP-EB1 comets per cell area in P0 keratinocytes. Squares indicate the frames selected for Figure 20.

Moreover, P0 MTs failed to undergo catastrophe after reaching the cell margins and continued to grow and bend at the periphery, contrary to wt MTs which paused upon reaching the cell membrane before disappearing (Fig. 20). Furthermore, by tracing single EB1 comets, MT tips were found to grow faster in P0 compared to wt cells (Fig. 21).

3.1.4 Glucose uptake is increased in P1c-deficient keratinocytes

To assess the physiological significance of plectin-modulated MT regulation I measured glucose uptake of mutant (P1c^{-/-} and P0) and wt keratinocytes. First, because glucose transport involving glucose transporter recycling is a MT-dependent process (Fletcher *et al*, 2000; Zaid *et al*, 2008), and second, because there is evidence for plectin's implication in wound healing (Abrahamsberg *et al*, 2005). Compromised wound healing and reduced skin proliferation are some of the severe complications associated with impaired glucose utilization in hyperglycemia and diabetes. When keratinocytes were incubated with 2-NBDG, a

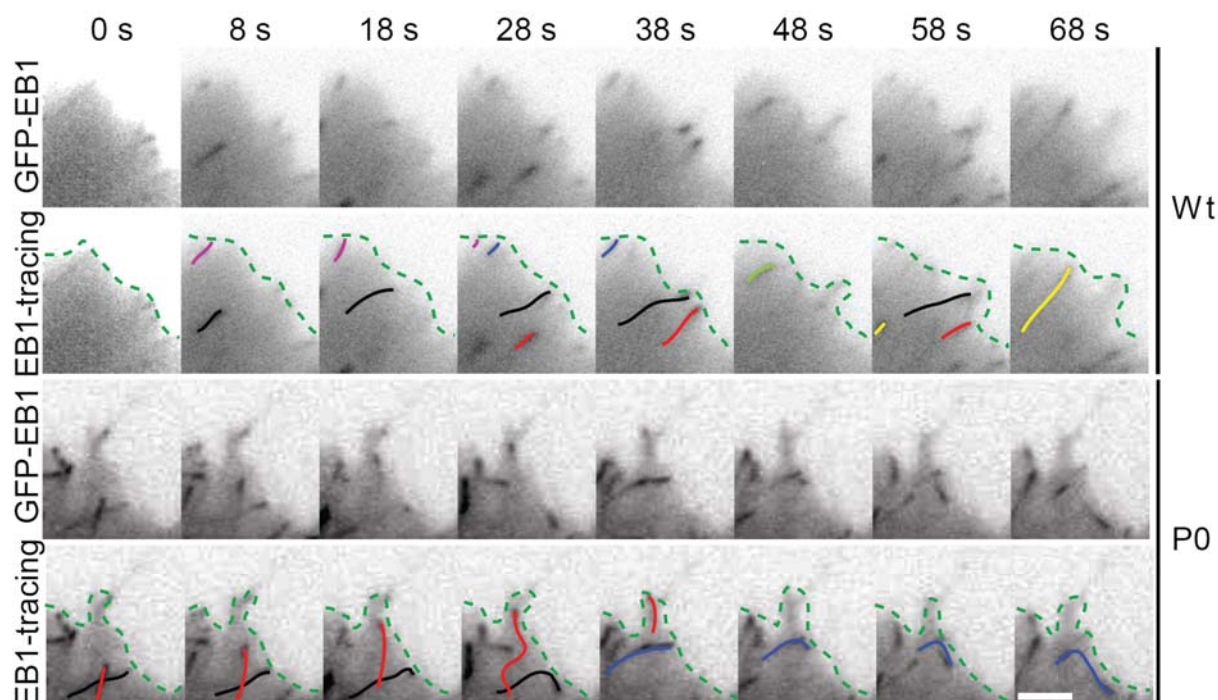


Figure 20. Sequence of single frame images taken from a time-lapse recording of GFP-EB1-expressing wt and P0 keratinocytes. Coloured lines mark trajectories of different EB1 comets (EB1-tracing). Green broken line marks cell margins. Coloured EB1 traces in wt images (upper rows) represent individual MTs that grow towards the periphery and disappear after reaching the margin; outlines trajectories in P0 cells mark MTs that continue to grow upon reaching the membrane and either meander (red line) or bend and grow parallel to the membrane (blue and black lines). Scale bar, 5 μ m.

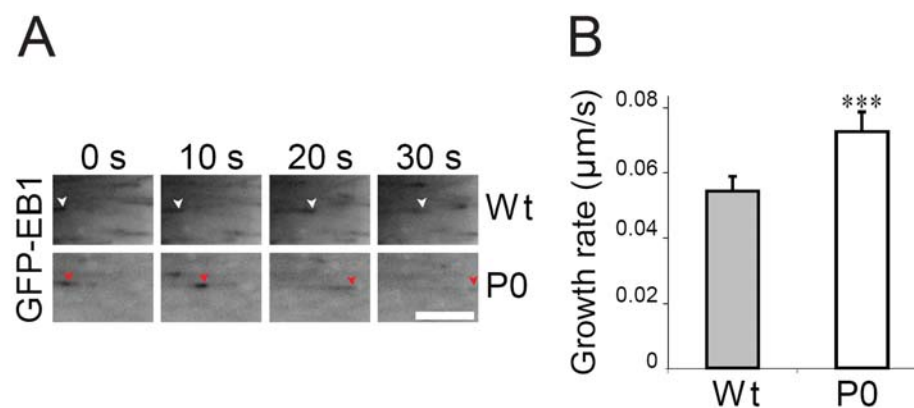


Figure 21 Time-lapse images of representative single EB1 comets in wt and P0 cells. **A)** Note faster growth of EB1 comets (corresponding to growing tips of MTs) in P0 cell (red arrowheads) compared to its wt counterpart (white arrowheads) during the same time period. **B)** Graph shows analysis of MT growth rates ($n=3$; ~ 20 cells/experiment). *** $P<0.001$. Error bars, \pm 95% CI. Scale bar, ~ 3 μ m.

fluorescent derivative of D-glucose (Yamada *et al*, 2000), and fluorescence intensities measured by confocal microscopy, a significantly higher uptake of 2-NBDG by P1c^{-/-} (~2.2-fold) and P0 (~1.5-fold), compared to wt cells was observed (Figure 22). Control experiments performed in the presence of the MT assembly blockers nocodazole (Figure 22) revealed a dramatic reduction in fluorescence intensity, confirming that 2-NBDG

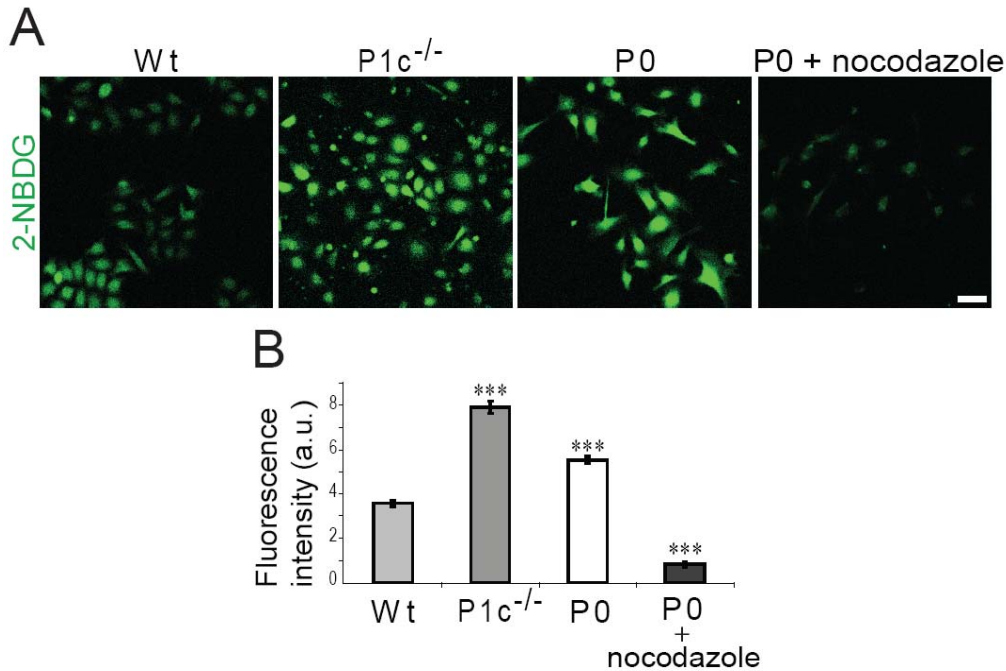


Figure 22. Alterations of glucose uptake in plectin-deficient keratinocytes. **A)** Primary wt, P1c^{-/-}, P0, and nocodazole-treated P0 keratinocytes were incubated with 2-NBDG and fluorescence intensity of cells was measured. Pictures obtained by immunofluorescence microscopy of 2-NBDG-treated keratinocytes show higher fluorescence intensity in P1c^{-/-} and P0 keratinocytes than wt or nocodazole-treated P0 keratinocytes. Scale bar, 1 mm. **B)** Data were evaluated by a one-way ANOVA-test and post-hoc Tukey correction compared to wt values (n=3; 200 cells/experiment) ***P<0.001. Error bars, ± 95% CI.

uptake was MT-dependent. Thus, a more efficient (MT-dependent) vesicular delivery of glucose transporters could readily explain the increase in glucose uptake shown by P1c^{-/-} and P0 keratinocytes. Indeed, when cells were immunolabeled for GLUT1 and signal intensities quantitated (for details see Material and methods), a ~4.5 times higher level of glucose transporters was measured for P0 compared to wt keratinocytes (Figure 23). Glucose uptake

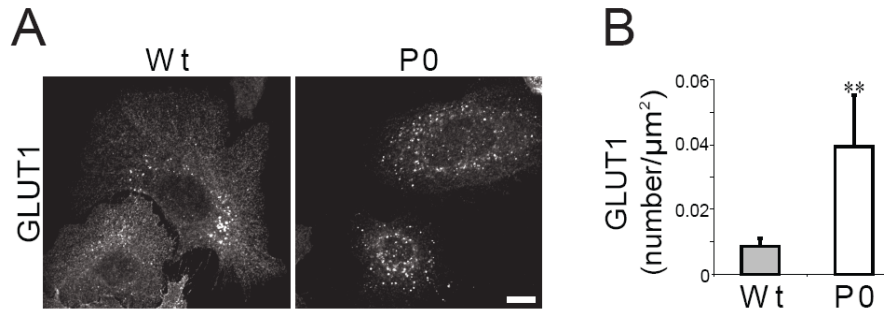


Figure 23. GLUT1 expression on keratinocytes. **A)** Keratinocytes were immunolabeled using antibodies to GLUT1. Note that GLUT1 staining remains in the perinuclear region in wt cells while in P0 cells the staining is spread over the cell. Scale bar, 10 μm . **B)** GLUT1 channel counts (normalized to total cell area) were subjected to a Student's t-test. ($n=3$; ~ 10 cells/experiment) $**P<0.01$. Error bars, \pm 95% CI.

might be additionally favored by the keratin network architecture of plectin-deficient keratinocytes, where keratin filaments typically extend all the way to the cell periphery instead of leaving a peripheral ring-shaped, filament-free zone characteristic of wt cells (Osmanagic-Myers, *et al* 2006). As recently suggested, keratins may participate in the regulation of cellular glucose uptake by properly localizing the glucose transporters GLUT1 and GLUT3, thereby increasing their density at the apical membrane (Vijayaraj *et al*, 2009).

3.1.5 Lack of P1c leads to aberrant mitotic spindles and diminished growth rate

As MTs are key players in cell division, I investigated whether their stabilization in P1c^{-/-} keratinocytes affects the division process of these cells. Interestingly, the immunostaining of primary P1c^{-/-} keratinocyte cultures using antibodies to α -tubulin, revealed a significant number of aberrant, multipolar as well as asymmetric, mitotic spindles (Figure 24A). A comparative quantitative analysis of aberrant mitotic spindles observed in primary P1c^{-/-} and wt keratinocytes, showed an unexpectedly high fraction (40%) of P1c^{-/-} mitotic cells to display

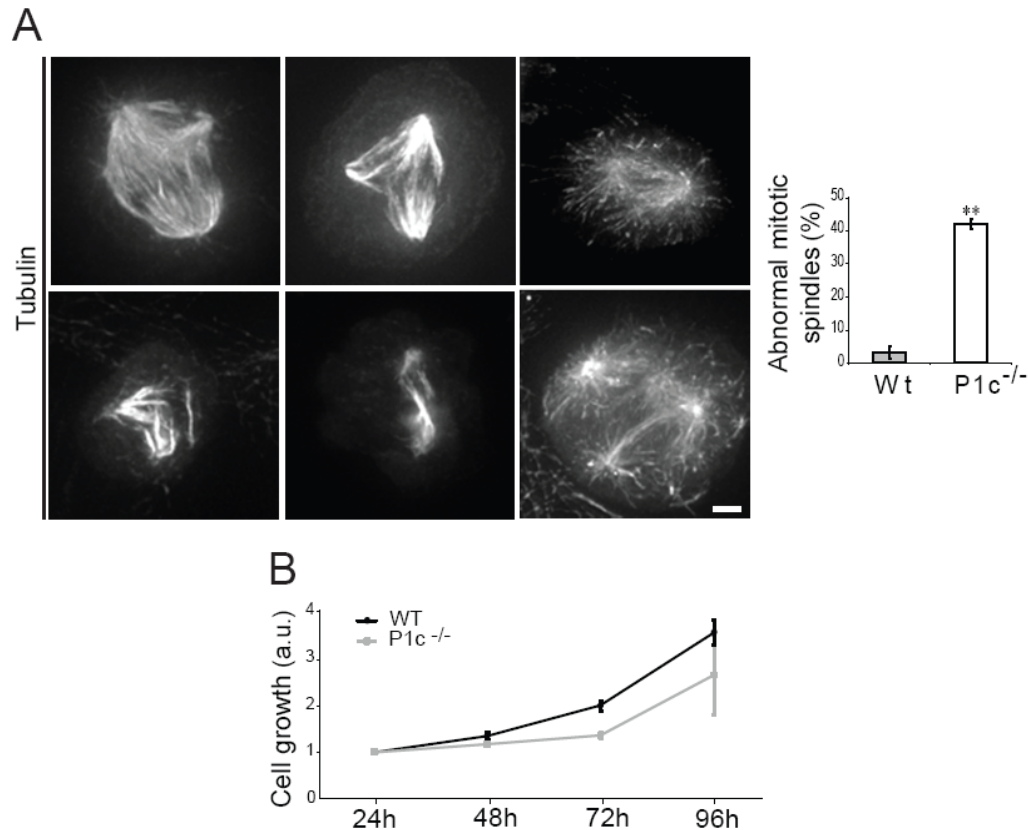


Figure 24. Alterations in mitotic spindle formation and cellular growth rate in plectin 1c-deficient keratinocytes. **A)** Spindle apparatuses of dividing cells were visualized by immunolabeling using antibodies to α -tubulin. Images display representative pictures of multipolar spindles (upper row) and asymmetric spindles (lower row) found in dividing P1c^{-/-} keratinocytes. Scale bar, 10 μ m. Abnormalities were statistically evaluated by a Student's t-test **P<0.01. Error bars, \pm 95% CI. (n=4; ~150 cells/experiment). **B)** Line graph represents growth rate of primary keratinocytes measured during 96 h (n=3). Error bars, \pm SEM.

multipolar or asymmetric spindles, compared to only ~3% of mitotic wt cells (Figure 24A, bar graph). The impairment of normal mitotic spindle formation correlated with a substantial delay in the growth rate of primary P1c-deficient compared to wt keratinocytes over the first 96 h after seeding of the cells (Figure 24B). Alterations in growth rate have already been observed in P0 fibroblasts (Spurny *et al*, 2008). Furthermore, plectin has been identified as a component of the mitotic spindle in several proteomic studies focused on the characterization of spindle-associated proteins (Mack & Compton, 2001; Sauer *et al*, 2005; Gache *et al*, 2010) and on the spindle phosphoproteome (Dephoure *et al*, 2008; Malik *et al*, 2009).

3.1.6 P1c-deficiency affects shape and directional migration of cells

It has previously been shown that primary as well as immortalized P0 keratinocytes migrate with higher velocities than their wt counterparts (Osmanagic-Myers, *et al* 2006), and it is known that polarized migration of mammalian cells requires stabilized MTs at the cell cortex (Watanabe *et al*, 2005; Kaverina & Straube, 2011). These observations prompted me to investigate a possible link between P1c-modulated MT dynamics and cellular features determining the shape and polarity of cells. Seeded at low densities to enable single cell monitoring, primary P1c^{-/-} keratinocytes showed a reduction in size (cell area) but an increase in their perimeter compared to wt cells (Figure 25, a-b); P0 cells, too, showed a reduction in size, but hardly a perimeter change (Figure 25, a-b). This suggested that primary P1c^{-/-} keratinocytes were displaying more protrusions than wt and P0 cells. Accordingly, a statistical analysis of calculated shape factors ($SF = 4\pi \times \text{area}/\text{perimeter}^2$) and aspect ratios ($AR = \text{shortest diameter}/\text{largest diameter}$) for each cell type revealed wt and P0 keratinocytes to be similar in shape, but P1c^{-/-} cells to have more protrusions and to be much more elongated (Figure 25 c-d, and Figure 26).

Time-lapse videos of single cells showed that primary P1c^{-/-} keratinocytes migrated faster (~1 $\mu\text{m}/\text{min}$) compared to wt cells (~0.8 $\mu\text{m}/\text{min}$), albeit still slower than P0 cells (~1.2 $\mu\text{m}/\text{min}$) (Figure 25, e). One explanation why P1c^{-/-} cells did not reach the velocity of P0 cells could have been that they were still expressing isoform P1a and thus were able to form intact HDs that were pinning them down, contrary to P0 cells that were lacking both isoforms. Interestingly, P1c^{-/-} keratinocytes showed also a drastic loss of directional migration potential compared to wt and P0 cells (Figure 26, migration tracks, and Figure 25, f). Promotion of migration through stabilized MTs and simultaneous retention of cells via P1a anchorage, leading to the extreme elongation of cells and loss of directional migration potential, could again be the reason why P1c-deficient, but not P0 cells showed this phenotype.

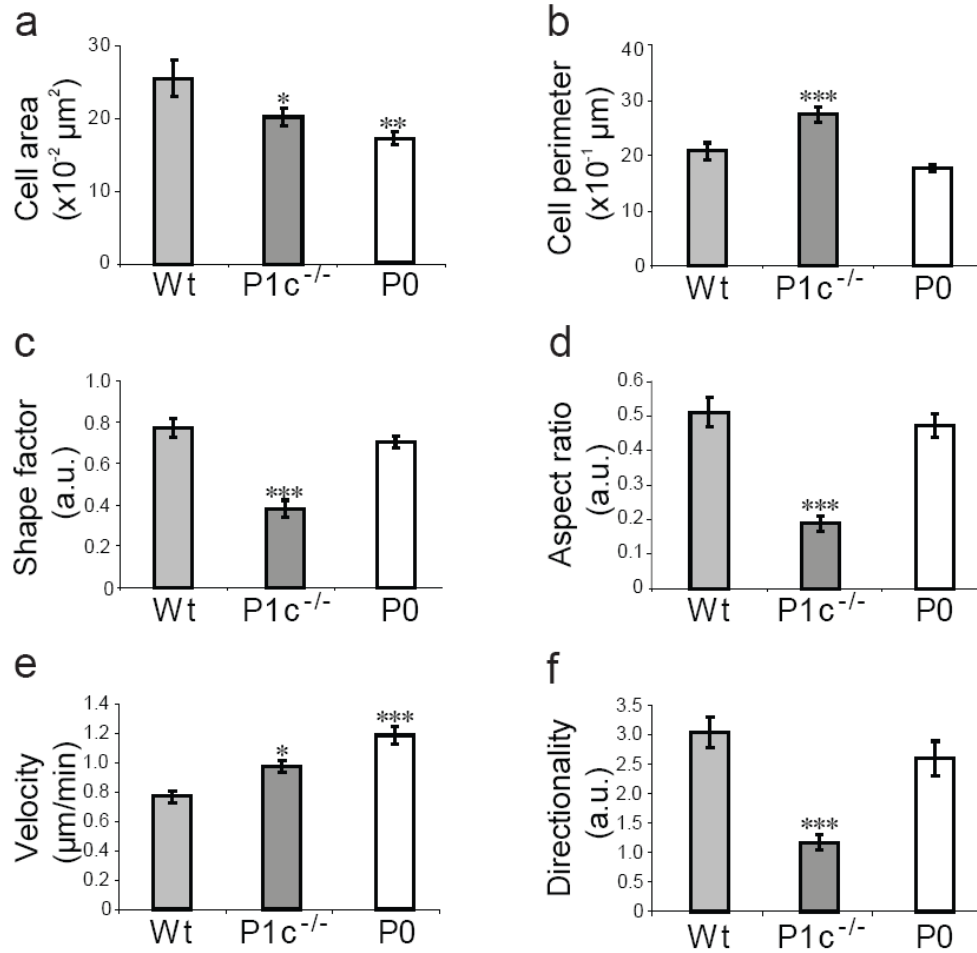


Figure 25. Statistical evaluation of keratinocyte shape and migration. Bar graphs show statistical analyses of cell area (a), cell perimeter (b), shape factor (c), aspect ratio (d), velocity (e), and directionality (f) of migrating primary wt, P1c^{-/-}, and P0 keratinocytes (n=3; 20 cells/experiment). *P<0.05; **P<0.005; ***P<0.001.

3.1.7 Lack of P1c causes alterations in FA dynamics

To explore possible mechanisms underlying the higher migration rate of plectin-deficient keratinocytes, I examined whether the greater stability of MTs in the mutant cells could compromise the stability of FAs. MT targeting events to FAs have been shown to induce their dissociation by delivering FA-relaxing factors and promoting FA turnover (for review see Kaverina et al., 2002). Accordingly, one may expect that the increased number of stable MTs

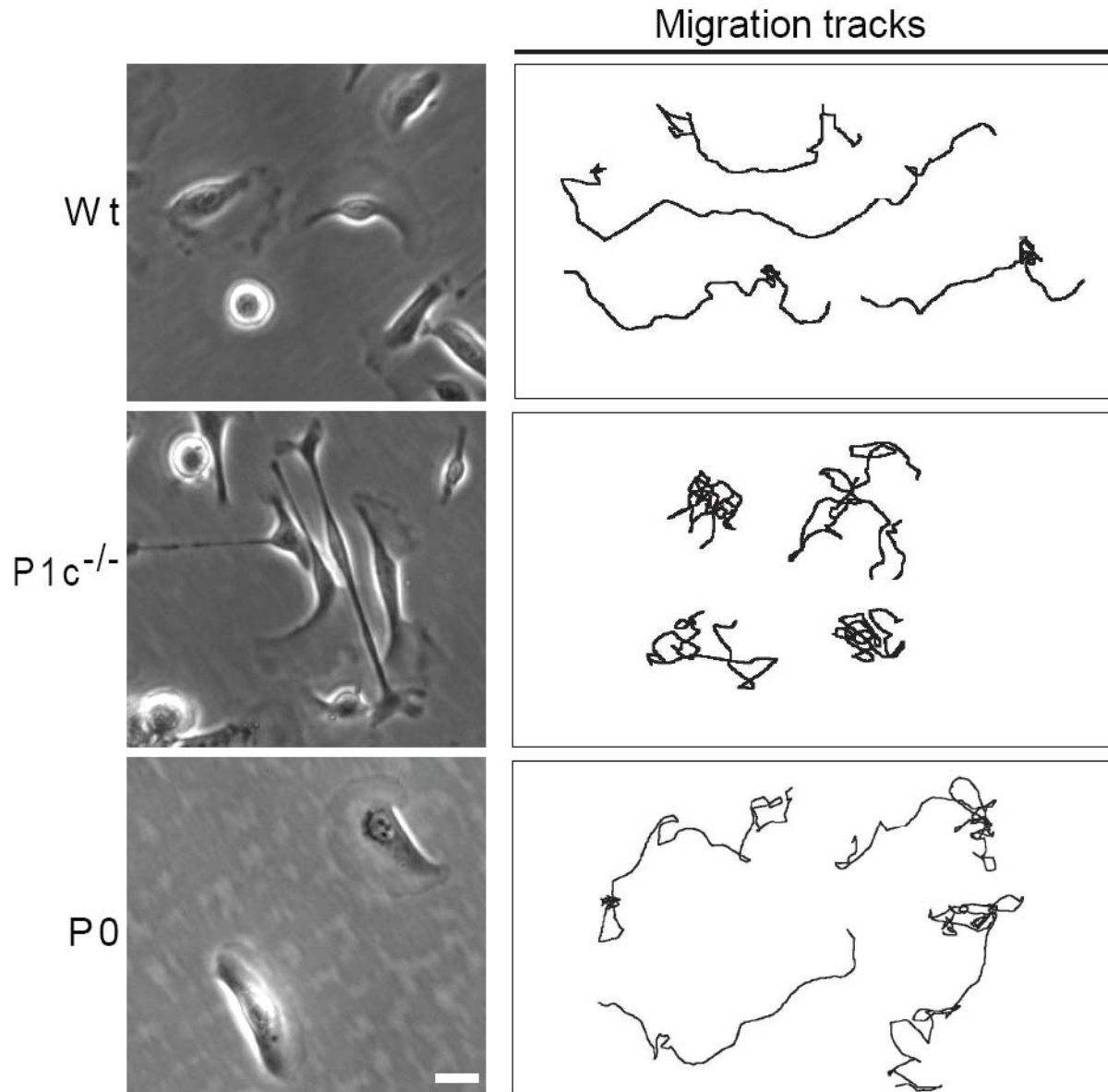


Figure 26. Loss of P1c affects polarized migration of keratinocytes. Phase contrast images of representative primary wt, P1c^{-/-} and P0 keratinocytes (left columns) and migration tracks of single keratinocytes monitored by video microscopy (migration tracks) are shown. Elongated shape of P1c^{-/-} keratinocytes (left column) and loss of polarization (migration tracks) can be observed. Scale bar, 100 μ m.

encountered in peripheral cytoplasmic regions of mutant keratinocytes leads to a higher number of MTs converging at peripheral FAs, with consequences for their turnover and size. In addressing these issues I focused on P0 and wt cells as they showed the largest divergence in

migration velocities. In order to analyze FA turnover, p53^{-/-} wt and P0 keratinocytes were transfected with EGFP-zyxin (Rottner et al., 1999) and subjected to time-lapse microscopy. In comparison to EGFP-zyxin-transfected wt keratinocytes, P0 cells display smaller and more numerous FAs (Figure 27A). After monitoring EGFP-zyxin labeled FAs, the ones of P0 cells showed a shorter life-time and thus increased turnover compared to wt cells (Figure 27A, bar graph). To test whether this difference was related to MT targeting, I analyzed in both cell types the proportions of MT-targeted versus not-targeted FAs by double staining for tubulin and vinculin (as FA marker) (Figure 27B). In contrast to wt cells, FA of P0 cells show more frequently colocalization of tubulin and vinculin (Figure 27B, arrowheads) than wt cells. I found that the cell type showing the higher proportion of MT-targeted FAs (Figure 27B, bar graph) was also the one displaying the more stable MT population (P0). To corroborate these data, I compared the size of vinculin-labeled FAs in wt and P0 keratinocytes and found that P0 FAs in general were smaller than wt (Figure 27C, bar graph), consistent with them being more frequently targeted by MTs and their higher turnover rates.

3.1.8 MTs in P1c-deficient keratinocytes show increased decoration by MAPs

To establish whether the data obtained *in vitro* showing MT destabilization using MAPs typical for neural cells (see Introduction) could be extrapolated to the situation prevailing in keratinocytes, I analyzed whether proteins of the MAP2/tau protein family were expressed in mouse epithelial cells; MAP2 expression in HaCat cells, an immortalized human keratinocyte cell line, had previously been reported by Liu *et al* (2007). As shown in Figure 25, when lysates of primary and immortalized mouse keratinocytes and of mouse epidermis were subjected to immunoblotting analysis using antibodies to MAP2, a ~70 kDa protein corresponding in size to MAP2c was detected in all samples tested (MAP2c is an isoform of MAP2 endowed with a potent MT assembly-promoting activity; Gamblin *et al*, 1996). In addition, proteins of ~95 kDa

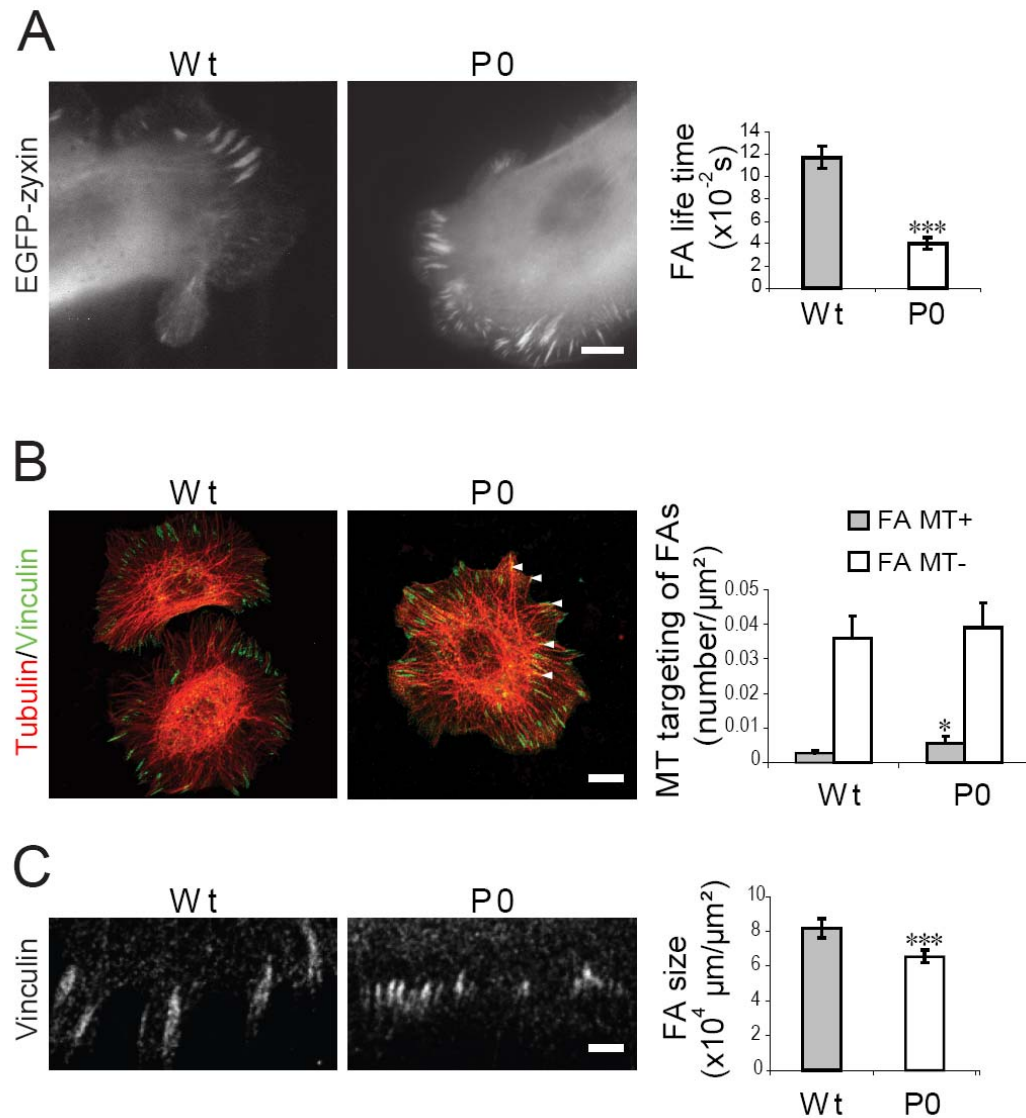


Figure 27. Loss of P1c alters FA dynamics and stability. **A)** Images of EGFP-zyxin-expressing immortalized wt and P0 keratinocytes (scale bar, 10 μm) and bar graph showing FA turnover rates ($n=3$, 10 cells/ experiment). *** $P<0.001$. Error bars, \pm SEM. **B)** Cells like in (A) double immunolabeled using antibodies to vinculin (green) and α -tubulin (red) to distinguish between MT-positive (arrowheads) and MT-negative FAs (scale bar, 15 μm). Bar graph, statistical analysis of MT-targeting of FAs in wt and P0 keratinocytes evaluated by a Chi-square test ($n=3$, 10 cells/experiment). * $P<0.05$. **C)** Detail images of vinculin-positive FAs at the periphery of cells (scale bar, 3 μm). Bar graph, statistical analysis of FA size in wt and P0 keratinocytes ($n=3$, 10 cells/experiment). *** $P<0.001$. Error bars, \pm SEM.

and ~60 kDa were detected that probably corresponded to isoforms of tau that were recognized by anti-MAP2 antibodies due to the partial structural homology of tau and MAP2

(Al-Bassam *et al*, 2002). This notion was confirmed by incubating similar blots with monoclonal antibodies to tau, revealing the presence of the high-molecular weight form of tau (~95 kDa) as well as of 50–70 kDa tau isoforms (Figure 28). These results indicated that brain- and epithelia-derived cells express similar MAP species.

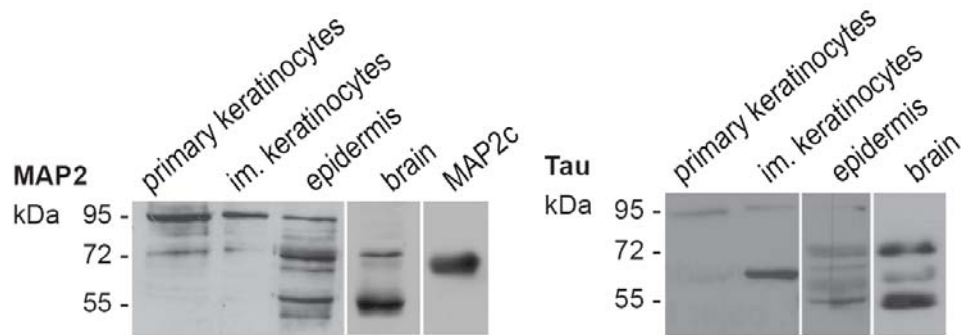


Figure 28. Tau and MAP2 are expressed in keratinocytes. Immunoblot showing the expression of MAP2 and tau in primary keratinocytes, immortalized (p53^{-/-}) keratinocytes, and epidermis, with a brain lysate and purified MAP2c protein run as positive controls (n=3).

To confirm these results on the transcript level, analysis of tau and MAP2 mRNA expression was assessed by RT-PCR analysis of total RNA isolated from primary and immortalized keratinocytes as well as from epidermal tissue. As shown in Figure 29, using primers binding

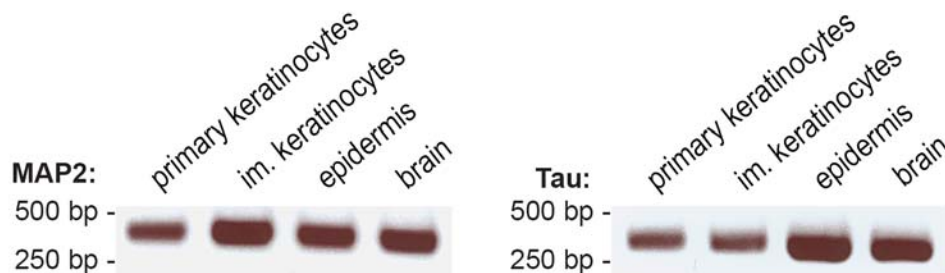


Figure 29. Keratinocytes expressed tau and MAP2 at mRNA levels. RT-PCR results using primers specified in the text can be observed. Note expression of tau and MAP2 RNA in primary keratinocytes, immortalized keratinocytes, epidermis and brain used as a positive control.

to sequences in exons 9 and 11 of the tau gene (flanking the second MT binding domain repeat-encoding exon 10; Poorkaj et al., 2001; Dehmelt and Halpain, 2005; Andreadis, 2005), a DNA fragment of the expected size (390 bp) was amplified in all cases including adult mouse brain RNA (run as positive control). The 390 bp fragment corresponded to transcripts of the 4 MT-binding repeats contained in exons 9, 10 and 11 (Duff *et al*, 2000; Takuma *et al*, 2003). DNA sequencing of the PCR products confirmed that they had been derived from tau transcripts. To detect MAP2 transcripts, primers binding to sequences in exons 5 and 6, which are common to all MAP2 splice variants (Dehmelt & Halpain, 2005) were used. Single bands of the expected size (344 bp) were amplified from all tissues analyzed, including the positive control. Again, DNA sequencing of the PCR products confirmed their authenticity. Since among the samples analyzed at least the immortalized mouse keratinocyte cell line has been shown to be devoid of any contaminating fibroblasts or melanocytes (Osmanagic-Myers *et al*, 2006), these data clearly demonstrated that tau and MAP2 mRNAs were expressed in mouse keratinocytes. To examine whether tau and MAP2 are expressed in skin also on the protein level, sections of frozen foot pad skin from adult mice were subjected to immunofluorescence microscopy. A pronounced, predominantly cytoplasmic staining of all live keratinocyte cell layers of the epidermis was detected using specific antibodies to tau or to MAP2 (Figure 30). Similar staining patterns were observed on sections from other skin areas, e.g. ear and tail skin (data not shown). Controls without using primary antibodies were negative (Figure 30).

According to these results one could have expected higher levels of MAPs to be bound to MTs in plectin-deficient cells. To investigate this idea, primary wt, P1c^{-/-}, and P0 keratinocytes were triple-immunostained using antibodies to MAP2, α -tubulin, and P1c. While in wt keratinocytes MAP2 showed a dotted staining pattern along MTs (similar to P1c) (Figure 31, upper panels), in both of the mutant cell types MTs were found decorated with MAP2 over much longer distances (Figure 31, lower panels, arrowheads), confirming our expectation.

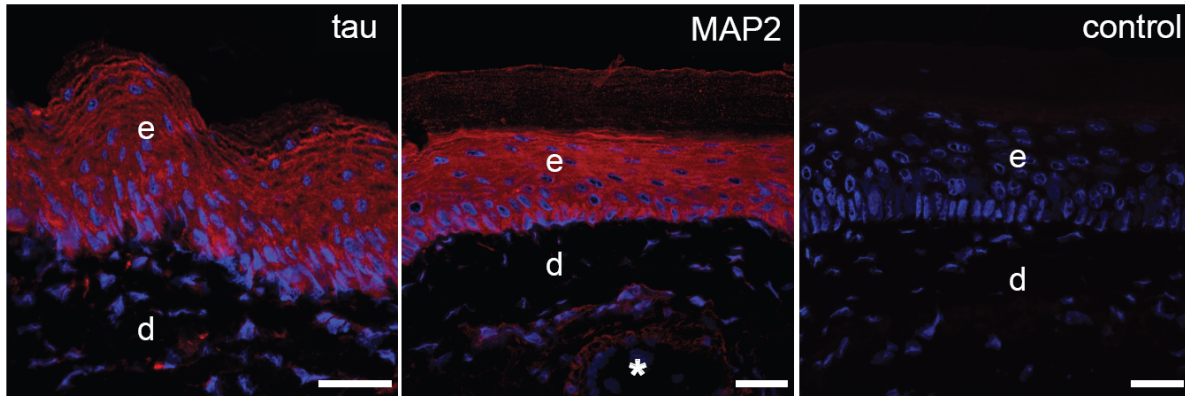


Figure 30. Skin sections are immunoreactive with anti-tau and MAP2 antibodies. Frozen foot pad skin sections from adult wt mice were immunolabeled using antibodies to tau and MAP2 (left and center panels). Sections were immunolabeled using antibodies to tau or MAP2. Nuclei were stained with DAPI. In negative controls (right panel), primary antibodies were omitted. Note relatively strong immunofluorescence signals for both antigens in epidermis (e), and weaker signals in hair follicles (asterisk), and in a few scattered cells in the dermis (d). Scale bars, 25 μ m.

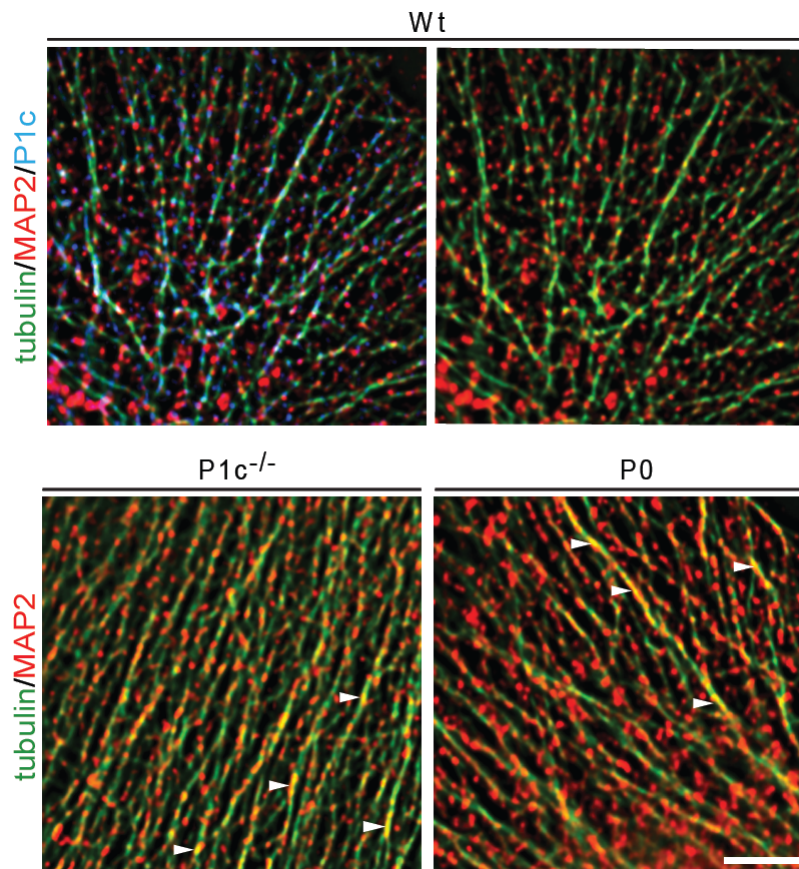


Figure 31. MAP2-MT colocalization in wt and P1c^{-/-} keratinocytes. Immunofluorescence microscopy of primary wt (upper row), P1c^{-/-}, and P0 (lower row) keratinocytes was performed using antibodies to MAP2 (red), α -tubulin (green), and P1c (blue). Note that decoration of MTs with MAP2 can be found over longer distances on P1c^{-/-} and P0 cells (arrowheads) than in wt keratinocytes. Scale bar, 2 μ m.

However, in contrast to P1c^{-/-} keratinocytes, their P0 counterparts showed MAP2 staining not only along MTs but also in association with structures seemingly unlinked to MTs. Different levels of MT-unbound MAPs in P0 and P1c^{-/-} cells might be caused by elevated basal activities of Erk1/2 MAP and Src kinases (Osmanagic-Myers et al., 2006) in P0, but not in P1c^{-/-} keratinocytes. Since MT-binding of MAPs is regulated by several kinases including Src (Lim & Halpain, 2000; Lee, 2005), increased activity of Src in P0 keratinocyte might result in higher levels of MT-unbound MAP2.

Part II - Plectin 1c in neurons

Having identified a MT-destabilizing activity of P1c and a series of physiological consequences of P1c deficiency in keratinocytes, it was of particular interest to further analyze whether P1c is involved in biological functions of other cell types. Since P1c is the major plectin isoform expressed in neural cells, and MT organization and dynamics are essential for neuronal function, I selected P1c-deficient dorsal root ganglia (DRG) neurons as a second system in which to study P1c's role in MT dynamics.

3.1.9 P1c-deficient neurons exhibit increased MT stability and altered MT dynamics

To investigate whether P1c causes changes in MT stability in neurons, DRG neurons were isolated from wt and P1c^{-/-} mice, cultivated and treated with low doses of the MT-depolymerizing drug nocodazole. Since neuronal axons and neurites are densely populated with MT bundles, individual MTs remaining after nocodazole treatment could not be traced. Instead they were traced and quantified at the growth cone of neurons where it was possible to monitor single MTs. Figure 32 A shows images of the growth cone of wt and P1c^{-/-} neurons immunostained with antibodies to tubulin after nocodazole treatment (upper row). To facilitate the visualization of nocodazole-resistant MTs, MTs were traced and their outlines together with growth cones boundaries are shown (Figure 32 A, lower row). P1c^{-/-} DRG neurons displayed ~3.5 times more intact MTs in the growth cone after drug treatment than wt cells (Figure 32 B). These results were similar to those observed in keratinocytes (see Part I).

In another approach to evaluate MT stability, the distribution of acetylated α -tubulin along neurites was investigated. P1c-deficient DRG neurons were compared to their wt counterparts by double immunofluorescence microscopy using anti-tubulin antibodies that did not discriminate between the modified (acetylated) and unmodified forms

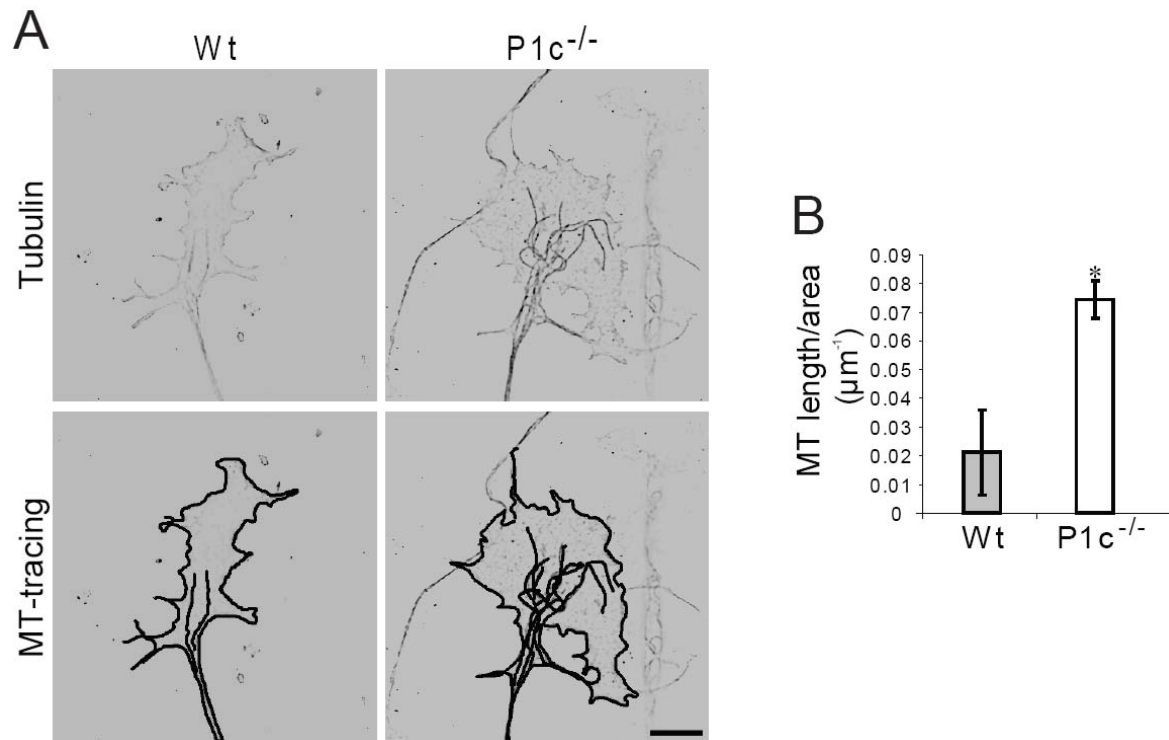


Figure 32. P1c affects drug resistance and stability of neuronal MTs **A)** Nocodazole-treated DRG neurons (wt and P1c^{-/-}) were immunolabeled using antibodies to α -tubulin. Black lines outline the periphery of the growth cone and the tracing of nocodazole-resistant MTs. Note the presence of higher number of MTs remaining after drug treatment in P1c^{-/-} growth cones (lower row, right panel). Scale bar, 4 μ m. **B)** Bar graph showing statistical evaluation of results shown in (A) applying a Student's t test (n=3). *P<0.05. Error bars, \pm 95% CI.

of the protein and antibodies that were specific for the acetylated version. The growth cones of wt DRG neurons were found to be barely immunoreactive with antibodies to acetylated tubulin, whereas in the growth cones of P1c^{-/-} DRG neurons acetylated MTs were clearly visible (Figure 33 A). A quantification of acetylated tubulin-positive areas (in pixels) versus unmodified (total) tubulin-positive areas showed the acetylated form to be ~2-fold increased in plectin-deficient DRG neurons compared to wt cells (Figure 33 B).

In order to confirm that the lack of P1c was directly responsible for the increased acetylation of MTs in P1c^{-/-} DRG neurons, isolated neurons were transiently transfected with expression plasmids encoding a P1c-mCherry fusion protein using nucleofection. Based on

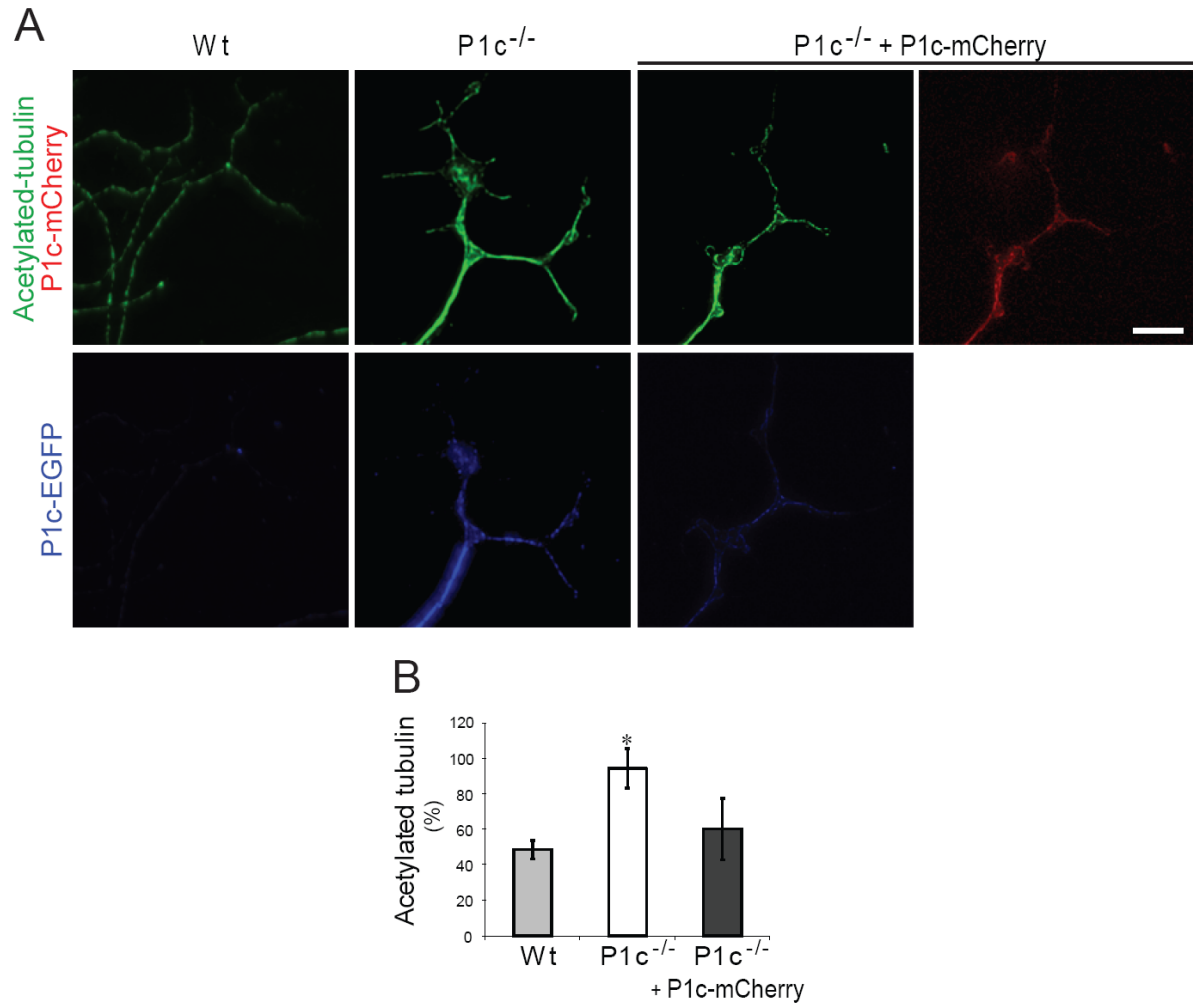


Figure 33. P1c affects MT acetylation in DRG neurons. **A)** Immunofluorescence microscopy was performed on wt, P1c^{-/-}, and P1c-mCherry-transfected P1c^{-/-} DRG neurons using rat monoclonal anti-tubulin (green) and mouse monoclonal anti-acetylated tubulin antibodies (blue). Note that only the growth cone of P1c^{-/-} DRG neurons is prominently immunoreactive with antibodies to acetylated tubulin. Scale bars, 4 μ m. **B)** Statistical evaluations (graph) of acetylated tubulin to total tubulin fluorescent signals were done by a one-way ANOVA-test and post-hoc Tukey correction compared to wt values (n=5). *P<0.05. Error bars, \pm SEM.

electroporation, this technique facilitates the transfer of cDNA constructs directly into the cell nucleus via short high-voltage pulses and optimized buffers to minimize damage to the cellular membranes (Zeitelhofer *et al*, 2007). As shown in Figure 33, the acetylated tubulin immunostaining of the P1c-mCherry-transfected P1c^{-/-} DRG neuronal growth cone is similar to the one of the wt growth cone. Measurements of acetylated tubulin-positive areas in

comparison to total tubulin-positive areas led to a statistically significant reduction of MT acetylation in P1c-mCherry-transfected P1c^{-/-} DRG neurons, approximating the levels of wt neurons (Figure 33 B). Thus, these data were fully consistent with the observed higher nocodazole resistance of MTs in mutant cells (see Figure 32) and they confirmed that the lack of P1c^{-/-} leads to increased stability of MTs.

Previous results from this laboratory and my own data, including the observed accumulation of MAPs along MTs of P1c-deficient keratinocytes (Figures 13 and 31), suggested that P1c antagonizes MAPs and thereby causes destabilization of MTs. According to this model, one may expect to find more MAPs to be bound to MTs in the absence of P1c. To investigate whether this was the case, the levels of tau bound to endogenous MTs were quantified in wt and P1c^{-/-} mouse brain lysates prepared under MT-stabilizing conditions. This so called endogenous MT-binding assay (Planel *et al*, 2008) allowed polymeric MTs and their co-assembling (bound) proteins to be sedimented by high-speed centrifugation. Immunoblotting of total lysates, supernatant and pellet fractions revealed three bands corresponding in size to the most common tau isoforms (between 50 and 60 kDa) in all fractions (Figure 34). While P1c^{-/-} and wt samples showed similar levels of tubulin in all fractions, tau levels were visibly decreased in the soluble, and increased in the insoluble (MT-bound) fraction of P1c^{-/-} (compared to wt samples), at least in the case of the ~50 kDa tau isoforms. Quantitative immunoblotting analysis more clearly revealed increased levels of MT-bound tau in P1c^{-/-} brain lysates (Figure 34 B).

In order to investigate whether the lack of P1c leads to altered MT dynamics in DRG neurons, time-lapse video microscopy of GFP-tagged EB1 was performed. This technique allows the visualization of MT tips in the growth cone as well as along the axon of the neurons (Stepanova *et al*, 2003; Su *et al*, 1995; Akhmanova & Steinmetz, 2008). The image shown in Figure 35 A represents a growth cone of a GFP-EB1-transfected DRG neuron showing three

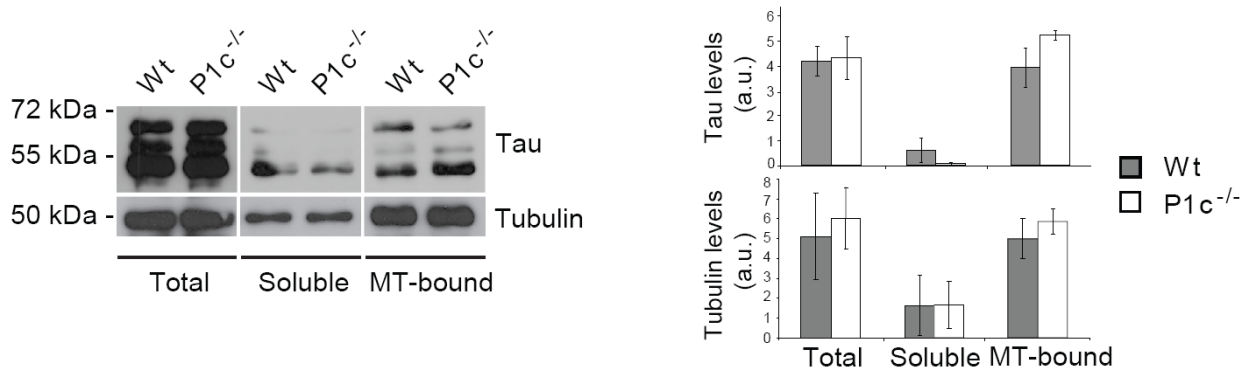


Figure 34. Tau is increased in the MT-bound fraction in P1c-deficient brain lysates. Endogenous MT-binding assay of tau was performed using wt and P1c^{-/-} brain lysates prepared under MT-stabilizing conditions. Tau and tubulin from total lysates, soluble, and the bound fractions were evaluated by immunoblotting analysis using anti-tau antibodies. Note that the ~50 kDa tau isoform is increased in the MT-bound fraction of P1c^{-/-} brain lysates, while tubulin levels are similar in both samples. Bar graph represents quantification of the immunoblotting data. Error bars, \pm SEM.

GFP-EB1 comets (black dots). Analysis of GFP-EB1 tracks of transiently transfected DRG neurons revealed faster MT growth in plectin-deficient cells (Figure 35 B), similar to what I had previously found in keratinocytes.

3.1.10 P1c-deficiency affects growth cone extension and neuritogenesis

Neuronal polarization, which is essential for neuronal development, requires active participation of actin filaments and MTs for growth cone extension. The neurite elongation process can be divided into three stages: protrusion, engorgement, and consolidation (Goldberg & Burmeister, 1986). Neuronal growth cones are rich in MTs in their central domain and in actin filaments at their periphery. Peripheral actin arcs prevent MTs from invading the peripheral region but during protrusion, actin filaments reorient towards growth direction, creating an actin-free zone that can be invaded by MTs. Vesicles and organelles transported by MTs enter in this area during the engorgement phase. In the subsequent consolidation stage, actin polymerization and protrusion stop and the MTs are bundled at the growth cone wrist, causing the elongation of the neurite shaft (Stiess & Bradke, 2011). The elongation

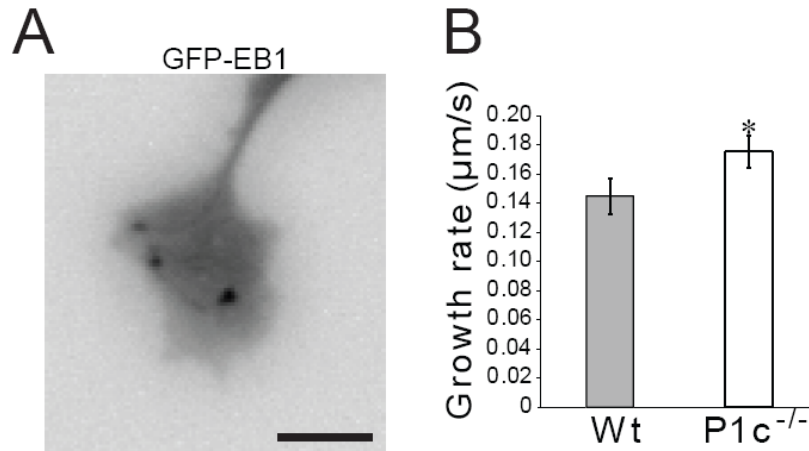


Figure 35. P1c affects MT growth rates in DRG neurons. **A)** A single frame of a time-lapse recording of GFP-EB1 visualized in the growth cone of a DRG neurons is shown. GFP-EB1 complexes are seen as black dots inside the growth cone. Scale bar, 0.8 μ m. **B)** Bar graph shows statistical analyses of MT growth rates subjected to a Wilcoxon-Mann-Whitney U-test (n=3; ~5 cells/experiment). *P<0.05. Error bars, \pm SEM.

process is positively regulated by enhanced MT stability and restrained actin arc formation (Neukirchen & Bradke, 2011). Moreover, MTs are also required for the accumulation of signaling molecules at the growth cone, including Src family kinases and Rho family GTP regulators involved in their cross-talk with actin filaments (Lowery & Vactor, 2009). Although the role of MTs during growth cone extension is still not well understood, it has been shown that dynamic MTs are indispensable for persistent growth cone advance (Tanaka *et al*, 1995).

In light of the fundamental role of MTs in neurite outgrowth, I tested whether the increased stability and growth rates of MTs in growth cones of P1c^{-/-} DRG neurons were affecting neurite extension. For this I measured growth cone extension of DRG neurons (isolated from P1c^{-/-} and wt mice) by phase-contrast and time-lapse video microscopy at 10 min intervals during at least 5 h. The comparison of neurite lengths reached by DRG neurons within the same time periods revealed a ~25% faster neurite extension rate in P1c^{-/-} compared to wt cells (Figure 36). Interestingly, also the morphology of P1c-deficient growth

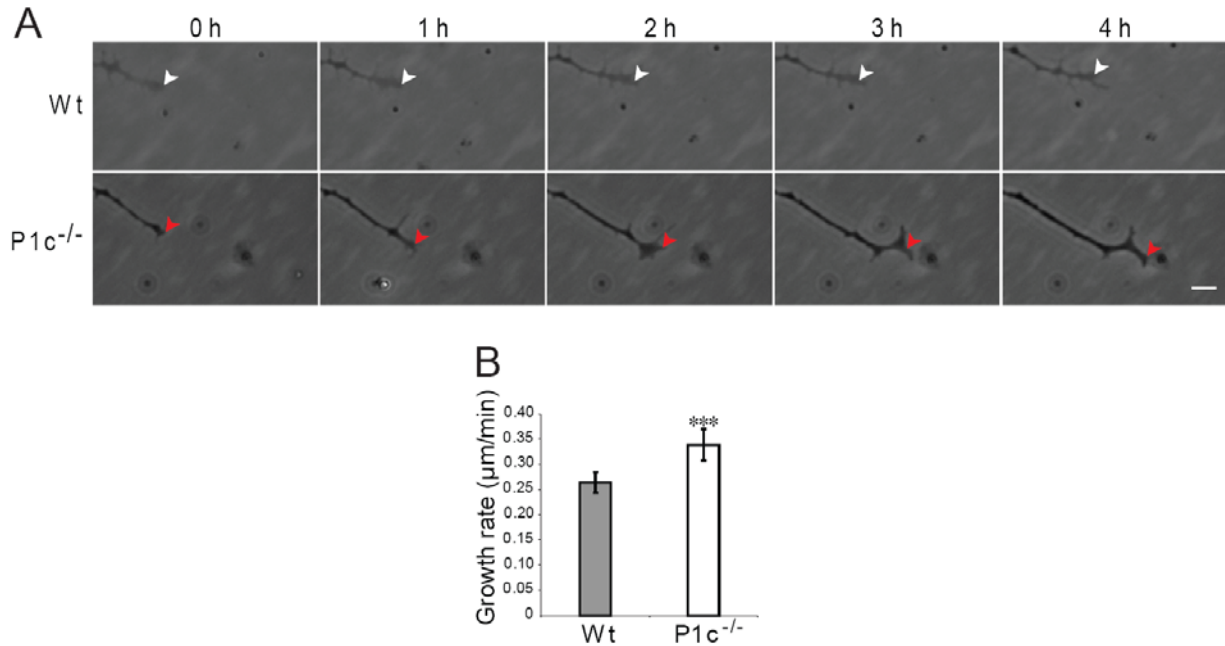


Figure 36. P1c-deficiency leads to faster growth cone extension. **A)** Growth cone extension of wt and P1c^{-/-} neurons was visualized overnight using phase-contrast time-lapse microscopy. Images show time points indicated. Scale bar, 8 μm. **B)** Graph represents statistical analysis of growth cone extension velocity subjected to a Student's t-test (n=8) ***P<0.001. Error bars, ± 95% CI.

cones was found to be different from that of their wt counterparts. Growth cones of P1c^{-/-} neurons appeared more robust compared to wt neurons, as indicated by its darker appearance. Thus unexpectedly, the higher stability of MTs in P1c^{-/-} DRG neurons led to a more efficient elongation of the growth cone, and consequently to faster neurite extension. A possible explanation for this phenotype presumably is a more pronounced engorgement phase. Indeed, P1c-deficient neurons displayed a higher proportion of growth cones that were spread out (resembling the engorgement phase) (Figure 36, 2h, lower panel). Since MTs are more stable in P1c^{-/-} neurons, they may invade the actin-free zone after protrusion, resulting in more vesicle and organelle transport into the growth cone required for the consolidation phase.

As neuronal morphology is dependent on cytoskeleton organization, and NFs, in

particular, have been reported to maintain the characteristic shape of axons during the structural changes that take place upon axonal elongation (Lin & Szaro, 1995), I investigated whether the changes in growth cone morphology of P1c-deficient DRG neurons were linked to changes in NF organization. Confocal immunofluorescence microscopy of wt and P1c^{-/-} DRG neurons using antibodies to NF proteins revealed that in the case of P1c-deficient neurons ~100% of the growth cones were filled with NFs, while this was the case for only ~25% of the wt growth cones (Figure 37). This phenotype was reminiscent of plectin-deficient cell types, keratinocytes and fibroblast, where IF networks had been found to extend to the

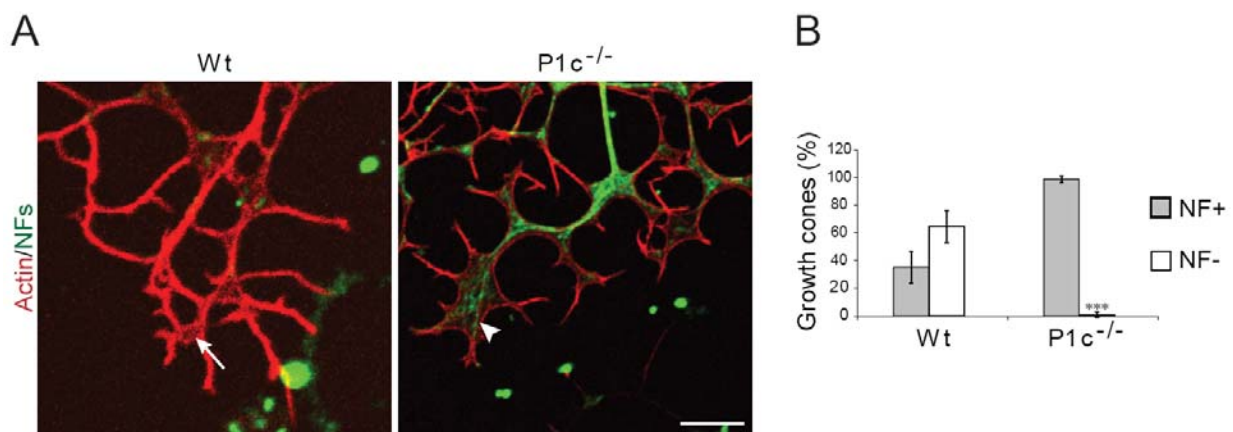


Figure 37. Lack of P1c in DRG neurons affects IF localization. **A)** Growth cones of wt and P1c^{-/-} DRG neurons were immunolabeled using antibodies to NFs (green) and stained for actin with phalloidin (red). Immunofluorescence microscopy images of P1c^{-/-} DRG neurons show NF-positive growth cones (arrowhead, right panel) in contrast to wt cells that display more NF-negative growth cones (arrows, left panel). Scale bar, 10 μ m. **B)** Graph shows quantification of NF- positive and NF-negative growth cones of wt and P1c^{-/-} DRG neurons subjected to Chi-square test (n=4). ***P<0.001. Error bars, \pm 95% CI.

outermost parts of the cell instead of being restrained to its central part, as is typical for wt cells (Osmanagic-Myers *et al*, 2006; Burgstaller *et al*, 2010).

Being part of the mechanism underlying neuronal branching and neurite extension, MT dynamics are essential for neuronal development (Conde & Cáceres, 2009). To investigate whether MT stabilization effected by P1c deficiency had an influence on neuronal

development, I decided to analyze the neurite outgrowth of DRG explants. For this, DRG explants, isolated from wt and $P1c^{-/-}$ mice, were cultivated embedded in matrigel and neurite outgrowth was measured after 24 h. As shown in Figure 38, $P1c$ -deficient DRGs showed less neurites growing out of explants than their wt counterparts. In addition, $P1c$ -deficient neurites seemed to be less branched than those of wt.

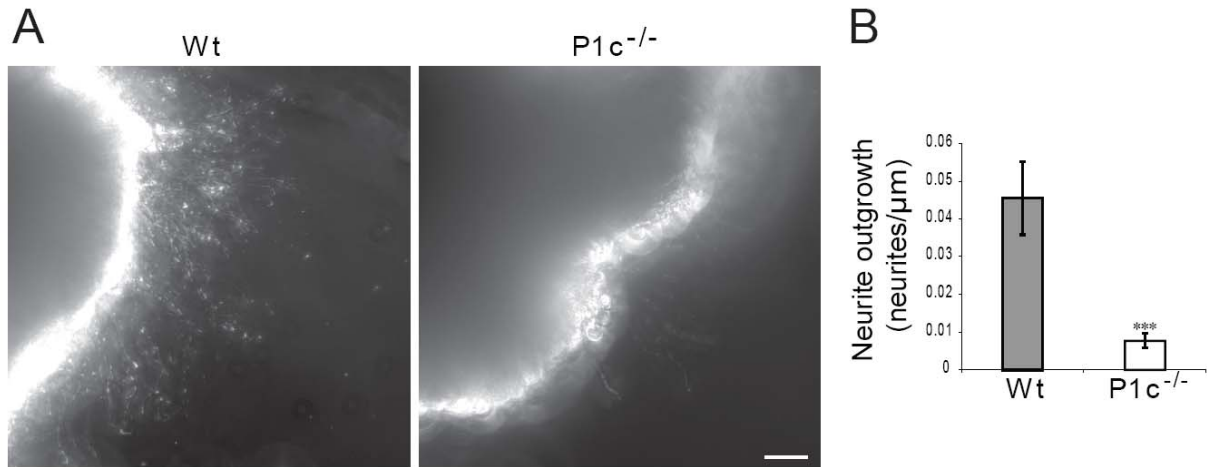


Figure 38. Lack of $P1c$ impairs neurite outgrowth. **A)** DRG explants of wt and $P1c^{-/-}$ mice were cultivated in matrigel. Phase contrast microscopy revealed less neurite outgrowth in $P1c^{-/-}$ DRG explants. Scale bar, 65 μ m. **B)** Graph shows quantitative comparison of neurite outgrowth (normalized to the DRG surface length in μ m) subjected to Student's t-test ($n \sim 20$). *** $P < 0.001$. Error bars, \pm SEM.

To further analyze whether $P1c^{-/-}$ neurons undergo less branching, cultivated primary $P1c^{-/-}$ DRG neurons were compared with primary wt DRG neurons. According to their level of branching three different populations of neurons, showing low, medium or high branching, could be distinguished in both genotypes. While most wt neurons showed a medium level of branching, in $P1c^{-/-}$ neurons the category of low level branching was most frequent (Figure 39). These results suggested that in $P1c$ -deficient DRG neurons branching was impaired. The reason for this could have been excessive amounts of tau bound to MTs, interfering with the severing activity of katanin, a protein triggering axonal branching (Yu *et al*, 2008).

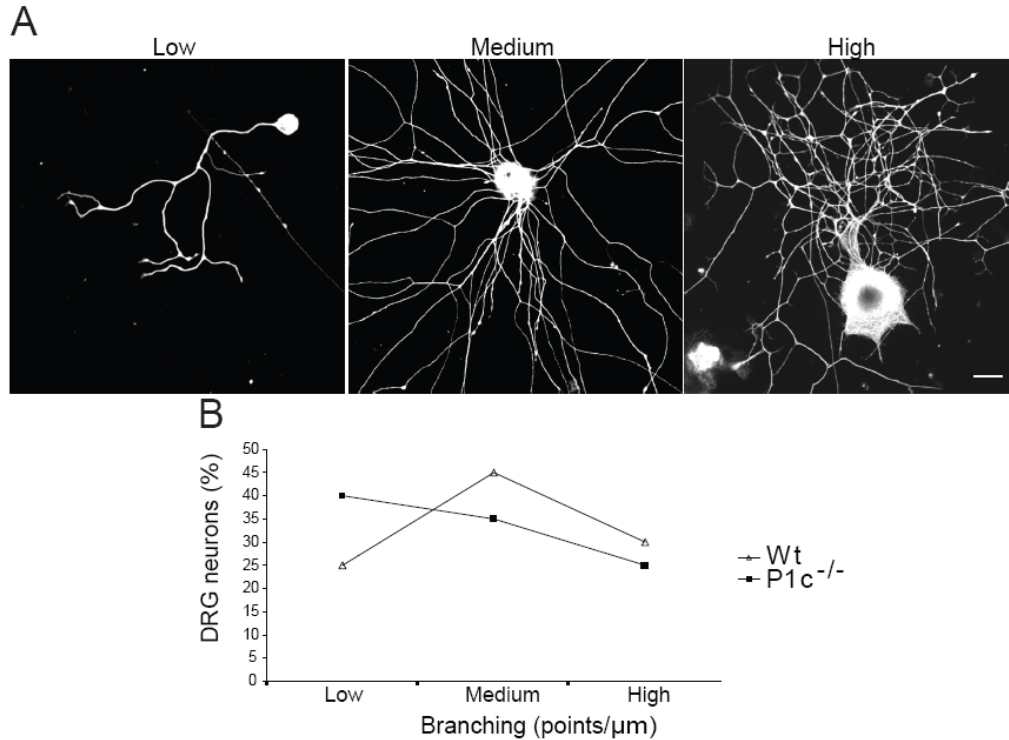


Figure 39. P1c-deficiency leads to decreased neurite branching. **A)** Images obtained by immunofluorescence microscopy show representative examples of the three populations of DRG neurons sorted by their branching levels (branching points normalized to neurite length): low (<0.015), medium ($0.015-0.030$), and high branching (>0.030). Scale bar, $20\mu\text{m}$. **B)** Line graph represents quantification of wt and P1c^{-/-} DRG neurons classified according to the number of branches per neurite length (low, medium, and high). Results were subjected to Wilcoxon-Mann-Whitney U-test ($n=20$). * $P<0.10$.

The Rho family of GTPases plays an important role in various developmental processes of neurons, including differentiation and neurite outgrowth. Activation of Rho is generally associated with the inhibition of neurite formation (Jeon *et al*, 2011). To assess whether the impaired ability of P1c-deficient DRGs to form neurites correlated with an overactivation of Rho, I measured the RhoA activation status in brain lysates. GTP-RhoA was pulled down from brain lysates using a GST-Rhotekin-binding domain (GST-RBD) fusion protein, containing a binding domain for activated (GTP-bound) RhoA. GTP-RhoA such isolated was analyzed by quantitative immunoblotting using antibodies to RhoA, and values measured were subjected to a Student's t test (Figure 40). While the total amount of RhoA was found to be similar in wt and

in P1c^{-/-} lysates, a tendency towards a higher content of active RhoA was found for P1c^{-/-} lysates, without being statistically significant, however.

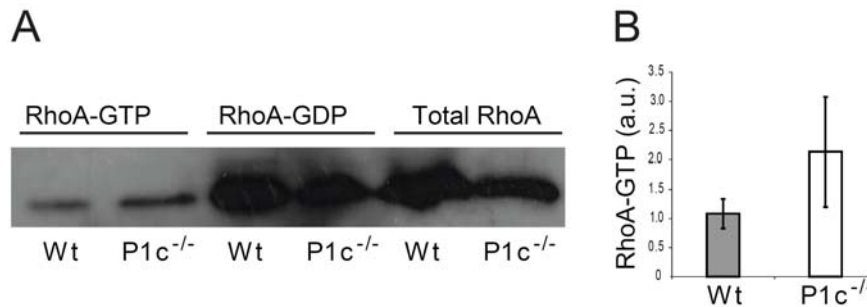


Figure 40. P1c-deficiency barely affects the activation of RhoA. A) Active RhoA pull down assays were performed using wt and P1c^{-/-} brain lysates. GTP-bound RhoA was precipitated using GST-RBD fusion protein and quantified by immunoblotting analysis using antibodies to RhoA. B) Graph show statistical analysis of the signals obtained (n=3). Error bars, \pm SEM.

3.1.11 Lack of P1c leads to abnormal vesicle transport in DRG neurons

One of the best-known functions of MTs is their role in mediating vesicle transport through the MT-based motor proteins kinesin and dynein. Alteration of MT organization and dynamics are shown to interfere with important neuronal functions such as synaptic vesicle transport or glucose uptake. Therefore, it was of interest to investigate whether the lack of P1c in DRG neurons and the stabilization of MTs had an effect on glucose uptake. Glucose is the major energy source for neurons, and the main glucose transporters identified in brain are GLUT1 and GLUT3 (Duelli & Kuschinsky, 2001), similar to keratinocytes. GLUT1 is the main isoform expressed in astrocytes and endothelial cells, while GLUT3 is mainly found in neurons. To test whether P1c-deficient DRG neurons, similar to P1c^{-/-} keratinocytes, showed increased glucose uptake. DRG-neurons were incubated with 2-NBDG, and fluorescence signals within cells were monitored by confocal microscopy. Comparing wt and P1c^{-/-} DRG neurons, increased glucose uptake was observed in P1c^{-/-} neurons according to expectations (Figure 41). Glucose uptake of P1c-deficient DRG neurons was in fact ~3 times higher than that of wt DRG neurons, similar to the results obtained with P1c^{-/-} keratinocytes.

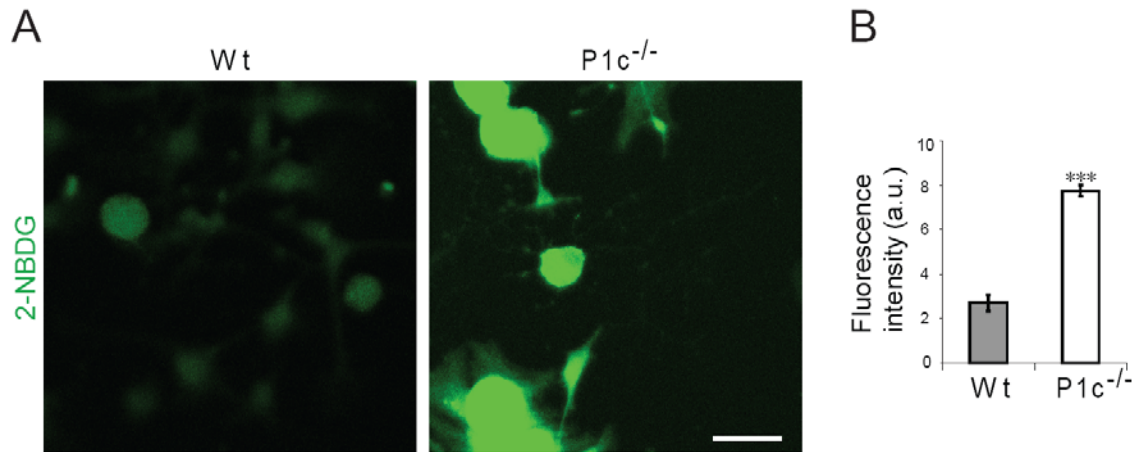


Figure 41. Alterations of glucose uptake in P1c-deficient DRG neurons. A) Primary wt and P1c^{-/-} DRG neurons were incubated with 2-NBDG and fluorescence intensity of cells was measured. Note higher fluorescence intensity of P1c^{-/-} DRG neurons after 2-NBDG treatment. Scale bar, 30 μ m B) Bar graph shows statistical analysis of data subjected to Student's t-test (n=3, ~20 cells/experiment). ***P<0.001. Error bars, \pm 95% CI.

Another well-known MT-dependent vesicular transport event is the transfer of peroxisomes to the cell periphery as a defence mechanism against oxidative stress. Alteration of tau levels in neurons can enhance oxidative stress by inhibiting transport and redistribution of peroxisomes, eventually leading to the absence of catalase in neurites (Stamer *et al*, 2002). To study whether this was also the case in P1c-deficient DRG neurons, I exposed wt and P1c^{-/-} DRG neuronal cultures to 250 μ M H₂O₂ for 5 min. Then, I assessed the vulnerability of the neurons to oxidative stress by quantifying the proportion of collapsed (bulb-shaped) growth cones as an indicator of oxidative stress damage. Quantitative measurements revealed ~4 times more collapsed growth cones in P1c^{-/-} DRG neurons compared to wt cells (Figure 42). These results suggested that enhanced levels of MT-bound MAPs, as is typical for P1c^{-/-} neurons, interfere with the cellular machinery protecting the cell against oxidative stress, probably by impeding vesicle (peroxisome) transport.

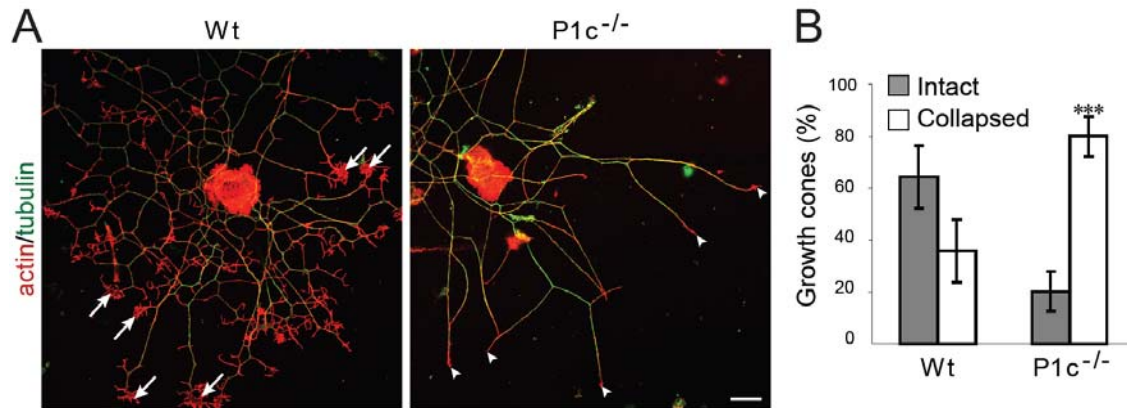


Figure 42. Neurites of P1c^{-/-} DRG neurons are highly sensitive to oxidative stress. A) Primary wt and P1c^{-/-} DRG neurons were exposed to 250 μ M H₂O₂ for 5 min, immunolabeled using antibodies to tubulin and stained for actin. Intact (arrows) and collapsed (arrowheads) growth cones were monitored using confocal microscopy. Scale bar, 20 μ m. **B)** Graph shows statistical analysis of intact and collapsed growth cones. Data were subjected to Chi-square (n=5). ***P<0.001. Error bars, \pm 95% CI. Note a higher proportion of intact versus collapsed growth cones in wt neurons, whereas the opposite was the case for P1c^{-/-} cells.

MT-bound MAPs can spatially control MT-dependent axonal transport, by differentially regulating the activity of MT-dependent motor proteins like kinesin and dynein (Dixit *et al*, 2008). Since MT-bound tau levels were found to be increased in P1c^{-/-} brain lysates, it was intriguing to explore whether tau levels can interfere with synaptic vesicle transport in DRG neurons. To directly visualize synaptic vesicle transport in DRG neurons, cells were loaded with FM1-43, an amphipathic dye used to monitor endosomal traffic, especially synaptic vesicle recycling at nerve terminals (Gaffield & Betz, 2006). FM dyes are non-fluorescent in aqueous media, but they become intensely fluorescent after their incorporation into a lipidic membrane. In neurons that are actively recycling neurotransmitters, these dyes are internalized within recycled synaptic vesicles. After activating DRG neurons by exposure to high concentration of potassium to trigger synaptic vesicle recycling (Gaffield & Betz, 2006), a higher percentage of retrogradely moving vesicles were detected in P1c^{-/-} DRG neurons compared to their wt counterparts (Figure 43). These results suggested that the activity of kinesin (the motor protein responsible for anterograde transport) was decreased as a result of more tau bound to MT in P1c^{-/-} cells (Figure 34).

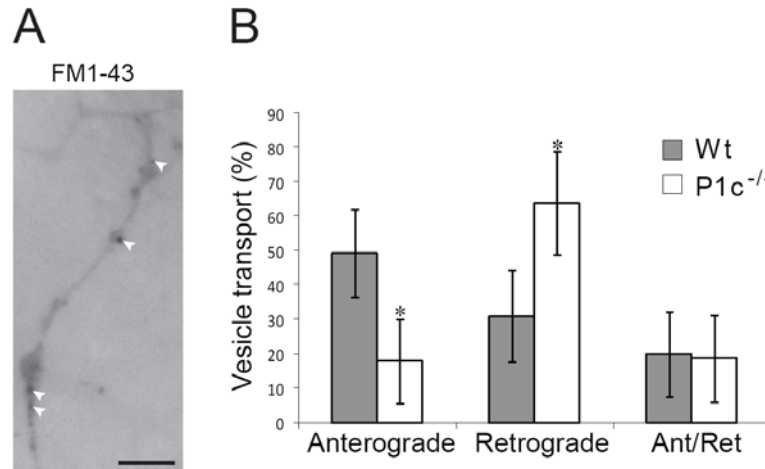


Figure 43. P1c deficiency impairs anterograde synaptic vesicle transport in DRG neurons. **A)** Neurons were subjected to K⁺-induced depolarization. A single frame image taken from a time-lapse recording of synaptic vesicles labeled with FM1-43 is shown. Representative vesicles are indicated with arrowheads. Scale bar, 2 μ m **B)** Chart represents the percentages of synaptic vesicles undergoing anterograde, retrograde, or bidirectional transport along the neurites. Data were subjected to Chi-square test (n=9) *P<0.05. Error bars, \pm SEM.

3.1.12 P1c deficiency causes abnormalities in membrane excitability of DRG neurons

It has been reported that tubulin in its acetylated form associated with Na⁺, K⁺-ATPase *in vitro* and *in vivo* and participates in the regulation of its enzymatic activity (Arce *et al*, 2008). Furthermore, it has been suggested that in cardiac myocytes modulation of Na⁺ current is a tubulin/GTP-coupled process (Casini *et al*, 2009). As acetylation of tubulin correlates with increased MT stability, it could be that the more stable MT population found in P1c^{-/-} DRG neurons has an influence on the Na⁺ influx into cells.

To investigate whether ion channel activity was altered in P1c-deficient DRG neurons, I measured the activity and expression levels of Na⁺ channels. Channel activity was measured using CoroNa green, a fluorescent Na⁺ indicator that allows the visualization of Na⁺ levels inside the cell. The fluorescence microscopy images suggested a slightly decreased channel activity in P1c^{-/-} DRG versus wt neurons, although after subjecting the data to a Student's t test

the observed difference was found not to be statistically significant (Figure 44). However, it could be that the Na^+ indicator used was not sensitive enough to measure minor Na^+ fluctuations. When I analyzed the expression levels of Na^+ channels at the membrane of wt and $\text{P1c}^{-/-}$ DRG neurons by immunofluorescence microscopy, a homogeneous distribution of the channels at the surface of wt DRG neurons was revealed (Figure 45), whereas in $\text{P1c}^{-/-}$ DRG neurons, channels appeared in a clustered way and unevenly distributed over the cell surface.

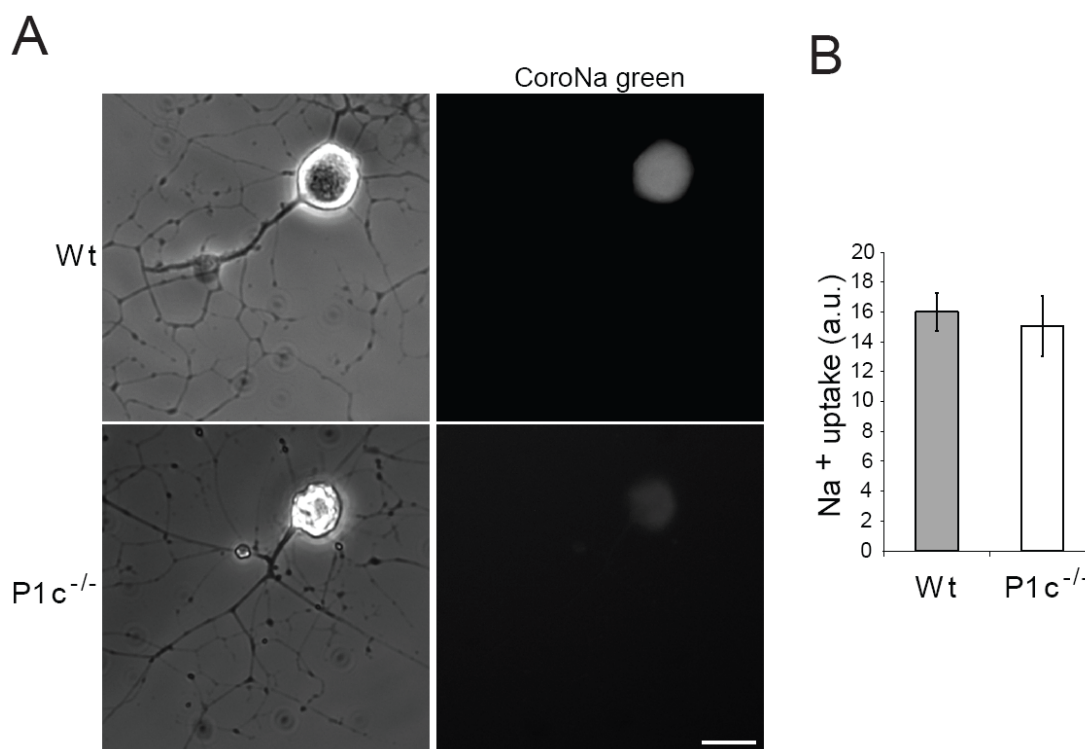


Figure 44. P1c deficiency does not affect intracellular Na^+ concentration. **A)** Phase contrast (left column) and fluorescent images of wt and $\text{P1c}^{-/-}$ DRG neurons loaded with CoroNa green (right column) are shown. Scale bar, 15 μm . **B)** Graph represents fluorescent intensities measured using ImageJ software (NIH Image, Bethesda, MD). (n=3, ~20 cells/experiment). Error bars, \pm SEM.

To directly investigate whether the ability of P1c -deficient DRG neurons to produce action potentials was affected, the membrane excitability of $\text{P1c}^{-/-}$ DRG neurons was measured

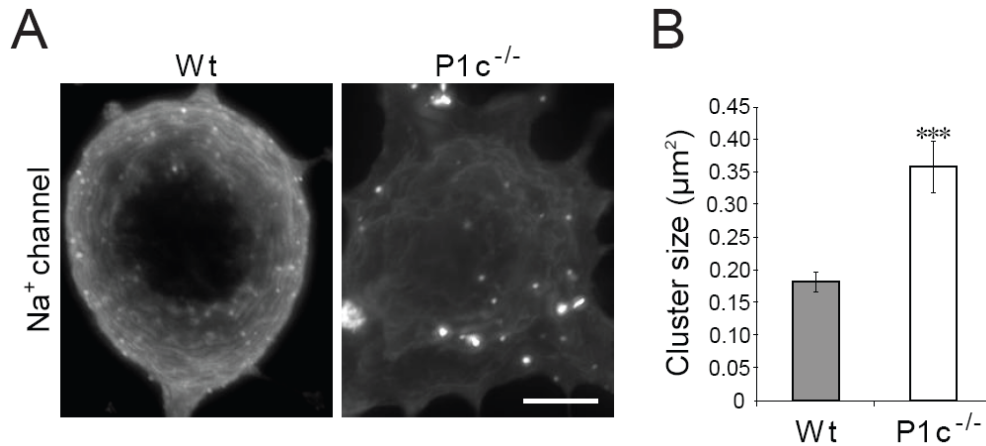


Figure 45. Clustering of P1c^{-/-} Na⁺ channels in P1c^{-/-} **A)** Immunofluorescence microscopy of wt and P1c^{-/-} DRG neurons immunolabeled using antibodies to Na⁺ channels. Note homogeneous dotted distribution of Na⁺ channels in wt DRG neurons contrasting their P1c^{-/-} counterparts. Scale bar, 6 μm. **B)** Bar graph show statistical analysis of the Na⁺ channel clusters size. Data were subjected to Student's t-test (n=3, ~25 cells/experiment). ***P<0.001. Error bars, ± 95%CI.

using current clamp electrophysiology. These experiments were performed in collaboration with A. Yousuf and K. Schicker in the laboratory of S. Böhm (Centre for Physiology and Pharmacology, Medical University of Vienna). The current clamp technique records whatever voltage the cell generates as a result of stimulation. When DRG neurons were subjected to these measurements, threshold levels reached by wt specimens were -35 mV and -42 mV (Figure 46). Although the data obtained with P1c^{-/-} DRG neurons on average were not significantly different, the data distribution was remarkably wider in this case with a much higher difference between the minimum and maximum value compared to wt cells. These results were consistent with possible alteration of membrane excitability regulation.

3.1.13 Differential extractability of tau from hippocampal wt and P1c^{-/-} lysates

Tau protein is very well known due to its implication in a group of neurodegenerative diseases known as tauopathies. The hallmark of tauopathies is the occurrence of tau aggregates and tau hyperphosphorylation (Kampers *et al*, 1999; Ballatore *et al*, 2007; Ittner *et*

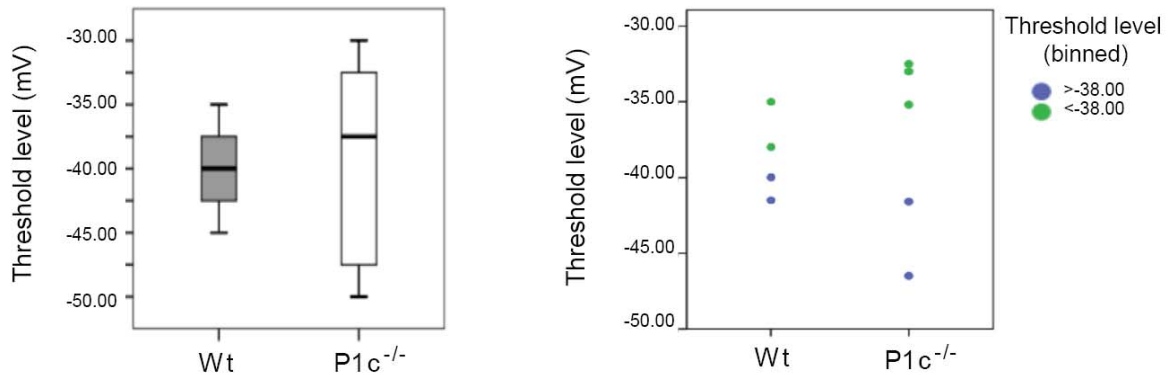


Figure 46. P1c deficiency causes a wide range of membrane potentials. Membrane potentials of wt and P1c^{-/-} DRG neurons were measured in current clamp mode. Box and whisker diagrams represent the statistical distribution of threshold voltages measured (n= 4).

al, 2010; Fu *et al*, 2010). Since the levels of tau bound to MTs are increased in P1c^{-/-} brain lysates, I considered of high interest to investigate whether tau aggregates were present in P1c-deficient brain. Normal tau is a highly soluble protein that loses its solubility under pathological conditions. A potential tendency of tau protein to form aggregates in P1c-deficient hippocampus was first examined by sarcosyl extraction of the tissue, whereby one obtains a soluble and an insoluble fraction (Sydow *et al*, 2011). When tau is forming part of aggregates, it will be found in the insoluble fraction. The analysis of sarcosyl-insoluble fractions produced from 12 P1c-deficient hippocampuses revealed a significantly reduced amount of insoluble tau in comparison to wt samples (Figure 47). This result suggested that tau in P1c-deficient brain did not form aggregates, but was more soluble, probably because it remained bound to tubulin which ends up primarily in the soluble fraction of the sarcosyl extract.

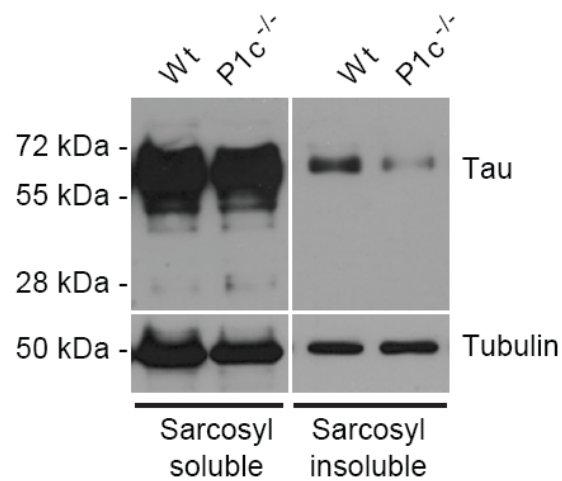


Figure 47. Sarcosyl-insoluble P1c^{-/-} fractions lysates contain reduced levels of tau. Sarcosyl soluble and insoluble fractions were subjected to immunoblotting analysis using antibodies to tau. Note the decreased tau-specific signal in the insoluble fraction of P1c^{-/-} hippocampus, while comparable levels of tau were found in the sarcosyl soluble fractions. Tubulin levels were similar in all fractions.

4 DISCUSSION

Plectin is one of the most abundant and versatile cytolinkers expressed in mammalian cells. One of its outstanding features is its functional diversity that is mainly based on the alternative splicing of a series of different first coding exons (Fuchs *et al*, 1999). A variety of isoforms generated in this way just differ in short N-terminal sequences that specify distinct properties of the cytolinker, including its cellular targeting and N-terminal binding partners (Reznicek *et al*, 2004; Abrahamsberg *et al*, 2005). In muscle, P1 is associated with the outer nuclear/ER membrane system, P1d with the Z-disks, P1f with the sarcolemmal dystrophin-glycoprotein complex and P1b with mitochondria (Konieczny *et al*, 2008; Reznicek *et al*, 2007). In epidermis, P1a links IFs to HDs and it undergoes selective degradation that seems to be required for epithelial differentiation (Walko *et al*, 2011). However, the role of P1c, a main isoform in the epidermis and the neural system, remained unclear up to date. In this thesis I provide evidence for a role of P1c in MT dynamics. Moreover, by studying MT-dependent basic cellular functions in keratinocytes and neuronal cells, the two cell types where P1c is most abundantly expressed, I could demonstrate that P1c-mediated MT regulation is of broad biological significance.

Plectin 1c acts as a MT destabilizer in a spatially-controlled manner

Based on three types of assays, resistance to MT depolymerizing drugs, assessment of acetylated tubulin levels, and direct observation of MT dynamics by video microscopy, this study provides evidence that P1c deficiency in keratinocytes and in DRG neurons results in increased MT stability. Increased stability was coupled with a decrease in the dynamics of MTs, manifesting as less frequent transitions between MT assembly and disassembly states. A destabilizing function of this kind was not expected for a cytolinker protein such as plectin. In fact, it was the opposite of what had been observed for other cytolinkers, such as ACF7 and

BPAG1, that have been shown to stabilize MTs (Kodama *et al*, 2003; Yang *et al*, 1999). Thus, plectin seems to be the first genuine cytolinker protein shown to act as a MT destabilizer. This finding, together with the observation that plectin can act also as a destabilizer of the actin cytoskeleton (Andrä *et al*, 1998), opens a new perspective on how cells maintain their cytoskeleton integrity. This study shows that this process is the result of a fine-tuned regulatory mechanism, in which cytolinker proteins are key players, not only by anchoring and providing stability to dynamic filaments, but also by destabilizing them and thus favoring their dynamic behavior, as demonstrated in this work for P1c.

My study demonstrates that abnormal MT stability in P1c^{-/-} keratinocytes could be rescued, i.e. restored to normal levels, in P1c-deficient keratinocytes by forced expression of P1c-EGFP fusion proteins. However, from experiments where I transfected cells with truncated forms of P1c lacking the IF-binding domain, evidence emerged that the rescue potential of P1c was dependent on the localization of the protein, in particular its association with IFs. Unable to be recruited to IF networks, and instead associating with actin filaments, the truncated versions tested showed only a limited, if any, rescue potential. These findings point towards a fascinating new feature of cytoskeletal filament cross-talk, namely the potential of IFs to destabilize rather than stabilize MTs via an associated cytolinker protein, thereby stimulating MT dynamics. In previous studies, actin was found to reinforce and stabilize MTs at the cell periphery via ACF7, resulting in polarization and more effective migration of cells (Kodama *et al*, 2003; Wu *et al*, 2011).

P1c destabilizes MTs by antagonizing MAP-mediated MT stabilization

As a possible mechanism underlying MT destabilization through plectin, previous results obtained in our laboratory suggest that plectin's SH3 domain interferes with MAP-MT binding and consequently antagonizes MAP-mediated MT stabilization (see model in Figure 48).

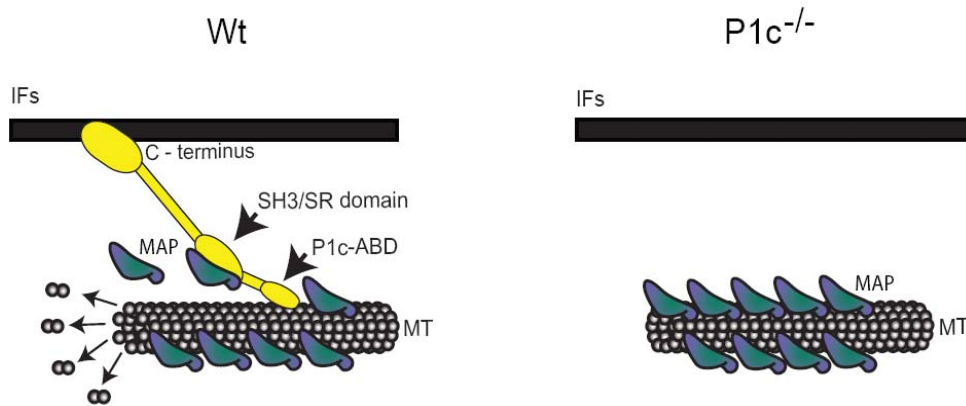


Figure 48. Model depicting plectin as MT destabilizer. Binding of P1c to MTs presumably occurs via its isoform-specific N-terminal sequence including the ABD. The SH3 domain located within the plakin domain binds to MAPs. Interference with the MT-stabilizing function of MAPs ensures a dynamic MT network in wt cells. When P1c is absent more MAPs can bind along MTs leading to their stabilization.

Several observations support such a mechanism. First, binding of plectin to HMW-MAPs was reported a few years ago (Herrmann & Wiche, 1987), and afterwards, using expression constructs encoding various domains of plectin, it could be shown that plectin's SH3 domain is responsible for this interaction (G. Walko, unpublished data). Second, MT co-assembly assays performed previously in the lab by L. Janda demonstrated that increasing concentrations of plectin's SH3 domain lead to decreased levels of MAPs binding to MTs and, as a consequence, less polymerized MTs (unpublished data). Third, based on an endogenous MT binding assay (see Results), it could be shown that plectin's SH3 domain was able to detach MAPs from stabilized MTs present in brain tissue lysates. Fourth, comparing wt, P1c^{-/-}, and P0 keratinocytes in this thesis project, I found MAP2 to be associated with larger portions of cellular MTs in mutant compared to wt cells, where P1c's presence interferes with MAP-MT binding. This observation was confirmed also by in vitro experiments performed with brain lysates where the amount of tau bound to MTs was analyzed. Comparison of wt and P1c^{-/-} MT-bound tau fractions revealed a greater amount of tau bound to MTs in plectin-deficient samples.

Is MT destabilization P1c-specific?

Since plectin's SH3 domain is expressed in all plectin isoforms known and is contained in many other proteins, including MT regulators, such as Fyn or Src (Lee *et al*, 1998), SH3 domain-mediated MT destabilization could be a function performed by plectin isoforms others than P1c as well as by many other proteins. However, although all plectin isoforms apparently have the potential to destabilize MTs via their SH3 domain, the destabilizing potential of P1c is likely to be more efficient than that of other isoforms. A possible reason for this could be a closer apposition of P1c to the MT surface accomplished by an additional tubulin-binding interface formed by its isoform-specific sequence and the succeeding ABD. The partial cosedimentation of endogenous keratinocyte P1c with MTs, but not of the equally abundant P1a, as previously observed in our laboratory (G. Walko, unpublished data), points in this direction. A weak, or even only transient binding of P1c to tubulin polymers might suffice to bring plectin's SH3 domain in contact with MAPs. However, the validity of such a mechanism has to be rigorously tested.

The hypothetical model depicted in Figure 48 proposes that, by antagonizing MAP-mediated MT stabilization, IF-associated P1c leads to a MT network that is more susceptible to localized disassembly in the vicinity of IFs. Conversely, in a plectin-deficient system, the fraction of MAPs attaching along MTs is higher, leading to promotion of assembly and stabilization of the polymer. This model does not exclude additional or alternative ways of how plectin may regulate MT dynamics, e.g. through its scaffolding and platform function for other putative MT regulators.

P1c deficiency impairs neurite outgrowth and branching

Interestingly, isolated DRG neurons as well neurite outgrowth from DRG explants of P1c-deficient mice showed reduced branching and neurite outgrowth in comparison with their wt

counterparts. As the results obtained in this work indicates, there are increased levels of tau bound to the MT fraction of P1c-deficient brain lysates. According to Yu *et al*, 2008, the decrease in neurite branching observed in P1c-deficient cells could be the result of tau protection against the MT-severing protein katanin, impairing the formation of new branches. However, although P1c-deficient DRG neurons show impaired branching and DRG explants have decreased potential to regenerate newly formed neurites, MT stabilization caused by P1c-deficiency promotes growth cone extension. P1c-deficient growth cones extend faster than wt growth cones. A possible explanation for this could be that stable MTs of P1c^{-/-} DRG neurons might act as a nucleation seed for the MT assembly and protrusion that is required during axon outgrowth (Conde & Cáceres, 2009). In addition they may provide tracks for MT-dependent motors that transport organelles and NFs to the growth cone during the outgrowth process (Lee *et al*, 2011). Together all these features would explain why growth cones observed in P1c-deficient DRG neurons are more spread out than their wt counterparts. They also correlate with the observed high percentage of P1c-deficient growth cones filled with NFs (~100%) in contrast to the much lower proportions (~35%) of NF-positive growth cones in the case of wt. The presence of NFs in P1c-deficient growth cones suggests an increased transport of NFs along MTs (Lee *et al*, 2011) that could result in more spread out growth cones as observed.

The neuronal outgrowth alterations observed in P1c-deficient DRG neurons suggest that P1c could be critical also in neuronal polarization. Since plectin has already been identified as a binding partner of ankyrin G (Maiweilidan *et al*, 2011), a marker for the axon initial segment (AIS) (Dzhashiashvili *et al*, 2007), it will be interesting to analyze whether ankyrin G localization at the AIS is impaired due to P1c deficiency. Moreover, tubulin acetylation (a characteristic feature of P1c^{-/-} DRG neurons) has been found to impair the concentration of ankyrin G at the AIS as well (Tapia *et al*, 2010). However, to further

investigate neuronal polarization in P1c-deficient neurons, a more suitable system than DRG neurons, such as hippocampal neurons, should be used due to their pyramidal shape that allows the monitoring of axon formation.

Is axonal transport altered in P1c-deficient DRG neurons?

Based on three different types of experiments, glucose uptake, synaptic vesicle transport visualization, and oxidative stress resistance, this thesis shows alteration in MT-dependent transport. However, while the results of synaptic vesicle transport and resistance towards oxidative stress point to an impairment of MT-dependent transport, the outcome of the glucose uptake shows the opposite. This apparent contradiction might be due to differences in the cellular localization where these phenomena were analyzed. While glucose uptake was mainly monitored in the cell body, vesicle transport and resistance towards oxidative stress were measured at the distal end of the neurites, where tau levels are increased in comparison to the cell body. Kinesin motility is responsible for anterograde vesicle transport and might be spatially regulated by tau, detaching from MTs when tau concentration is high (Dixit *et al*, 2008). Since tau concentration increases following a proximal-distal gradient, kinesin anterograde transport at the end of the growth cones would be inhibited. However, data reported from Yuan *et al* (2008) contradict this hypothesis showing unaffected axonal transport rates in mice lacking or overexpressing tau protein. The results that I report here would support Dixit *et al*'s hypothesis, as synaptic vesicle anterograde transport and resistance towards oxidative stress mediated by peroxisomes transport along the neurites in P1c-deficient cells were found reduced, correlating with the higher levels of tau associated with MTs along the neurite in comparison to wt DRG neurons.

Is membrane excitability affected in P1c-deficient neurons?

Na⁺ influx in P1c-deficient cells showed a tendency to be reduced in comparison with wt cells, although the difference found was not statistically significant. The distribution of Na⁺ channels was abnormal as well. Unlike wt cells Na⁺ channels were not homogeneously distributed across P1c-deficient DRG neurons distributed (Figure 46). As described in the Results, wt neurons were stimulated between -35 mV and -42 mV, while the corresponding threshold levels reached by P1c-deficient DRGs were more varied. Since P1c-mediated MT destabilization appears to be a spatially controlled event, the diversity of results obtained from current clamp technique could be due to the different points where the current was applied, making it difficult to compare and evaluate the different measurements. Anyway, these results do not provide any explanation for the reduced motor nerve conduction velocity observed in P1c-deficient mice. Thus, it could be that the higher number of small caliber axons observed in these mice is the sole reason for the reported phenotype (Fuchs *et al*, 2009).

Are there any similarities between P1c deficiency and tauopathy or neurodegenerative disorder phenotypes?

Tauopathies and neurodegenerative disorders share some common features like protein aggregate formation, alterations of MT stability, and hyperphosphorylation of proteins (Lee *et al*, 2001; Avila *et al*, 2004). For example Alzheimer disease is characterized by the presence of neurofibrillary tangles or aggregates formed by hyperphosphorylated tau and NFs (Rudrabhatla *et al*, 2011). Similarly, the neurodegenerative disorder Charcot-Marie-Tooth disease manifests with NF aggregates, impaired MT-dependent transport, aberrant mitochondria distribution, reduced motor nerve conduction velocity, and increased MT stability (Schröder, 2005). Interestingly, P1c-deficient mice share some of these phenomena including, impaired MT-dependent transport, increased MT stability and reduced motor nerve conduction

velocity. Moreover increased NF-positive staining but no aggregates were found.

Results presented in this thesis show increased levels of tau bound to MTs in P1c-deficient brain lysates. Whether MT-bound tau in P1c^{-/-} neurons is hyperphosphorylated is still an open question. Although hyperphosphorylation of tau (usually connected with impaired memory) has been found to be the cause for tau detachment of MTs (Biernat *et al*, 1993; Drewes *et al*, 1995), these studies were focused on human tau and not murine tau. Human differs from murine tau in the ratio of the isoforms, containing more 3R (3 MT-binding domain repeats) tau than 4R (4 MT-binding domain repeats) tau. In contrast, murine tau is almost all 4R tau and is more difficult to detach from MTs. Thus, it would be still possible that the increased levels of tau bound to MTs in P1c^{-/-} brain lysates would be hyperphosphorylated. In fact, hyperphosphorylated tau bound to MTs present in brain lysates has been recently reported (Planel *et al*, 2008).

It has been suggested that as well as an increase in the amount of intracellular tau, structural changes to this protein, modifications by phosphorylation, or its aggregation could produce toxic effects in cells (Avila, 2010). Future investigations using P1c-deficient mice could help to clarify the mechanism underlying the toxic effects of tau. Questions to be addressed include whether toxicity is a result of tau detachment from MTs, or whether tau could still promote toxicity even when it remains bound to the polymers. Extracellular tau was also found to promote cellular toxicity by increasing the levels of intracellular calcium (Gómez-Ramos *et al*, 2006). In addition, tau overexpression results in its secretion via membrane vesicles as a mechanism to avoid intracellular toxicity (Simón *et al*, 2012). However, it remains to be elucidated how excess tau protein gets associated with these membrane vesicles. Interestingly, preliminary data from this laboratory suggest that the rodless isoform of P1 (an isoform targeted to membranes) might be actively transported to the exterior of differentiated myoblast. In fact, plectin was found to co-fractionate with Golgi stacks suggesting an

association of plectin with the Golgi apparatus (P. Möseneder, Master thesis). Thus, it might be of interest to study whether plectin is involved in tau association with membrane vesicles.

Closing remarks

In conclusion, my study adds a new facet to the already broad spectrum of plectin functions. The fact that plectin can act as a MT destabilizer opens a new perspective on the role of cytolinkers in regulating cytoskeletal integrity. In fact, P1c is the first cytolinker protein reported to possess a MT-destabilizing function. The analyses of P1c-deficient keratinocytes and DRG neurons combined with in vitro data using recombinant proteins, suggest that plectin antagonizes MAP-mediated MT-stabilization in a spatially controlled manner. As a consequence, P1c-deficient keratinocytes show aberrations in MT-dependent functions, such as mitotic spindle formation, glucose uptake, FA turn over, and polarized migration. Similarly, P1c-deficient DRG neurons show alterations in glucose uptake, axonal vesicle transport, Na⁺ channel distribution, membrane excitability, and reduced tau solubility. The broad spectrum of MT-dependent cellular processes affected by P1c deficiency makes P1c not only a uniquely versatile plectin isoform variant, but also an essential element in the orchestration and proper functioning of the MT network. It will be a challenging task for future investigations to dissect in detail the mechanism underlying MT destabilization mediated by plectin. Of particular interest will be to investigate whether plectin is involved in tau phosphorylation, and how it regulates NF network assembly and its extension into the growth cone of neurons. Eventually it will be a challenging task to analyze whether plectin-related phenotypes have consequences at the cognitive levels of P1c-deficient mice, and whether P1c-deficiency could prevent tau's toxic effects by keeping tau attached to MTs, avoiding aggregate formation.

5 MATERIAL AND METHODS

Plasmids

Mammalian expression plasmids encoding GFP-EB1 (Stepanova et al., 2003), EGFP-tubulin and EGFP-zyxin (Rottner et al., 1999), and the bacterial expression plasmid pET3d/MAP2c encoding rat MAP2c (Ludin et al., 1996) were kindly provided by A. Akhmanova (Erasmus Medical Center, Rotterdam, The Netherlands), J. Wehland (Gesellschaft für Biotechnologische Forschung, Braunschweig, Germany), M. Gimona (University of Salzburg, Austria), and A. Matus (Friedrich Miescher Institute, Basel, Switzerland), respectively. Mammalian expression plasmids encoding full-length mouse P1c and P1c-8 with C-terminal EGFP or mCherry tags have been described previously (Rezniczek et al., 2003; Burgstaller et al., 2010). Plectin fragments corresponding to exons 1c-8 (p1c-8, amino acids 1-299, NCBI Reference Sequence: NP_035247); exons 1c-30 (p1c-30, amino acids 1-1374); exons 16-24 (p16-24, amino acids 632-1018); exons 20-21 (p20-21, amino acids 815-889) were excised from existing plasmids (constructed as described in Rezniczek et al., 2003), and inserted into the EcoRI site of the bacterial expression vector pGEX-4T-1 (GST gene fusion system).

Antibodies, antisera and dyes

Table 1. Primary antibodies and dyes used for immunofluorescence microscopy (IFM) and immunoblotting (IB).

Antibody/Dye	Antibody type	Antigen/Epitope	Dilution	Source
#32	serum, rabbit	purified MAP2 of hog brain	1:500 (IFM) 1:2000 (IB)	G. Wiche
Acetylated tubulin, T6793, clone 6-11B-1	monoclonal, mouse	<i>Chlamydomonas</i> axonemal acetylated tubulin	1:300 (IFM) 1:1000 (IB)	Sigma-Aldrich®
Actin, A-2066	polyclonal, rabbit	C-terminal end of actin	1:100 (IFM)	Sigma-Aldrich®

Actin, A4700, clone AC-40	monoclonal, mouse	C-terminal end of actin	1:200 (IFM)	Sigma-Aldrich®
Fyn-59, sc-73388	monoclonal, mouse	amino acids 7-176 of human Fyn	1:100 (IFM) 1:2000 (IB)	Santa Cruz Biotechnology, Inc.
GAPDH, G9545	polyclonal, rabbit	amino acids 314-333 of mouse GAPDH	1:15000 (IB)	Sigma-Aldrich®
GLUT1, 07-1401	polyclonal, rabbit	C-terminal end of GLUT1	1:100 (IFM)	Millipore
GFAP (GA5), #3670	monoclonal, mouse	purified GFAP of pig spinal cord	1:300 (IFM) 1:1000 (IB)	Cell signaling technology®
GST, G1160, clone GST2	monoclonal, mouse	<i>Schistosoma japonicum</i> GST	1:1000 (IB)	Sigma-Aldrich®
Na ⁺ channel α , cardiac (III-IV loop)	polyclonal, rabbit	Na ⁺ channel intracellular III-IV loop	1:80 (IFM)	Upstate (Millipore)
Neurofilament 160 kD, MAB5254, clone NN18	monoclonal, mouse	neurofilament 160 kD	1:50 (IB)	Chemicon® International
Neurofilament 200kD, clone RT97	monoclonal, rat	neurofilament heavy chain of rat brain	1:10 (IFM)	J. Wood
Phalloidin conjugated with Texas Red®-X, T-7471	dye	actin	1:100 (IFM)	Molecular Probes
Plectin 1c	polyclonal, rabbit	N-terminal sequence M ₁ -S ₁₇ of plectin 1c	1:100 (IFM) 1:800 (IB)	G. Wiche
Plectin #9	serum, rabbit	plectin (exons 9-12)	1:3330 (IB)	B. Nicolic, G. Wiche
Plectin#10F6	serum, mouse	plectin (rod-domain)	1:2 (IFM)	G. Wiche
Plectin #46	serum, rabbit	plectin (rod-domain)	1:100 (IFM)	G. Wiche

RhoA, sc-418, clone 26C4	monoclonal, mouse	RhoA	1:500 (IB)	Santa Cruz Biotechnology, Inc.
Synaptophysin-Prediluted	polyclonal, rabbit	C-terminus of human synaptophysin	1:5 (IFM) 1:50 (IB)	Invitrogen
Tau, A-0024	polyclonal, rabbit	amino acids 243-241 of human tau (containing 4R of MT-binding site)	1:100 (IFM) 1:2000 (IB)	Dako
Tau-1, MAB3420, clone PC1C6	monoclonal, mouse	purified denatured bovine MAPs	1:100 (IFM) 1:2000 (IB)	Chemicon® International
Tubulin, SM2202P	monoclonal, rat	C-terminal end of yeast α -tubulin	1:300 (IFM)	Acris antibodies
Tubulin, T5168, clone B-5-1-2	monoclonal, mouse	purified α -tubulin of sea urchin sperm axonemes	1:1000 (IFM) 1:10000 (IB)	Sigma-Aldrich®
Vinculin, clone VIN-11-5	Monoclonal, mouse	purified vinculin of chicken gizzard smooth muscle	1:50 (IFM)	Sigma-Aldrich®

Table 2. Secondary antibodies used in immunofluorescence microscopy (IFM) and immunoblotting (IB). Horseadish peroxidase (HRPO).

Secondary antibody	Host	Dilution	Source
Alexa Fluor 488 anti-mouse IgM (μ chain)	donkey	1:1000 (IFM)	Jackson ImmunoResearch Laboratories, Inc.
Alexa Fluor 488 anti-rabbit IgGs	donkey	1:1000 (IFM)	Jackson ImmunoResearch Laboratories, Inc.
Alexa Fluor 488 anti-mouse IgGs	goat	1:1000 (IFM)	Jackson ImmunoResearch Laboratories, Inc.
Alexa Fluor 488 anti-rabbit IgGs	goat	1:1000 (IFM)	Jackson ImmunoResearch Laboratories, Inc.
Cy5 anti-mouse IgGs	donkey	1:300 (IFM)	Jackson ImmunoResearch Laboratories, Inc.

Cy5 anti-rabbit IgGs	donkey	1:300 (IFM)	Jackson ImmunoResearch Laboratories, Inc.
Cy5 anti-rat IgGs	donkey	1:300 (IFM)	Jackson ImmunoResearch Laboratories, Inc.
DyLight 649 anti-mouse IgGs	donkey	1:500 (IFM)	Jackson ImmunoResearch Laboratories, Inc.
DyLight 649 anti-rabbit IgGs	donkey	1:500 (IFM)	Jackson ImmunoResearch Laboratories, Inc.
DyLight 649 anti-rat IgGs	donkey	1:500 (IFM)	Jackson ImmunoResearch Laboratories, Inc.
HRPO anti-mouse IgM (μ chain)	donkey	1:10000 (IB)	Jackson ImmunoResearch Laboratories, Inc.
HRPO anti-mouse IgGs	goat	1:10000 (IB)	Jackson ImmunoResearch Laboratories, Inc.
HRPO anti-rabbit IgGs	goat	1:20000 (IB)	Jackson ImmunoResearch Laboratories, Inc.
Rhodamine red anti-mouse IgGs	donkey	1:200 (IFM)	Jackson ImmunoResearch Laboratories, Inc.
Rhodamine red anti-rabbit IgGs	donkey	1:100 (IFM)	Jackson ImmunoResearch Laboratories, Inc.
Texas red anti-mouse IgGs	goat	1:200 (IFM)	Jackson ImmunoResearch Laboratories, Inc.
Texas red anti-mouse IgGs	donkey	1:200 (IFM)	Jackson ImmunoResearch Laboratories, Inc.
Texas red anti-rabbit IgGs	donkey	1:200 (IFM)	Jackson ImmunoResearch Laboratories, Inc.
Texas red anti-rat IgGs	goat	1:200 (IFM)	Jackson ImmunoResearch Laboratories, Inc.

DNA methods

5.1.1 Preparation of plasmid DNA

Plasmid DNA purification from bacteria was carried out using anion exchange JetStarTM resin

columns according to manufacturer's instructions (Genomed). Endotoxin-free plasmid DNA suitable for transfection of primary cells was isolated from bacteria using JetStar™ Endotoxin-free Plasmid kit.

5.1.2 Determination of DNA concentration

DNA concentration was calculated according to its optical density. Spectrophotometric measurements were performed at 260 nm. An optical density of 1 corresponds to a concentration of 50 µg/ml of double-stranded DNA.

Protein methods

5.1.3 Determination of concentration

Protein concentration was determined by colorimetric detection of the cuprous cation (Cu^{1+}) by bicinchoninic acid using the BCA™ Protein Assay kit (Pierce) according to manufacturer's instructions.

5.1.4 SDS-Polyacrilamide gel electrophoresis (PAGE)

Proteins were separated using standard SDS-6%, -10% or -12% PAGE (Laemmli, 1970). Gels were prepared using the Mini-PROTEAN® Electrophoresis System (Bio-Rad). First, the cassette was filled with resolving gel solution, overlaid with isopropanol and allowed to polymerize. Then, the stacking gel was poured on the top of the resolving gel, and a comb was inserted to allow sample loading. Samples were boiled at 95°C during 5 min prior to loading into the gel slots. Gels were run at 25 mAmp/gel and 500 V.

Buffers and solutions:

- 5x SDS Laemmli sample buffer:
 - Tris-HCl, pH 6.8 ----- 125 mM
 - DDT ----- 250 mM
 - SDS ----- 5%

- Bromophenol-Blue ----- 0.25%
- Glycerol ----- 25%
- SDS-PAGE running buffer:
 - Tris ----- 25 mM
 - Glycine ----- 250 mM
 - SDS ----- 0.1%
- 30% Acrylamide mix (29:1):
 - Acrylamide----- 29 g
 - Bis-acrylamide ----- 1 g
 - ddH₂O up to 100 ml

5.1.5 Coomassie staining

Gels were stained after electrophoresis by incubation with Coomassie staining solution. After adding the solution, gels were warm up in the microwave for 10 s and incubated at room temperature for 15 min. Then, gels were destained with destaining solution during 1 h at room temperature or at 4°C overnight.

Solutions:

- Coomassie staining solution:
 - Coomassie R-250 (Sigma-Aldrich) ----- 0.05% (w/v)
 - Methanol----- 40%
 - Acetic acid ----- 7%
 - ddH₂O ----- 53%
- Destaining solution:
 - Acetic acid ----- 10%
 - Methanol ----- 30%
 - ddH₂O ----- 60%

5.1.6 Immunoblotting

After electrophoresis, gels were electrophoretically transferred onto nitrocellulose membranes at 25 V, 4°C, overnight, or 100 V, 4°C for 2 h. Then, the transfer efficiency was tested by staining with Ponceau S (Sigma-Aldrich) and washed with ddH₂O. Membranes were blocked

for 30 min, incubated with primary antibodies diluted in PBST at room temperature for 1h or at 4°C overnight, wash 2 x 15 min with PBST, incubated with secondary antibodies diluted in PBST at room temperature for 1h and washed 2 x 15 min with PBST. Detection was carried out using the SuperSignal West Pico Chemiluminescent Substrate (Pierce) and exposing the membranes to an X-ray sensitive film (Fuji).

Buffers and solutions:

- Blot Buffer:
 - Tris ----- 48 mM
 - Glycine ----- 40 mM
 - SDS ----- 0.1%
- PBS (phosphate buffered saline):
 - NaCl ----- 8.18 g
 - KCl ----- 0.201 g
 - KH_2PO_4 ----- 0.204 g
 - $\text{Na}_2\text{H}_2\text{PO}_4$ ----- 1.132 g
 - pH 7.4
 - ddH₂O up to 1000 ml
- PBST:
 - PBS containing 0.1% Tween-20
- Ponceau S staining solution:
 - Ponceau S (Sigma-Aldrich) ----- 0.5% (w/v)
 - Acetic acid ----- 1%
 - ddH₂O
- Blocking solution:
 - 5% non-fat dry milk in PBST

5.1.7 Quantification of protein bands on immunoblots

Densitometrical quantification of protein bands was performed after scanning the X-ray films on a flat-bed scanner using QuantiScan v1.5 software (Biosoft, Cambridge, UK).

5.1.8 Preparation of total cell and tissue lysates

Tissues were snap frozen in liquid nitrogen, pulverized and suspended in 1% Triton X-100, 0.5% NP-40, 150 mM NaCl, 20 mM Tris-HCl, pH7.5 supplemented with Complete Mini Protease Inhibitor Cocktail tablets (CMPI) (Roche). Cell lysates were prepared from confluent cultures and lyse in 1x PBS, 0.5% Triton X-100, 1 mM PMSF, 2 mM DTT.

5.1.9 Endogenous MT-binding assay

The protocol of this assay was based on a similar one described by Planel *et al*, 2008; except where indicated otherwise, all working steps were carried out above 20°C to prevent MT depolymerization. Brains isolated from mice were homogenized in 80 mM MES, pH 6.8, 1 mM MgCl₂, 2 mM EGTA, 30% glycerol, 0.1% Triton X-100, 1 mM PMSF, 1 mM Na₃VO₄, 1 mM NaF, and CMPI (Roche) using a mechanical tissue homogenizator. Lysates were centrifuged for 6 min at 16,000 x g to obtain supernatant fraction containing intact MTs. The MT fraction was centrifuged (20 min at 25°C) in a vacuum Optima™ TLX Ultracentrifuge (Beckman) at 40,000 rpm (100000 x g) to obtain a MT-free supernatant and a MT-containing pellet fraction. MTs in the pellet fraction were resuspend in 100 mM MES pH 6.5, 0.5 mM MgSO₄, 30% glycerol, 1 mM EGTA, 0.1% Triton X-100, 1 mM Na₃VO₄, 1 mM NaF, 2 mM DTT, 1 mM PMSF, and CMPI (Roche). Samples of both fractions were mixed with O+ buffer (O'Farrel, 1975) supplemented with CMPI (Roche) and boiled 5 min prior to immunoblotting. Tau levels were analyzed by immunoblotting MT-free and MT-containing fractions.

5.1.10 RhoA pull down assay

pGEX-2T-RBD culture

100 ml LB medium were inoculated with pGEX-2T-RBD (GST-RBD) bacterial stock (DH5α), and let it grow at 37°C overnight. GST-RBD fusion protein encodes the Rho-binding domain of

Rhotekin, used as an activation specific probe for RhoA-GTP.

- LB medium (Luria-Bertani medium):
 - Bacto-tryptone ----- 1% (w/v)
 - Bacto-yeast extract ----- 0.5% (w/v)
 - NaCl ----- 1% (w/v)
 - pH 7.5
 - ddH₂O up to 1000 ml

pGEX-2T-RBD: Growth and Induction

300 ml LB medium were inoculated with 400 µl of overnight bacterial stock supplemented with corresponding antibiotics and 15 ml glucose and incubated at 37°C until the culture reaches OD₆₀₀ of 0.7 to 0.8. Protein expression was induced by adding 0.5 mM IPTG and culture was incubated at 30°C for 2-4 h. Cells were harvested by centrifugation at 10000 x g (Heraeus centrifuge) during 15 min at 4°C. Pellets were shock freeze in liquid nitrogen and store at -80°C.

pGEX-2T-RBD: Cell lysis

Bacteria pellets were resuspended in 4.5 ml ice-cold STE-Buffer supplemented with 1 mM PMSF and homogenized using a 19G needle. Suspensions were supplemented with lysozyme, 5 mM DTT, 1% Tween-20, 0.03% SDS and centrifuged at 16000 xg for 20 min at 4°C.

- STE Buffer:
 - Tris, pH 8.0 ----- 10 mM
 - NaCl ----- 150 mM
 - EDTA ----- 10 mM EDTA

Purification of GST-Rhotekin-BD (GST-RBD)

Glutathione Sepharose™ 4B (GE, Healthcare) is supplied as 75%, in order to prepare 50% slurry the bottle of Glutathione Sepharose 4B slurry was gently shaken, 399 µl of 75% slurry for 300 µl desired volume were taken and centrifuged at 500 xg for 5 min at room temperature. Supernatant was discarded and 1 ml STE Buffer was added to remove ethanol after 2x centrifugation at 500 xg for 5 min at room temperature. 5ml from the previously obtained lysates was added to the 300 µl 50% slurry and mixed gently for 30 min at 4°C. Then the mixed was washed 3 x with 5ml ice-cold STE Buffer by centrifuging at 500 xg for 5 min at 4°C. Pellets were resuspended in 120 µl of STE buffer, aliquoted into 30-35 µl and stored at -80°C until use on pull down assay.

RhoA pull down assay

Brain was lysed in 500 µl ice-cold pull down lysis buffer, transferred to pre-chilled eppendorf tubes and centrifuge at 14000 x g for 5 min at 4°C. Pre-cleared lysates were transferred into new pre-chilled tubes with 30 -35 µl of GST-RBD (30-45 µg) and incubated for 1 h at 4°C. Then, the samples were spun down at 700xg for 3 min at 4°C and washed 2x with 600 µl ice-cold 1 x Mg²⁺Buffer. RhoA was eluted from beads with 45 µl of 2x SDS sample buffer and boiled for 5 min at 95°C. Samples were loaded on SDS 15%-PAGE gels.

- Pull down lysis buffer:
 - Hepes/HCl ----- 25 mM
 - NaCl ----- 150 mM
 - MgCl₂ ----- 10 mM
 - NP-40 ----- 1%
 - PMSF ----- 100 µM
 - CMPI (Roche)
 - ddH₂O

- 1x Mg²⁺ Buffer:
 - NaF ----- 25 mM
 - Aprotinine ----- 10 µg/ml
 - Benzamidine ----- 10 µg/ml
 - Glycerol ----- 10%
 - PMSF ----- 100 µM
 - ddH₂O

5.1.11 Extraction of sarcosyl-insoluble tau

Extraction of sarcosyl-insoluble tau was carried similarly as described (Greenberg & Davies, 1990). In brief, the brain tissue was homogenized in 3 volumes of cold Buffer H and centrifuged at 27000 g for 20 min at 4°C (21000 rpm with TLA-45 rotor). The supernatant was collected and the resulting pellet was homogenized in buffer H. The homogenization was centrifuged at 27000 g for 20 min at 4°C (21000 rpm with TLA-45 rotor). The supernatant obtained was collected and combined with the one resulting from the first centrifugation. N-lauroylsarcosine was added to the supernatant at 1% (w and/v) final concentration and then incubated at 37°C shaking for 60-90 min. The samples were centrifuged at 150000g for 35 min at 20°C (58800 rpm TLA 120.2 rotor) and the resulting pellets were resuspended in 50 mM Tris-HCl, pH 7.4, using 0.5 µl of buffer per mg of initial weight. The samples were diluted in SDS sample buffer, boiled at 95°C for 5 min and loaded in SDS-15% gels at a ration 1:2 (soluble: insoluble). Sarcosyl-insoluble tau was evaluated after immunoblotting using tau antibodies.

- Buffer H:
 - Tris-HCl ----- 10 mM
 - EGTA ----- 1 mM
 - NaCl ----- 0.8 M
 - Sucrose ----- 10%
 - pH = 7.4

Mammalian cell culture

5.1.12 Cultivation of p53^{-/-} keratinocytes

Immortalized plectin wt and P0 mouse keratinocytes cell cultures were obtained from plectin wt/p53^{-/-} and P0/p53^{-/-} mice (Andr  et al, 2003). Wt and P0 p53^{-/-} keratinocytes were cultured on 100 µg/ml bovine collagen I (Sigma-Aldrich®)-coated plastic dishes (Nunc) using keratinocyte growth medium (KGM). Cultivation was done at 37°C in a humidified atmosphere of 5% CO₂. Cells were let grow until 80-90% confluency before splitting. Splitting of cells was carried out using strong trypsin solution for 8-10 min at 37°C. Then, cells were spun down at 200 xg for 3 min at room temperature. Supernatant was discarded, cell pellet resuspended in KGM and plated.

- Keratinocyte growth medium:
 - KBMTM w/o Ca²⁺ (Lonza) ----- 500 ml
 - KGMTM BulletKitTM w/o Ca²⁺ (Lonza):
 - BPE (bovine pituitary extract) ----- 2ml
 - hEGF (human epidermal growth factor) --- 0.5 ml
 - Insulin (recombinant human) ----- 0.5 ml
 - Hydrocortisone ----- 0.5 ml
 - GA-1000(gentamicin, amphotericin B) ---- 0.5 ml
 - Chelex-treated FCS (Gibco®) ----- 2%
 - ITS (Insulin-Transferrin-Selenium) (Gibco®) ----- 1%
 - CaCl₂ ----- 0.05 mM
- Chelex- (Gibco®) treated fetal calf serum (FCS) (Sigma-Aldrich):
 - 20 g of Chelex to 200 ml ddH₂O
 - adjust pH to 7.4 overnight
 - place Chelex for 1h at 4°C to form a compact pellet
 - add Chelex to 50 ml FCS
 - stir for 1h at 4°C
 - place the mixture for 1h at 4°C to form a compact Chelex pellet
 - decant serum through a bottle top filter into an autoclaved glass bottle

- Strong trypsin solution:
 - 0.25% Trypsin (Gibco®)
 - 0.37 mg/mol EDTA
 - HBSS (Gibco®)

5.1.13 Isolation of primary keratinocytes

Primary keratinocytes were isolated from newborn mice skin or adult tail skin. Skins were flatten and put dermis-side down on Dispase II solution (Roche) for 1h at 37°C or on strong trypsin solution at 4°C overnight. After incubation, epidermis was separated from dermis and minced into small pieces with two scalpels. Cells were dissociated from tissue by incubation in 3 ml strong trypsin solution under shaking conditions at 37°C for 8 min (newborn mices) or 6 min (adult mice). Epidermal pieces were resuspended by pipetting up and down 60 times and then filtered through a 70 µm mesh of a cell strainer attached to a 50 ml tube filled with 40 ml of KGM at 4°C to remove pieces of stratum corneum. Suspension was centrifuged 150 g for 7 min at room temperature. Supernatant was discarded, cell pellet was resuspend in KGM-Gold medium and cell suspension was plated on collagen-I-coated dishes. Primary keratinocytes cultivation was performed as described previously.

- Dispase II solution (Roche):
 - 10 mg/ml of dispase II (Roche) in KBM™ (CC-3112, Lonza)
- Keratinocyte growth medium (KGM)-Gold:
 - KBM-Gold™ w/o Ca²⁺ (Lonza) ----- 500 ml
 - KGM-Gold™ BulletKit™ (CC-3111, Lonza):
 - BPE (bovine pituitary extract) ----- 2ml
 - hEGF (human epidermal growth factor) --- 0.5 ml
 - Insulin (recombinant human) ----- 0.5 ml
 - Hydrocortisone ----- 0.5 ml
 - GA-1000 (gentamicin, amphotericin B) ---- 0.5 ml
 - Epinephrin ----- 0.25 ml
 - Transferrin ----- 0.5 ml

- Chelex-(Gibco®) treated FCS (Sigma-Aldrich) ----- 8%
- ITS (Insulin-Transferrin-Selenium) (Gibco®) ----- 1%
- CaCl_2 ----- 0.05 mM

5.1.14 Isolation and cultivation of DRG neurons

DRG neuron isolation was performed similarly as described by Stroissnigg *et al*, 2007. DRGs of adult mice were dissected and harvested in ice-cold RPMI 1640 (Gibco®) medium, cut into small pieces before enzymatic dissociation by 4000 U/ml collagenase solution (SERVA Electrophoresis, GmbH) for 90 min at 37°C followed by treatment with normal trypsin solution supplemented with DNase I (Sigma-Aldrich) for 7-15 min at 37 °C. Trypsinization was inhibited adding stop solution, and finally the DRGs were triturated several times through a narrowed Pasteur pipette. Suspension was spun down at 120xg 5 min, resuspended in growth medium and plated onto precoated coverslips with poly-L-lysine (10 µg/ml in ddH₂O; Sigma-Aldrich) overnight at 37 °C, followed by laminin (10 µg/ml in PBS; at least 3 h at 37 °C; Sigma-Aldrich). DRG neurons were cultivated at 37°C in a humidified atmosphere of 5% CO₂.

Media and solutions:

- Collagenase solution (1 ml/mice):
 - 200 µl collagenase (4000 U/ml, Sigma-Aldrich)
 - 20 µl horse serum (Gibco®)
 - 780 µl RPMI 1640 (Gibco®)
- Trypsin solution (1 ml/mice):
 - 500 µl normal trypsin solution
 - 20 µl DNase I (Roche)
- Stop solution (2 ml/mice):
 - 400 µl horse serum (Gibco®)
 - 1.6 ml RPMI 1640 (Gibco®)

- Growth medium (2 ml/mice):
 - 10 µl penicillin/streptomycin (5000 U/ml-5000 µg/ml, Gibco®)
 - 100 µl horse serum (Gibco®)
 - 35.5 µl glucose (50%)
 - 35.5 µl N3 mix
 - 1840 µl RPMI 1640 Gibco®
- Normal trypsin solution:
 - 0.05% Trypsin (Gibco®)
 - 0.2 mg/mol EDTA
 - HBSS (Gibco®)
- 57x N3 mix (Bottenstein and Sato, 1979):
 - 1 mg/ml BSA fraction V in HBSS (PAA)
 - 10 mg/ml apotransferrin in HBSS (T1147, Sigma-Aldrich®)
 - 1 µg/ml Na-Selenit in HBSS (S9133, T1147, Sigma-Aldrich®)
 - 3.2 mg/ml putrescine in HBSS (P5780, Sigma-Aldrich®)
 - 1.25 µg/ml progesterone in EtOH (P6149, Sigma-Aldrich®)
 - 4 µg/ml corticosterone in EtOH (C2505, Sigma-Aldrich®)
 - 2 µg/ml tri-iodothyronine in 0.01% NaOH (T6397, Sigma-Aldrich®)
 - 1 mg/ml insulin (I6634, Sigma-Aldrich®)
 - HBSS - Ca²⁺ - Mg²⁺ (Gibco®)

5.1.15 Freezing and thawing of cells

Cells were frozen in freezing solution containing 90% FCS (Sigma-Aldrich) and 10% DMSO, kept at -80°C for 24h and then transfer to liquid nitrogen for long-term storage. Thawing of cells were done diluting the frozen aliquots in 15 ml of growth medium, spinning down at 200 xg for 3 min, resuspending the cell pellets in growth medium and plating the cells in appropriate medium.

5.1.16 Transient transfection

FuGene6 (Roche)

FuGENE6 Transfection Reagent (Roche) is a lipid-base transfection reagent used to transfect cell lines. For transfecting 35 mm dishes, 200 µl of medium without serum or growth factors

were added into polystyrene tubes (do not use polypropylene tubes). 8 µl of room temperature pre-warmed FuGENE6 reagent was added directly into the medium and tap gently to mix. Then, 5 µg of DNA were added and tap gently again to mix the contents. The mixture was incubated for 30 min at room temperature. After incubation, 300 µl of serum-free medium were added and the solution was dropwise added onto the cells. Cells were plated and allowed to grow to 60-70% confluency in the presence of growth medium.

Nanofectin (PAA)

Nanofectin (PAA) consists of a positively charged polymer with a high DNA-binding capacity, which is embedded into a porous nanoparticle that is optimized for the endocytosis machinery of the cell. Transfection of cell lines was done following manufacture's instructions. DNA and nanofecting diluted in Diluent (1:50) were mixed in a 1:32 proportion. The mixture was incubated for 15 to 30 min at room temperature and added drop wise onto the cells. Prior transfection cells were plated and allowed to grow to 70-80% confluency in the presence of growth medium.

Nucleofector™ Technology (Lonza)

Nucleofector™ Technology (Lonza) is especially designed for primary cell transfection. It is a non-viral method, which is based on a combination of electrical parameters and cell-type specific solutions.

Amaxa® human keratinocyte Nucleofector® kit

Primary keratinocytes were transiently transfected using the Amaxa® human keratinocyte Nucleofector® kit similarly to manufacturer's instructions. 7×10^5 cells per transfection were resuspended in 100 µl of human keratinocyte Nucleofector® solution and combined with 4-5 µg of endotoxin-free DNA. The cell/DNA suspension was transferred to a cuvette avoiding cell bubbles and the cuvette was inserted into the Nucleofector® cuvette holder. Program T-024 for high transfection efficiency was applied and immediately after transfection 500 µl of growth medium was added. The transfected cell suspension was gently plated onto plastic dishes.

Amaxa[®] basic neuron SCN Nucleofector[®] kit

Primary DRG neurons were transiently transfected using the Amaxa[®] basic neuron SCN Nucleofector[®] kit similarly to manufacturer's instructions. 2×10^4 cells per transfection were resuspended in 20 μ l of basic neuron SCN Nucleofector[®] solution and combined with 0.5-1 μ g of endotoxin-free DNA. The cell/DNA suspension was transferred to a cuvette avoiding cell bubbles and the cuvette was inserted into the Nucleofector[®] cuvette holder. Program SCN basic neuro program 6 was applied and immediately after transfection 500 μ l of growth medium was added. The cuvette containing the cell suspension was placed inside an incubator to avoid high mortality. After 5-10 min incubation the transfected cell suspension was gently plated onto coverslips.

5.1.17 Nocodazole and colchicine treatment

To assess MT stability, cells were kept in culture medium supplemented with 1 μ M nocodazole in DMSO (Sigma-Aldrich) or 10 μ M colchicine in DMSO (Sigma-Aldrich) for 30 min in the case of keratinocytes or 3 min in the case of DRG neurons, before being fixed and processed for microscopy. Immunolabeled single MTs remaining in nocodazole-treated cells were traced, their length measured using LSM software (Zeiss), and normalized to total cell area.

5.1.18 Oxidative stress

Oxidative stress of DRG neurons was tested treating primary DRG neurons with 250 μ M H₂O₂ for 5 min before being fixed and processed for microscopy. After visualization by confocal microscopy, oxidative stress was quantified as the proportion of collapse growth cones (bulb-shaped growth cones) to the total number of growth cones and comparing the results obtained from wt and P1c^{-/-} DRG neurons.

5.1.19 DRG explants

DRGs of adult mice were dissected and harvested in ice-cold RPMI 1640 (Gibco[®]) medium and cut in half. Half-cut DRG explants were placed on 5-10 μ l drops of ice-cold matrigel (BD-Science) onto uncoated coverslips and completely covered with 10 μ l matrigel drop.

5.1.20 2-NBDG uptake

Primary mouse keratinocytes and DRG neurons were incubated with 600 μ M 2-NBDG (Invitrogen) for 15 min following the protocol described by Yamada *et al*, 2000. Fluorescence intensities of 2-NBDG were collected using a confocal microscope and after background subtraction, fluorescence intensity was measured using ImageJ software (NIH Image, Bethesda, MD).

5.1.21 Na⁺ uptake

Na⁺ uptake of primary DRG neurons was measured using CoroNa Green Na⁺ Indicator (Invitrogen). CoroNa Green dye is a Na⁺ indicator that exhibits an increase in fluorescence intensity upon binding Na⁺ (excitation/emission = 492/516 nm). Cells were loaded by adding 1 μ M CoroNa Green Na⁺ in DMSO (Invitrogen), incubated for 10 min at 37°C and washed with dye-free medium. Fluorescence intensities of CoroNa Green Na⁺ Indicator (Invitrogen) were collected using a confocal microscope and after background subtraction, and measured using ImageJ software (NIH Image, Bethesda, MD).

5.1.22 Synaptic vesicle exocytosis and endocytosis with FM dyes

Visualization of synaptic vesicles exocytosis and endocytosis was performed similarly as described by Gaffield & Betz (2006). Cells were treated with 15 μ M FM1-43 (Invitrogen) diluted in high K⁺ Ringer solution to trigger synaptic vesicle recycling for 10 min at 37°C and washed 3 x 5 min normal Ringer solution before performing time-lapse microscopy.

- High K⁺ Ringer solution:
 - NaCl ----- 31.5 mM
 - KCl ----- 90 mM
 - CaCl₂ ----- 2 mM
 - MgCl₂ ----- 2 mM
 - Glucose ----- 30 mM
 - Hepes ----- 25 mM
 - pH 7.3

- Normal Ringer solution:
 - NaCl ----- 119 mM
 - KCl ----- 2.5 mM
 - CaCl₂ ----- 2 mM
 - MgCl₂ ----- 2 mM
 - Glucose ----- 30 mM
 - Hepes ----- 25 mM
 - pH 7.3

5.1.23 Current clamp electrophysiology

Electrophysiology experiments were performed by A. Yousuf and K. Schicker at S. Böhm laboratory (Centre for Physiology and Pharmacology, Medical University of Vienna). DRG neuronal current potentials were recorded by current clamp technique at room temperature after 1 to 2 days in culture. Measurements were carried out using Axopatch 200B amplifier and the pCLAP 8.1 hard- and software (Molecular Devices, Sunnyvale, CA) as described by A. Yousuf *et al*, 2011.

Microscopy

5.1.24 Immunolabeling for immunofluorescence microscopy

Keratinocyte cell cultures were rinsed (1 min) with pre-warmed (37°C) 60 mM PIPES, pH 6.9, 25 mM HEPES, 10 mM EGTA, and 2 mM MgCl₂ (MT-stabilizing solution). Cells were then fixed with 2.5% PFA, quenched with 0.1 M glycine, permeabilized with 0.1% Triton X-100, and block with 5% BSA in PBS for 1h at room temperature. After blocking cells were immunolabeled incubating with primary antibodies previously described diluted in 3% BSA in PBS for 1h at room temperature. Then, cells were washed 3 x 10 min with PBS and incubated with corresponding secondary antibodies diluted in PBS for 1h at room temperature. After 3 x 10 min washing with PBS, cells were mounted in mowiol 4-88 (Hoechst).

Primary DRG neurons were fixed with pre-warmed (37°C) 4%PFA in 22% sucrose solution added directly to growth medium for 45 min at room temperature. Cells were then washed 3 x 5 min with PBS and blocked with 10% BSA, 0.3% Triton X-100 for 1h at room temperature. After blocking cells were incubated with primary antibody diluted in 5% BSA, 0.15% Triton X-100 for 3h at room temperature or overnight at 4°C and then washed 3 x 5 min with PBS. Cells were then incubated with secondary antibody diluted in PBS for 2h at room temperature, washed 3 x 5 min with PBS and mount in mowiol 4-88 (Hoechst).

5.1.25 Confocal microscopy

Microscopy was performed at room temperature using a confocal microscope (Zeiss, LSM 510) equipped with a Plan-Apochromat 63x 1.4 NA or 100x 1.4 NA objective lens. Images were recorded using the LSM 510 module and the LSM software.

5.1.26 Wide-field microscopy

Wide-field microscopy was performed at room temperature using a DeltaVision Image Restoration microscope system (Applied Precision Instruments, LLC, Issaquah, WA, USA), equipped with a Plan-Apochromat 60x1.4 NA objective lens or using an AxioObserver Z1 microscope coupled to AxioCam MRm (Carl Zeiss MicroImaging) equipped with phase contrast optics. Images were acquired with softWoRx software (Applied Precision Instruments) and Zeiss AxioVision 4.8.1. software respectively.

5.1.27 Deconvolution

Acquired pictures were deconvolved using 3D Huygens Deconvolution & Analysis software (Scientific Volume Imaging) or using softWoRx software (Applied Precision Instruments).

5.1.28 Time-lapse video microscopy

Visualization of MT dynamics

Cells expressing GFP-EB1 or EGFP-tubulin were kept in a closed POCmini cultivation system (Zeiss), and live-cell imaging was performed using an inverted microscope (Zeiss, Axiovert S100TV) at 37°C and in a humidified atmosphere of 5% CO₂. Frames of GFP-EB1 and EGFP-tubulin were collected with a Plan-Apochromat 100x 1.4 NA objective lens every 2 s during 5 min. Individual comets or MTs were traced using Metamorph 6.3 software (MDS Analytical Technologies).

Visualization of FA dynamics

Cells expressing EGFP-zyxin were kept in a closed POCmini cultivation system (Zeiss), and live-cell imaging was performed using an inverted microscope (Zeiss, Axiovert S100TV) at 37°C and in a humidified atmosphere of 5% CO₂. Frames of EGFP-zyxin images were acquired every 2 min during 30 min. Individual FAs were tracked using Metamorph 6.3 software (MDS Analytical Technologies).

Single cell migration

Migrating keratinocytes were recorded using an AxioObserver Z1 microscope coupled to AxioCam MRm (Carl Zeiss MicroImaging) equipped with phase contrast optics at 37°C and humidified atmosphere of 5% CO₂. Frames were taken with an EC Plan-Neofluar 10x/0.3NA objective lens in 7 min intervals over a period of 12 h. Images were processed with Zeiss AxioVision 4.8.1 image analysis software and further analyzed with ImageJ software (NIH Image, Bethesda, MD) for manual tracking of migrating cells. To track the whole cell trajectory, cell nuclei were marked for each frame throughout the entire time-lapse sequence.

Visualization of synaptic vesicles

Cells stained with FM1-43 (Invitrogen) were kept in a closed POCmini cultivation system (Zeiss), and live-cell imaging was performed using an inverted microscope (Zeiss, Axiovert S100TV) at 37°C and in a humidified atmosphere of 5% CO₂. Frames of FM1-43 images were acquired every 2 s during 15 min. Individual synaptic vesicles were tracked using Metamorph 6.3 software (MDS Analytical Technologies).

Growth cone extension

Extending growth cones were recorded using an AxioObserver Z1 microscope coupled to AxioCam MRm (Carl Zeiss MicroImaging) equipped with phase contrast optics at 37°C and humidified atmosphere of 5% CO₂. Frames were taken with a LD A Plan 32x/0.4 NA objective lens in 10 min intervals over periods from 5 h to 12h. Images were processed with Zeiss AxioVision 4.8.1 image analysis software and further analyzed with ImageJ software (NIH Image, Bethesda, MD) for manual tracking of migrating cells.

5.1.29 Image processing and semiquantification

Images were subjected equally across the entire image to minimum degree of Gaussian filter or histogram stretch necessary to facilitate visualization using ImageJ software (NIH Image, Bethesda, MD), LSM software (Zeiss), softWoRx software (Applied Precision Instruments) or AxioVision 4.8.1. software (Zeiss).

The proportion of acetylated to total tubulin in MTs was measured in double labeled specimens by selecting acetylated tubulin-positive and tubulin-positive areas (in pixels) using the magic wand tool in Adobe® Photoshop® CS2 and keeping the tolerance constant. Immunolabeled GLUT1 and Na⁺ clusters were counted and measured using ImageJ software (NIH Image, Bethesda, MD) and values normalized to cell area after GLUT1 immunolabeling.

Statistical analyses

Comparisons between values of two groups were made using Student's t-test, Wilcoxon-Mann-Whitney U-test or Chi-square test ($\alpha=0.001-0.10$). Comparisons among values of multiple groups were performed using one-way analysis of variance (ANOVA) ($\alpha=0.001-0.10$). The significance between the individual groups was subsequently determined using the Tukey post-hoc test ($\alpha=0.05$). Analyses were performed using SPSS Statistics v.19 (IBM®).

LIST OF FIGURES AND TABLES

Figure 1. Schematic representation of MT dynamics.....	21
Figure 2. Schematic representation of MAPs.....	23
Figure 3. Mammalian cytolinker proteins.....	26
Figure 4. Model of MT-regulating proteins and PTMs.....	27
Figure 5 Scheme representing actin-MT crosstalk.....	33
Figure 6. Domain map of plectin.....	35
Figure 7. Transcripts generated by alternative splicing at the 5'-end of the plectin gene.....	36
Figure 8. Simplified representation of plectin's function as organizer of fibroblast cytoarchitecture.....	38
Figure 9. Model depicting the role of plectin in skeletal muscle fibers.....	39
Figure 10. Tissue distribution of murine exon 1c.....	41
Figure 11. Scheme representing positional mapping of plectin mutations	42
Figure 12. P1c interacts with MTs.....	43
Figure 13. Plectin's SH3 domain (fragment p20-21) compromises recombinant MAP-MT interaction.....	45
Figure 14. P1c deficiency affects drug resistance of keratinocyte MTs.....	49
Figure 15. P1c deficiency affects acetylation of keratinocyte MTs.....	50
Figure 16. P1c variants lacking the IF-binding domain fail to rescue nocodazole sensitivity in P1c-deficient keratinocytes.....	51

Figure 17. P1c variants lacking the IF-binding domain fail to reverse increased MT acetylation in P1c-deficient keratinocytes.....	53
Figure 18. P1c affects dynamic properties of MTs.	54
Figure 19. Time-lapse images of GFP-EB1 comets in wt and P0 keratinocytes.....	55
Figure 20. Sequence of single frame images taken from a time-lapse recording of GFP-EB1-expressing wt and P0 keratinocytes.....	56
Figure 21 Time-lapse images of representative single EB1 comets	56
Figure 22. Alterations of glucose uptake in plectin-deficient keratinocytes.....	57
Figure 23. GLUT1 expression on keratinocytes.....	58
Figure 24. Alterations in mitotic spindle formation and cellular growth rate in plectin1c-deficient keratinocytes.....	59
Figure 25. Statistical evaluation of keratinocyte shape and migration.....	61
Figure 26. Loss of P1c affects polarized migration of keratinocytes.....	62
Figure 27. Loss of P1c alters FA dynamics and stability.....	64
Figure 28. Tau and MAP2 are expressed in keratinocytes.....	65
Figure 29. Keratinocytes expressed tau and MAP2 at mRNA levels.....	65
Figure 30. Skin sections are immunoreactive with anti- tau and MAP2 antibodies.....	67
Figure 31. MAP2-MT colocalization in wt and P1c ^{-/-} keratinocytes.....	67
Figure 32. P1c affects drug resistance and stability of neuronal MTs.....	70
Figure 33. P1c affects MT acetylation in DRG neurons.....	71
Figure 34. Tau is increased in the MT-bound fraction in P1c-deficient brain lysates.....	73

Figure 35. P1c affects MT growth rate of DRG neurons.....	74
Figure 36. P1c deficiency leads to faster growth cone extension.....	75
Figure 37. Lack of P1c in DRG neurons affects IF localization.....	76
Figure 38. Lack of P1c impairs neurite outgrowth.....	77
Figure 39. P1c deficiency causes decreased neurite branching.....	78
Figure 40. P1c-deficiency barely affects the activation of RhoA.....	79
Figure 41. Alterations of glucose uptake in P1c-deficient DRG neurons.....	80
Figure 42. Neurites of P1c ^{-/-} DRG neurons are highly sensitive to oxidative stress.....	81
Figure 43. P1c deficiency impairs anterograde synaptic vesicle transport.....	82
Figure 44. P1c deficiency does not alter intracellular Na ⁺ concentration.....	83
Figure 45. Clustering of P1c ^{-/-} Na ⁺ channels in P1c ^{-/-}	84
Figure 46. P1c deficiency causes a wide range of membrane potential	85
Figure 47. Sarcosyl-insoluble P1c ^{-/-} fraction lysates contain reduced levels of tau.....	86
Figure 48. Model depicting plectin as MT destabilizer.....	89
Table 1. Primary antibodies and dyes used for immunofluorescence microscopy (IFM) and immunoblotting (IB).....	96
Table 2. Secondary antibodies used in immunofluorescence microscopy (IFM) and immunoblotting (IB). Horseadish peroxidase (HRPO).....	98

ABBREVIATIONS

2-NBDG	2-[N-(7-nitrobenz-2-oxa-1,3-diazol-4-yl) amino]-2-deoxy-D-glucose
ABD	actin-binding domain
ACF7	microtubule-actin crosslinking factor 7
AIS	axon initial segment
BCA	bicinchoninic acid
BPAG1	bullous pemphigoid antigen 1
BPE	bovine pituitary extract
BSA	bovine serum albumin
cAMP	cyclic adenosine monophosphate
cDNA	complementary deoxyribonucleic acid
cdc2	cell division control protein 2
CH	calponin-homology domain
CMPI	complete mini protease inhibitor
DDT	dithiothreitol
DMSO	dimethyl sulfoxide
DNA	deoxyribonucleic acid
DRG	dorsal root ganglia
EB1	end-binding protein 1
EBS	epidermolysis bullosa simplex

EBS-MD	epidermolysis bullosa simplex with muscular dystrophy
EGFP	enhanced green fluorescent protein
EtOH	ethanol
FA	focal adhesion
FbA	fibrillar adhesion
GA-1000	gentamicin, amphotericin B
GAPDH	glyceraldehyde 3-phosphate dehydrogenase
GAR	gas2-homology region
GC	globular carboxy-terminal domain
GFAP	glial fibrillary acidic protein
GFP	green fluorescence protein
GLUT1	glucose transporter 1
GLUT3	glucose transporter 3
GN	globular amino-terminal domain
GST	glutathione S-transferase
GTP	guanosine-5'-triphosphate
hEGF	human epidermal growth factor
EDTA	ethylenediaminetetraacetic acid
EGTA	ethylene glycol tetraacetic acid
ER	endoplasmic reticulum

FCS	fetal calf serum
HBSS	Hank's buffered salt solution
HD	hemidesmosome
Hepes	4-(2-hydroxyethyl)-1-piperazineethanesulfonic acid
HMW	high molecular weight
HS-SN	high-speed supernatant
HS-P	high-speed pellet
IB	immunoblotting
IF	intermediate filament
IFM	immunofluorescence microscopy
IPTG	isopropyl β -D-1-thiogalactopyranoside
ITS	insulin-transferrin-selenium
KBM	keratinocyte basal medium
KGM	keratinocyte growth medium
LB	Luria-Bertani
MACF	microtubule-actin crosslinking factor 7
MAP	microtubule associated protein
MCK	muscle creatine kinase
MES	2-(N-morpholino)-ethanesulfonic acid
MT	microtubule

NF	neurofilaments
NP-40	nonyl phenoxypolyethoxylethanol 40
RPMI	Roswell Park Memorial Institute
SDS	sodium dodecyl sulfate
SDS-PAGE	SDS-polyacrylamide-gel electrophoresis
SH	Src homology domain
SR	spectrin repeat
STE	sodium chloride-tris-EDTA
P	pellet
P0	plectin-null
P1	plectin 1
P1a	plectin 1a
P1b	plectin 1b
P1c	plectin 1c
P1c ^{-/-}	plectin 1c-deficiency
P1d	plectin 1d
P1f	plectin 1f
PBS	phosphate buffered saline
PBST	phosphate buffered saline-tween
PFA	paraformaldehyde

PIPES	piperazine-N,N'-bis(2-ethanesulfonic acid)
PMSF	phenyl-methyl-sulfonyl-fluoride
PMT	post-translation modifications
PRD	plakin repeat domain
RBD	rhotekin-binding domain
S	supernatant
Tris	tris-(hydroxymethyl) aminomethane
Wt	wild-type

REFERENCES

- Abal M, Piel M, Bouckson-Castaign V, Mogensen M, Sibarita JB, Bornens M (2002) Microtubule release from the centrosome in migrating cells *J Cell Biol* **159**: 731-737
- Abrahamsberg C, Fuchs P, Osmanagic-Myers S, Fischer I, Propst F, Elbe-Bürger A, Wiche G (2005) Targeted ablation of plectin isoform 1 uncovers role of cytolinker proteins in leukocyte recruitment *Proc Natl Acad Sci USA* **102**: 18449-18454
- Ackerl R, Walko G, Fuchs P, Fischer I, Schmuth M, Wiche G (2007) Conditional targeting of plectin in prenatal and adult mouse stratified epithelia causes keratinocyte fragility and lesional epidermal barrier defects *J Cell Sci* **120**: 2435-2443
- Al-Bassam J, Kim H, Brouhard G, van Oijen A, Harrison SC, Chang F (2010) CLASP promotes microtubule rescue by recruiting tubulin dimers to the microtubule *Dev Cell* **19**: 245–258
- Al-Bassam J, Ozer RS, Safer D, Halpain S, Milligan RA (2002) MAP2 and tau bind longitudinally along the outer ridges of microtubule protofilaments *J Cell Biol* **157**: 1187-1196
- Akhmanova A, Hoogenraad CC, Drabek K, Stepanova T, Dortland B, Verkerk T, Vermeulen W, Burgering BM, De Zeeuw CI, Grosveld F, Galjart N (2001) CLASPs are CLIP-115 and -170 associating proteins involved in the regional regulation of microtubule dynamics in motile fibroblasts *Cell* **104**: 923–935
- Akhmanova A, Steinmetz MO (2008) Tracking the ends: a dynamic protein network controls the fate of microtubule tips. *Nat Rev Mol Cell Biol* **9**: 309-322
- Andrä K, Kornacker I, Jörgl A, Zörer M, Spazierer D, Fuchs P, Fischer I, Wiche G (2003) Plectin-isoform-specific rescue of hemidesmosomal defects in plectin (–/–) keratinocytes *J*

Invest Dermatol **120**: 189-197

Andrä K, Lassmann H, Bittner R, Shorny S, Fässler R, Propst F, Wiche G (1997) Targeted inactivation of plectin reveals essential function in maintaining the integrity of skin, muscle and heart cytoarchitecture *Genes Dev* **11**: 3143-3156

Andrä K, Nikolic B, Stöcher M, Drenckhahn D, Wiche G (1998) Not just scaffolding: plectin regulates actin dynamics in cultured cells *Genes Dev* **12**: 3442-3451

Andrews PD, Ovechkina Y, Morrice N, Wagenbach M, Duncan K, Wordeman L, Swedlow JR (2004) Aurora B regulates MCAK at the mitotic centromere *Dev Cell* **6**: 253–268

Angst BD, Nilles LA, Green KJ (1990) Desmoplakin II expression is not restricted to stratified epithelia *J Cell Sci* **97**: 247-257

Arce CA, Casale CH, Barra HS (2008) Submembraneous microtubule cytoskeleton: regulation of ATPases by interaction with acetylated tubulin *FEBS J* **275**:4664–4674

Avila J (2010) Intracellular and extracellular tau *Front Neurosci* **4**: 49

Avila J, Lucas JJ, Perez M, Hernandez F (2004) Role of tau protein in both physiological and pathological conditions *Physiol Rev* **84**: 361–384

Ballatore C, Lee VM, Trojanowski JQ (2007) Tau-mediated neurodegeneration in Alzheimer's disease and related disorders *Nat Rev Neurosci* **8**: 663-672

Ban R, Matsuzaki H, Akashi T, Sakashita G, Taniguchi H, Park SY, Tanaka H, Furukawa K, Urano T (2009) Mitotic regulation of the stability of microtubule plus-end tracking protein EB3 by ubiquitin ligase SIAH-1 and aurora mitotic kinases *J Biol Chem* **284**: 28367–28381

Belmont L, Mitchison T, Deacon HW (1996) Catastrophic revelations about Op18/stathmin *Trends Biochem Sci* **21**: 197-198

Bhat KM, Setaluri V (2007) Microtubule-associated proteins as targets in cancer chemotherapy

Clin Cancer Res **13**: 2849-2854

Biernat J, Gustke N, Drewes G, Mandelkow EM, Mandelkow E (1993) Phosphorylation of Ser²⁶² strongly reduces binding of tau to microtubules: distinction between PHF-like immunoreactivity and microtubule binding *Neuron* **11**: 153-163

Bonnet C, Boucher D, Lazereg S, Pedrotti B, Islam K, Denoulet P, Larcher JC (2001) Differential binding regulation of microtubule-associated proteins MAP1A, MAP1B, and MAP2 by tubulin polyglutamylation *J Biol Chem* **276**: 12839–12848

Bottenstein JE, Sato GH (1979) Growth of a rat neuroblastoma cell line in serum-free supplemented medium *Proc Natl Acad Sci* **76**: 514-517

Bowen JR, Hwang D, Bai X, Roy D, Spiliotis ET (2011) Septin GTPases spatially guide microtubule organization and plus end dynamics in polarizing epithelia *J Cell Biol* **194**: 187–197

Brouhard GJ, Stear JH, Noetzel TL, Al-Bassam J, Kinoshita K, Harrison SC, Howard J, Hyman AA (2008) XMAP215 is a processive microtubule polymerase *Cell* **132**: 79-88

Brown A, Bernier G, Mathieu M, Rossant J, Kothary R (1995) The mouse dystonia musculorum gene is a neural isoform of bullous pemphigoid antigen 1 *Nat Genet* **10**: 301-306

Bugnard E, Zaal KJM, Ralston E (2005) Reorganization of microtubule nucleation during muscle differentiation *Cell Motil Cytoskeleton* **60**: 1–13

Bulinski JC, Richards JE, Piperno G (1988) Posttranslational modifications of alpha tubulin: detyrosination and acetylation differentiate populations of interphase microtubules in cultured cells *J Cell Biol* **106**: 1213-1220

Burgstaller G, Gregor M, Winter L, Wiche G (2010) Keeping the vimentin network under control: cell-matrix adhesion-associated plectin 1f affects cell shape and polarity of

- fibroblasts *Mol Biol Cell* **21**: 3362-3375
- Carlsson L, Thornell LE (2001) Desmin-related myopathies in mice and man *Acta Physiol Scand* **171**: 341-348
- Casini S, Tan HL, Demirayak I, Remme CA, Amin AS, Scicluna BP, Chaytan H, Ruijter JM, Bezzina CR, van Ginneken ACG, Veldkamp MW (2009) Tubulin polymerization modifies cardiac sodium channel expression and gating *Cardiovasc Res* **85**:691–700
- Chhabra ES, Higgs HN (2007) The many faces of actin: matching assembly factors with cellular structures *Nat Cell Biol* **9**: 1110-1121
- Choi JH, Bertram PG, Drenan R, Carvalho J, Zhou HH, Zheng XF (2002) The FKBP12-rapamycin-associated protein (FRAP) is a CLIP-170 kinase *EMBO Rep* **3**: 988–994
- Chou YH, Bischoff JR, Beach D, Goldman RD (1990) Intermediate filament reorganization during mitosis is mediated by p34^{cdc2} phosphorylation of vimentin *Cell* **62**: 1063-1071
- Conde C, Cáceres A (2009) Microtubule assembly, organization and dynamics in axon and dendrites *Nat Rev Neurosci* **10**: 319-332
- Cook TA, Nagasaki T, Gundersen GG (1998) Rho guanosine triphosphatase mediates the selective stabilization of microtubules induced by lysophosphatidic acid *J Cell Biol* **141**: 175-185
- Dalpe G, Leclerc N, Vallee A, Messer A, Mathieu M, De Repentigny Y, Kothary R (1998) Dystonin is essential for maintaining neuronal cytoskeleton organization *Mol Cell Neurosci* **10**: 243-257
- Dalpe G, Mathieu M, Comtois A, Zhu E, Wasiak S, De Repentigny Y, Leclerc N, Rothary R (1999) Dystonin-deficient mice exhibit an intrinsic muscle weakness and an instability of skeletal muscle cytoarchitecture *Dev Biol* **210**: 367-380

- Dammermann A, Desai A, Oegema K (2003) The minus end in sight *Curr Biol* **13**: R614–R624
- de Forges H, Bouissou A, Perez F (2012) Interplay between microtubule dynamics and intracellular organization *Int J Biochem Cell Biol* **44**: 266–274
- Dehmelt L, Halpain S (2004) The MAP2/Tau family of microtubule-associated proteins *Genome Biol* **6**: 204
- Dephoure N, Zhou C, Villén J, Beausoleil SA, Bakalarski CE, Elledge SJ, Gygi SP (2008) A quantitative atlas of mitotic phosphorylation *Proc Natl Acad Sci USA* **105**: 10762–10767
- Dimitrov A, Quesnoit M, Moutel S, Cantaloube I, Pous C, Perez F (2008) Detection of GTP-tubulin conformation in vivo reveals a role for GTP remnants in microtubule rescues *Science* **322**: 1353–1356
- Dixit R, Ross JL, Goldmann YE, Holzbaur EL (2008) Differential regulation of dynein and kinesin motor proteins by tau *Science* **319**: 1086–1089
- Doherty GJ, McMahon HT (2008) Mediation, modulation, and consequences of membrane-cytoskeleton interactions *Annu Rev Biophys* **37**: 65–95
- Drewes G, Trinczek B, Illenberger S, Biernat J, Schmitt-Ulms G, Meyer HE, Mandelkow EM, Mandelkow E (1995) Microtubule-associated protein/microtubule affinity-regulating kinase (p110^{mark}). A novel protein kinase that regulates tau-microtubule interactions and dynamic instability by phosphorylation at the Alzheimer-specific site serine 262 *J Biol Chem* **270**: 7679–7688
- Duelli R, Kuschinsky W (2001) Brain glucose transporters: relationship to local energy demand *News Physiol Sci* **16**: 71–76
- Dujardin DL, Vallee RB (2002) Dynein at the cortex *Curr Opin Cell Biol* **14**: 44–49
- Dzhashiashvili Y, Zhang Y, Galinska J, Lam I, Grumet M, Salzer JL (2007) Nodes of Ranvier

- and axon initial segments are ankyrin G-dependent domains that assemble by distinct mechanisms *J Cell Biol* **177**: 857–870
- Edde B, Rossier J, Le Caer J, Desbruyeres E, Gros F, Denoulet P (1990) Posttranslational glutamylation of alpha-tubulin *Science* **247**: 83–85
- Elliott CE, Becker B, Oehler S, Castañón MJ, Hauptmann R, Wiche G (1997) Plectin transcript diversity: Identification and tissue distribution of variants with distinct first coding exons and rodless isoforms *Genomics* **42**: 115-125
- Ems-McClung SC, Walczak CE (2010) Kinesin-13s in mitosis: Key players in the spatial and temporal organization of spindle microtubules *Semin Cell Dev Biol* **21**: 276–282
- Eriksson JE, He T, Trejo-Skalli AV, Härmälä-Braskén AS, Hellman J, Chou YH, Goldman RD (2004) Specific in vivo phosphorylation sites determine the assembly dynamics of vimentin intermediate filaments *J Cell Sci* **117**: 919-932
- Felgner H, Frank R, Biernat J, Mandelkow EM, Mandelkow E, Ludin B, Matus A, Schliwa M (1997) Domains of neuronal microtubule-associated proteins and flexural rigidity of microtubules *J Cell Biol* **138**: 1067-1075
- Fields AP, Thompson LJ (1995) The regulation of mitotic nuclear envelope breakdown: a role for multiple lamin kinases *Prog Cell Cycle Res* **1**: 271-286
- Fletcher LM, Welsh GI, Oatey PB, Tavaré JM (2000) Role for the microtubule cytoskeleton in GLUT4 vesicle trafficking and in the regulation of insulin-stimulated glucose uptake *Biochem J* **352**: 267-276
- Foisner R, Wiche R (1987) Structure and hydrodynamic properties of plectin molecules *J Mol Biol* **198**: 515-531
- Franke WW, Moll R (1987) Cytoskeletal components of lymphoid organs. I. Synthesis of

- cytokeratins 8 and 18 and desmin in subpopulations of extrafollicular reticulum cells of human lymph nodes, tonsils, and spleen *Differentiation* **36**: 145-163
- Friedman JR, Webster BM, Mastronarde DN, Verhey KJ, Voeltz GK (2010) ER sliding dynamics and ER-mitochondrial contacts occur on acetylated microtubules *J Cell Biol* **190**: 363–375
- Fu YJ, Nishihira Y, Kuroda S, Toyoshima Y, Ishihara T, Shinokazi M, Miyashita A, Piao YS, Tan CF, Tani T, Koike R, Iwanaga K, Tsujihata M, Onodera O, Kuwano R, Nishizawa M, Kakita A, Ikeuchi T, Takahashi H (2010) Sporadic four-repeat tauopathy with frontotemporal lobar degeneration, parkinsonism, and motor neuron disease: a distinct clinicopathological and biochemical disease entity *Acta neuropathol* **120**: 21-32
- Fuchs E, Karakesisoglou I (2001) Bridging cytoskeletal intersections *Genes Dev* **15**: 1–14
- Fuchs E, Weber K (1994) Intermediate filaments: Structure, dynamics, function, and disease *Annu Rev Biochem* **63**: 345-382
- Fuchs P, Zörer M, Rezniczek GA, Spazierer D, Oehler S, Castañón MJ, Hauptmann R, Wiche G (1999) Unusual 5' transcript complexity of plectin isoforms: Novel tissue-specific exons modulate actin binding activity *Hum Mol Genet* **8**: 2461-2472
- Fuchs P, Zörer M, Reipert S, Rezniczek GA, Propst F, Walko G, Fischer I, Bauer J, Leschnik MW, Lüscher B, Thalhammer JG, Lassmann H, Wiche G (2009) Targeted inactivation of a developmentally regulated neural plectin isoform (Plectin 1c) in mice leads to reduced motor nerve conduction velocity *J Biol Chem* **284**: 26502-26509
- Fujiwara S, Shinkai H, Takayasu S, Owaribe K, Tsukita S, Kageshita T (1992) A case of subepidermal blister disease associated with autoantibody against 450 kD protein *J Dermatol* **19**: 610–613

- Fujiwara S, Kohno K, Iwamatsu A, Naito I, Shinkai H (1996) Identification of a 450-kDa human epidermal autoantigen as a new member of the plectin family *J Invest Dermatol* **106**: 1125–1130
- Fukata TN, Watanabe H, Iwamatsu A, Kaibuchi K (2005) Tubulin and CRMP-2 complex is transported via Kinesin-1 *J Neurochem* **93**: 1371–1382
- Gache V, Waridel P, Winter C, Juhem A, Schroeder M, Shevchenko A, Popov AV (2010) *Xenopus* meiotic microtubule-associated interactome *PLoS One* **5**: e9248
- Gache Y, Chavanas S, Lacour JP, Wiche G, Owaribe K, Meneguzzi G, Ortonne JP (1996) Defective expression of plectin/HD1 in epidermolysis bullosa simplex with muscular dystrophy *J Clin Invest* **97**: 2289-2298
- Gaffield MA, Betz WJ (2006) Imaging synaptic vesicles exocytosis and endocytosis with FM dyes *Nat Protoc* **1**: 2916-2921
- Gamblin TC, Nachmanoff K, Halpain S, Williams RC Jr (1996) Recombinant microtubule-associated protein 2c reduces the dynamic instability of individual microtubules *Biochemistry* **35**: 12576-12586
- Geraldo S, Khanzada UK, Parsons M, Chilton JK, Gordon-Weeks PR (2008) Targeting of the F-actin-binding protein drebrin by the microtubule plus-tip protein EB3 is required for neuritogenesis *Nat Cell Biol* **10**: 1181–1189
- Getsios S, Huen AC, Green KJ (2004) Working out the strength and flexibility of desmosomes *Nat Rev Mol Cell Biol* **5**: 271-281
- Goldberg DJ, Burmeister DW (1986) Stages in axon formation: observations of growth of *Aplysia* axons in culture using video-enhanced contrast-differential interference contrast microscopy *J Cell Biol* **103**: 1921–1931

- Gomes ER, Jani S, Gundersen GG (2005) Nuclear movement regulated by cdc42, MRCK, myosin, and actin flow establishes MTOC polarization in migrating cells *Cell* **121**: 451-463
- Gómez-Ramos A, Díaz-Hernández M, Cuadros R, Hernández F, Avila J (2006) Extracellular tau is toxic to neuronal cells *FEBS Lett* **580**: 4842–4850
- Greenberg SG, Davies P (1990) A preparation of Alzheimer paired helical filaments that displays distinct tau proteins by polyacrylamide gel electrophoresis *Proc Natl Acad Sci* **87**: 5827-5831
- Gregor M, Zeöld A, Oehler S, Marobela KA, Fuchs P, Weigel G, Hardie DG, Wiche G (2006) Plectin scaffolds recruit energy-controlling AMP-activated protein kinase (AMPK) in differentiated myofibres *J Cell Sci* **119**: 1864-1875
- Gu Y, Oyama F, Ihara Y (1996) Tau is widely expressed in rat tissues *J Neurochem* **67**: 1235-1244
- Gundesli H, Talim B, Korkusuz P, Balci-Hayta B, Cirak S, Akarsu NA, Topaloglu H, Dincer P (2010) Mutation in exon 1f of PLEC, leading to disruption of plectin isoform 1f, causes autosomal-recessive Limb-Girdle muscular dystrophy *Am J Human Genet* **87**:834–841
- Herrmann H, Wiche G (1987) Plectin and IFAP-300K are homologous proteins binding to microtubule-associated proteins 1 and 2 and to the 240-kilodalton subunit of spectrin *J Biol Chem* **262**: 1320-1325
- Huang DY, Goedert M, Jakes R, Weisgraber KH, Garner CC, Saunders AM, Pericak-Vance MA, Schmechel DE, Roses AD, Strittmatter WJ (1994) Isoform-specific interactions of apolipoprotein E with the microtubule-associated protein MAP2c: implications for Alzheimer's disease *Neurosci Lett* **182**: 55-58
- Huang X, Li J, Foster D, Lemanski SL, Dube DK, Zhang C, Lemanski LF (2002) Protein kinase

- C-mediated desmin phosphorylation is related to myofibril disarray in cardiomyopathic hamster heart *Exp Biol Med* **227**: 1039-1046
- Intong LR, Murrell DF (2012) Inherited epidermolysis bullosa: new diagnostic criteria and classification *Clin Dermatol* **30**: 70-77
- Ishikawa H, Bischoff R, Holtzer H (1968) Mitosis and intermediate-sized filaments in developing skeletal muscle *J Cell Biol* **38**: 538-555
- Ittner LM, Ke YD, Delerue F, Bi M, Gladbach A, van Eersel J, Wölfling H, Chieng BC, Christie MJ, Napier IA, Eckert A, Staufenbiel M, Hardeman E, Götz J (2010) Dendritic function of tau mediates amyloid- β toxicity in Alzheimer's Disease mouse models *Cell* **142**: 387-397
- Janke C, Bulinski JC (2011) Post-translational regulation of the microtubule cytoskeleton: mechanisms and functions *Nat Rev Mol Cell Biol* **12**: 773–786
- Janué A, Olive M, Ferrer I (2010) Tau phosphorylation in myotilinopathies and desminopathies *Open Pathol J* **4**: 1-10
- Jefferson JJ, Ciatto C, Shapiro C, Liem RK (2006) Structural analysis of the plakin domain of bullous pemphigoid antigen1 (BPAG1) suggests that plakins are members of the spectrin superfamily *J Mol Biol* **366**: 244-257
- Jeon CY, Moon MY, Kim HJ, Kim JG, Li Y, Jin JK, Kim PH, Kim HC, Meier KE, Kim YS, Park JB (2011) Control of neurite outgrowth by RhoA inactivation *J Neurochem* **Epub**
- Jiang K, Akhmanova A (2011) Microtubule tip-interacting proteins: a view from both ends *Curr Opin Cell Biol* **23**: 94–101
- Kampers T, Pangalos M, Geerts H, Wiech H, Mandelkow E (1999) Assembly of paired helical filaments from mouse tau: implications for the neurofibrillary pathology in transgenic mouse models for Alzheimer's disease *FEBS Lett* **451**: 39-44

- Kaverina I, Krylyshkina O, Small JV (2002) Regulation of substrate adhesion dynamics during cell motility *Int J Biochem Cell Biol* **34**: 746-761
- Kaverina I, Straube A (2011) Regulation of cell migration by dynamic microtubules *Semin Cell Dev Biol* **22**: 968-974
- Kodama A, Karakesisoglou I, Wong E, Vaezi A, Fuchs E (2003) ACF7: An essential integrator of microtubule dynamics *Cell* **115**: 343-354
- Komarova YA, Akhmanova A, Kojima S, Galjart N, Borisy GG (2002) Cytoplasmic linker proteins promote microtubule rescue in vivo *J Cell Biol* **159**: 589-599
- Komarova Y, De Groot CO, Grigoriev I, Gouveia SM, Munteanu EL, Schober JM, Honnappa S, Buey RM, Hoogenraad CC, Dogterom M, Borisy GG, Steinmetz MO, Akhmanova A (2009) Mammalian end binding proteins control persistent microtubule growth *J Cell Biol* **184**: 691-706
- Konieczny P, Fuchs P, Reipert S, Kunz WS, Zeöld A, Fischer I, Paulin D, Schröder R, Wiche G (2008) Myofiber integrity depends on desmin network targeting to Z-disks and costameres via distinct plectin isoforms *J Cell Biol* **181**: 667-681
- Kostan J, Gregor M, Walko G, Wiche G (2009) Plectin isoform-dependent regulation of keratin-integrin alpha6beta4 anchorage via Ca^{2+} /calmodulin *J Biol Chem* **284**: 18525-18536
- Kreitzer G, Liao G, Gundersen GG (1999) Detyrosination of tubulin regulates the interaction of intermediate filaments with microtubules in vivo via a kinesin-dependent mechanism *Mol Biol Cell* **10**: 1105-1118
- Krendel M, Zenke FT, Bokoch GM (2002) Nucleotide exchange factor GEF-H1 mediates cross-talk between microtubules and the actin cytoskeleton *Nat Cell Biol* **4**: 294-301
- Krylyshkina O, Kaverina I, Kranewitter K, Steffen W, Alonso MC, Cross RA, Small JV (2002)

- Modulation of substrate adhesion dynamics via microtubule targeting requires kinesin-1 *J Cell Biol* **156**: 349-359
- Kumar P, Lyle KS, Gierke S, Matov A, Danuser G, Wittmann T (2009) GSK3 phosphorylation modulates CLASP-microtubule association and lamella microtubule attachment *J Cell Biol* **184**: 895–908
- Lacroix B, van Dijk J, Gold ND, Guizetti J, Aldrian-Herrada G, Rogowski K, Gerlich DW, Janke C (2010) Tubulin polyglutamylation stimulates spastin-mediated microtubule severing *J Cell Biol* **189**: 945–954
- Laemmli UK (1970) Cleavage of structural proteins during the assembly of the head of bacteriophage T4 *Nature* **227**: 680-685
- Lan W, Zhang X, Kline-Smith SL, Rosasco SE, Barrett-Wilt GA, Shabanowitz J, Hunt DF, Walczak CE, Stukenberg PT (2004) Aurora B phosphorylates centromeric MCAK and regulates its localization and microtubule depolymerization activity *Curr Biol* **14**: 273–286
- Lansbergen G, Akhmanova A (2006) Microtubule plus end: A hub of cellular activities *Traffic* **7**: 499–507
- Lechler T, Fuchs E (2007) Desmoplakin an unexpected regulator of microtubule organization in the epidermis *J Cell Biol* **176**: 147–154
- Lee G, Newman ST, Gard DL, Band H, Panchamoorthy G (1998) Tau interacts with Src-family non-receptor tyrosine kinases *J Cell Sci* **111**: 3167-3177
- Lee HS, Komarova YA, Nadezhdina ES, Anjum R, Peloquin JG, Schober JM, Danciu O, van Haren J, Galjart N, Gygi SP, Akhmanova A, Borisy GG (2010) Phosphorylation controls autoinhibition of cytoplasmic linker protein-170 *Mol Biol Cell* **21**: 2661–2673
- Lee S, Sunil N, Tejada JM, Shea TB (2011) Differential roles of kinesin and dynein in

- translocation of neurofilaments into axonal neurites *J Cell Sci* **124**: 1022-1031
- Lee VM, Goedert M, Trojanowski JQ (2001) Neurodegenerative tauopathies *Annu Rev Neurosci* **24**: 1121-1159
- Leung CL, Green KJ, Liem RK (2002) Plakins: a family of versatile cytolinker proteins *Trends Cell Biol* **12**: 37-45
- Leung CL, Sun D, Zheng M, Knowles DR, Liem RK (1999) Microtubule actin cross-linking factor (MACF): a hybrid of dystonin and dystrophin that can interact with the actin and microtubule cytoskeletons *J Cell Biol* **147**: 1275-1286
- Lewis SA, Ivanov IE, Lee GH, Cowan NJ (1989) Organization of microtubules in dendrites and axons is determined by a short hydrophobic zipper in microtubule-associated proteins MAP2 and tau *Nature* **342**: 498-505
- Liao G, Gundersen GG (1998) Kinesin is a candidate for cross-bridging microtubules and intermediate filaments. Selective binding of kinesin to detyrosinated tubulin and vimentin. *J Biol Chem* **273**: 9797–9803
- Liem RK, Messing A (2009) Dysfunctions of neuronal and glial intermediate filaments in disease *J Clin Invest* **119**: 1812-1824
- Lin CC, Cheng TS, Hsu CM, Wu CH, Chang LS, Shen ZS, Yeh HM, Chang LK, Howng SL, Hong YR (2006) Characterization and functional aspects of human ninein isoforms that regulated by centrosomal targeting signals and evidence for docking sites to direct gamma-tubulin *Cell Cycle* **5**: 2517–2527
- Lin W, Szaro BG (1995) Neurofilaments help maintain normal morphologies and support elongation of neurites in *Xenopus laevis* cultured embryonic spinal cord neurons *J Neurosci* **15**: 8331-8344

- Liu CG, Maercker C, Castañón MJ, Hauptmann R, Wiche G (1996) Human plectin: organization of the gene, sequence analysis and chromosome localization (8q24) *Proc Natl Acad Sci USA* **93**: 4278-4283
- Liu SY, Chen YT, Tseng MY, Hung CC, Chiang WF, Chen HR, Shieh TY, Chen CH, Jou YS, Chen JY (2007) Involvement of microtubule-associated protein 2 (MAP2) in oral cancer cell motility: a novel biological function of MAP2 in non-neuronal cells. *Biochem Biophys Res Commun* **366**: 520-525
- Lowery LA, Van Vactor D (2009) The trip of the tip: understanding the growth cone machinery *Nat Rev Mol Cell Bio* **10**: 332-343
- Mack GJ, Compton DA (2001) Analysis of mitotic microtubule-associated proteins using mass spectrometry identifies astrin, a spindle associated protein *Proc Natl Acad Sci USA* **98**: 14434-14439
- Maiweilidan Y, Klauza I, Kordeli E(2011) Novel interactions of ankyrins-G at the costameres: The muscle-specific Obscurin/Titin-Binding-related Domain (OTBD) binds plectin and filamin C *Exp Cell Res* **317**: 724–736
- Malecz N, Foisner R, Wiche G (1996) Identification of plectin as a p34^{cdc2} kinase substrate and mapping of a single phosphorylation site *J Biol Chem* **271**: 8203-8208
- Malik R, Lenobel R, Santamaria A, Ries A, Nigg EA, Körner R (2009) Quantitative analysis of the human spindle phosphoproteome at distinct mitotic stages *J Proteome Res* **8**: 4553-4563
- Martínez-López MJ, Alcántara S, Mascaró C, Pérez-Brangulí F, Ruiz-Lozano P, Maes T, Soriano E, Buesa C (2005) Mouse neuron navigator 1, a novel microtubule-associated protein involved in neuronal migration *Mol Cell Neurosci* **28**: 599–612

- Masson D, Kreis TE (1993) Identification and molecular characterization of E-MAP-115, a novel microtubule-associated protein predominantly expressed in epithelial cells *J Cell Biol* **123**: 357-371
- Mazarguil H, Le Caer JP, Wehland J, Job D (1991) Characterization of a major brain tubulin variant which cannot be tyrosinated *Biochemistry* **43**: 10523–10528
- Meng W, Mushika Y, Ichii T, Takeichi M (2008) Anchorage of microtubule minus ends to adherens junctions regulates epithelial cell-cell contacts *Cell* **135**: 948–959
- Mimori-Kiyosue Y, Grigoriev I, Lansbergen G, Sasaki H, Matsui C, Severin F, Galjart N, Grosveld F, Vorobjev I, Tsukita S, Akhmanova (2010) CLASP1 and CLASP2 bind to EB1 and regulate microtubule plus-end dynamics at the cell cortex *J Cell Biol* **168**: 141-153
- Mitchison T, Kirschner M (1984) Dynamic instability of microtubule growth *Nature* **312**: 237-242
- Moll R, Moll I (1998) Epidermal adhesion molecules and basement membrane components as target structures of autoimmunity *Virchows Arch* **432**: 487-504
- Möseneder, P (2010) Assessment of the putative secretion of plectin molecules and generation of expression plasmids containing noncoding isoform-specific nucleotide sequences. Master thesis. University of Vienna.
- Nakano A, Kato H, Watanabe T, Min KD, Yamazaki S, Asano Y, Seguchi O, Higo S, Shintani Y, Asanuma H, Asakura M, Minamino T, Kaibuchi K, Mochizuki N, Kitakaze M, Takashima S (2010) AMPK controls the speed of microtubule polymerization and directional cell migration through CLIP-170 phosphorylation *Nat Cell Biol* **12**: 583–590
- Neukirchen D, Bradke F (2011) Cytoplasmic linker proteins regulate neuronal polarization through microtubule and growth cone dynamics *J Neurosci* **31**: 1528–1538
- Nikolic B, Mac Nulty E, Mir B, Wiche G (1996) Basic amino acid residue cluster within nuclear

- targeting sequence motif is essential for cytoplasmic plectin-vimentin network junctions *J Cell Biol* **134**: 1455-1467
- O' Farrel PH (1975) High resolution two-dimensional electrophoresis of proteins *J Biol Chem* **250**: 4007-4021
- Olmsted JB (1986) Microtubule-associated proteins *Ann Rev Cell Biol* **2**: 421-457
- Ortega E, Buey RM, Sonnenberg A, de Pereda JM (2011) The structure of the plakin domain of plectin reveals a non-canonical SH3 domain interacting with its fourth spectrin repeat *J Biol Chem* **286**: 12429–12438
- Osmanagic-Myers S, Gregor M, Walko G, Burgstaller G, Reipert S, Wiche G (2006) Plectin-controlled keratin cytoarchitecture affects MAP kinases involved in cellular stress response and migration *J Cell Biol* **174**: 557-568
- Parysek M, Wolosewicz JJ, Olmsted JB (1984) MAP4: a microtubule-associated protein specific for a subset of tissue microtubules *J Cell Biol* **99**: 2287-2896
- Patel K, Nogales E, Heald R (2012) Multiple domains of human CLASP contribute to microtubule dynamics and organization in vitro and in Xenopus egg extracts *Cytoskeleton (Hoboken)* **Epub**
- Peris L, Thery M, Fauré J, Saoudi Y, Lafanechère L, Chilton JK, Gordon-Weeks PR, Galjart N, Bornens M, Worderman L, Wehland J, Andrieux A, Job D (2006) Tubulin tyrosination is a major factor affecting the recruitment of CAP-Gly proteins at microtubule plus ends *J Cell Biol* **174**: 839–849
- Piperno G, LeDizet M, Chang XJ (1987) Microtubules containing acetylated alpha-tubulin in mammalian cells in culture *J Cell Biol* **104**: 289-302
- Planel E, Krishnamurthy P, Miyasaka T, Liu L, Herman M, Kumar A, Bretteville A, Figueroa HY,

- Yu WH, Whittington RA, Davies P, Takashima A, Nixon RA, Duff KE (2008) Anesthesia-induced hyperphosphorylation detaches 3-repeat tau from microtubules without affecting their stability in vivo *J Neurosci* **28**: 12798-12807.
- Pytela R, Wiche G (1980) High molecular weight polypeptides (270,000-340,000) from cultured cells are related to hog brain microtubule-associated proteins but copurify with intermediate filaments *Proc Natl Acad Sci USA* **77**: 4808-4812
- Qiang L, Yu W, Andreadis A, Luo M, Baas PW (2006) Tau protects microtubules in the axon from severing by katanin *J Neurosci* **26**: 3120-3129
- Raybin D, Flavin M (1977) Enzyme which specifically adds tyrosine to the alpha chain of tubulin *Biochemistry* **10**: 2189-2194
- Redeker V, Levilliers N, Schmitter J, Le Caer J, Rossier J, Adoutte A, Bre M (1994) Polyglycylation of tubulin: a posttranslational modification in axonemal microtubules *Science* **266**: 1688-1691
- Reed NA, Cai D, Blasius TL, Jih GT, Meyhofer E, Gaertig J, Verhey KJ (2006) Microtubule acetylation promotes Kinesin-1 binding and transport *Curr Biol* **16**: 2166-2172
- Reilein A, Nelson WJ (2005) APC is a component of an organizing template for cortical microtubule networks *Nat Cell Biol* **7**: 463-473
- Ren XD, Kiosses WB, Schwartz MA (1999) Regulation of the small GTP-binding protein Rho by cell adhesion and the cytoskeleton *EMBO J* **18**: 578-585
- Rezniczek GA, Abrahamsberg C, Fuchs P, Spazierer D, Wiche G (2003) Plectin 5'-transcript diversity: short alternative sequences determine stability of gene products, initiation of translation and subcellular localization of isoforms *Hum Mol Genet* **12**: 3181-3194
- Rezniczek GA, de Pereda JM, Reipert S, Wiche G (1998) Linking integrin $\alpha 6\beta 4$ -based cell

- adhesion to intermediate filament cytoskeleton: direct interaction between the $\beta 4$ subunit and plectin at multiple molecular sites *J Cell Biol* **141**: 209-225
- Rezniczek GA, Janda L, Wiche G (2004) Plectin *Methods Cell Biol* **78**: 721-755
- Rezniczek GA, Konieczny P, Nikolic B, Reipert S, Schneller D, Abrahamsberg C, Davies KE, Winder SJ, Wiche G (2007) Plectin 1f scaffolding at the sarcolemma of dystrophic (mdx) muscle fibers through multiple interactions with beta-dystroglycan *J Cell Biol* **176**: 965-977
- Rickard JE, Kreis TE (1991) Binding of pp170 to microtubules is regulated by phosphorylation *J Biol Chem* **266**: 17597–17605
- Rodriguez OC, Schaefer AW, Mandato CA, Forscher P, Bement WM, Waterman-Storer CM (2003) Conserved microtubule–actin interactions in cell movement and morphogenesis *Nat Cell Biol* **5**: 599–609
- Roll-Mecak A, McNally FJ (2010) Microtubule-severing enzymes *Curr Opin Cell Biol* **22**: 96–103
- Rottner K, Behrendt B, Small JV, Wehland J (1999) VASP dynamics during lamellipodia protrusion *Nat Cell Biol* **1**: 321-322
- Rudrabhatla P, Jaffe H, Pant HC (2011) Direct evidence of phosphorylated neuronal intermediate filament proteins in neurofibrillary tangles (NFTs): phosphoproteomics of Alzheimer’s NFTs *FASEB J* **25**: 3896-3905
- Ruhrberg C, Hajibagheri MA, Parry DA, Watt FM (1997) Periplakin, a novel component of cornified envelopes and desmosomes that belongs to the plakin family and forms complexes with envoplakin *J Cell Biol* **139**: 1835-1849
- Ruhrberg C, Hajibagheri MA, Simon M, Dooley TP, Watt FM (1996) Envoplakin, a novel precursor of the cornified envelope that has homology to desmoplakin *J Cell Biol* **134**: 715-

729

- Ruhrberg C, Watt FM (1997) The plakin family: versatile organizers of cytoskeletal architecture *Curr Opin Genet Dev* **7**: 392-397
- Sanchez C, Diaz-Nido J, Avila J. (2000) Phosphorylation of microtubule-associated protein 2 (MAP2) and its relevance for the regulation of the neuronal cytoskeleton function *Prog Neurobiol* **61**:133-168
- Sapir T, Elbaum M, Reiner O (1997) Reduction of microtubule catastrophe events by LIS1, platelet-activating factor acetylhydrolase subunit *EMBO J* **16**: 6977–6984
- Sauer G, Körner R, Hanisch A, Ries A, Nigg E, Silljé HH (2005) Proteome analysis of the human mitotic spindle *Mol Cell Proteomics* **4**: 35-43
- Schröder JM (2005) Neuropathology of Charcot-Marie-Tooth and related disorders *Neuromolecular Med* **8**: 23-42
- Schulze E, Kirschner M (1986) Microtubule dynamics in interphase cells *J Cell Biol* **102**: 1020-1031
- Shea TB, Lee S (2011) Neurofilament phosphorylation regulates axonal transport by an indirect mechanism: A merging of opposing hypotheses *Cytoskeleton* **68**: 589-595
- Simón D, García-García E, Royo F, Falcón-Pérez JM, Avila J (2012) Proteostasis of tau. Tau overexpression results in its secretion via membrane vesicles *FEBS Lett* **586**: 47–54
- Smith FJ, Eady RA, Leigh IM, McMillan JR, Rugg EL, Kelsell DP, Bryant SP, Spurr NK, Geddes JF, Kirtschig G, Milana G, de Bono AG, Owaribe K, Wiche G, Pulkkinen L, Uitto J, McLean WH, Lane EB (1996) Plectin deficiency results in muscular dystrophy with Epidermolysis Bullosa *Nat Genet* **13**: 450-457
- Sonnenberg A, Liem RK (2007) Plakins in development and disease *Exp Cell Res* **313**: 2189-

2203

- Spazierer D, Fuchs P, Proll V, Janda L, Oehler S, Fischer I, Hauptmann R, Wiche G (2003) Epiplakin gene analysis in mouse reveals a single exon encoding a 725-kDa protein with expression restricted to epithelial tissues *J Biol Chem* **278**: 31657-31666
- Spiliotis ET (2010) Regulation of microtubule organization and functions by septin GTPases *Cytoskeleton* **67**: 339–345
- Spiliotis ET, Hunt SJ, HuQ, Kinoshita M, Nelson WJ (2008) Epithelial polarity requires septin coupling of vesicle transport to polyglutamylated microtubules *J Cell Biol* **180**: 295–303
- Spurny R (2008) Plectin-vimentin interactions: intermediate filament network formation, dynamics, and nitrosylation-induced collapse. PhD thesis. University of Vienna.
- Spurny R, Gregor M, Castañón MJ, Wiche G (2008) Plectin deficiency affects precursor formation and dynamics of vimentin networks *Exp Cell Res* **15**: 3570-3580
- Stamer K, Vogel R, Thies E, Madelkow E, Mandelkow EM (2002) Tau blocks traffic of organelles, neurofilaments, and APP vesicles in neurons and enhances oxidative stress *J Cell Biol* **156**: 1051-1063
- Steinböck FA, Wiche G (1999) Plectin: a cytolinker by design *Biol Chem* **380**: 151–158
- Stepanova T, Slemmer J, Hoogenraad CC, Lansbergen G, Dortland B, De Zeeuw CI, Grosveld F, van Cappellen G, Akhmanova A, Galjart N (2003) Visualization of microtubule growth in cultured neurons via the use of EB3-GFP (end-binding protein 3-green fluorescent protein) *J Neurosci* **23**: 2655-2664
- Stiess M, Bradke F (2011) Neuronal polarization: The cytoskeleton leads the way *Dev Neurobiol* **71**: 430–444
- Straube A, Merdes A (2007) EB3 regulates microtubule dynamics at the cell cortex and is

- required for myoblast elongation and fusion *Curr Biol* **17**: 1318–1325
- Stroissnigg H, Trancikova A, Descovich L, Fuhrmann J, Kutschera W, Kostan J, Meixner A, Nothias F, Propst F (2007) S-nitrosylation of microtubule-associated protein 1B mediates nitric-oxide-induced axon retraction *Nat Cell Biol* **9**: 1035-1045
- Su LK, Burrell M, Hill DE, Gyuris J, Brent R, Wiltshire R, Trent J, Vogelstein B, Kinzler KW (1995) APC binds to the novel protein EB1 *Cancer Res* **55**: 2972-2977
- Sudo H, Baas PW (2010) Acetylation of microtubules influences their sensitivity to severing by katanin in neurons and fibroblasts *J Neurosci* **30**: 7215–7226
- Sunil N, Lee S, Shea TB (2012) Interference with kinesin-based anterograde neurofilament axonal transport increases neurofilament-neurofilament bundling *Cytoskeleton* In Press
- Svitkina TM, Verkhovsky AB, Borisy GB (1998) Plectin sidearms mediate interactions of intermediate filaments with microtubules and other components of the cytoskeleton *Biol Bull* **194**: 409-410
- Sydow A, Van der Jeugd A, Zheng F, Ahmed T, Balschun D, Petrova O, Drexler D, Zhou L, Rune G, Mandelkow E, D’Hooge R, Alzheimer C, Mandelkow EM (2011) Tau-induced defects in synaptic plasticity, learning, and memory are reversible in transgenic mice after switching off the toxic Tau mutant *J Neurosci* **31**: 2511-2525
- Tanaka E, Ho T, Kirschner MW (1995) The role of microtubule dynamics in growth cone motility and axonal growth *J Cell Biol* **128**: 139-155
- Tapia M, Wandosell F, Garrido JJ (2010) Impaired function of HDAC6 slows down axonal growth and interferes with axon initial segment development *PLoS ONE* **9**: e12908
- Tian R, Gregor M, Wiche G, Goldman JE (2006) Plectin regulates the organization of glial fibrillary acidic protein in Alexander disease *Am J Pathol* **168**: 888-897

- Tischfield MA, Cederquist GY, Gupta ML Jr, Engle EC (2011) Phenotypic spectrum of the tubulin-related disorders and functional implications of disease-causing mutations *Curr Opin Genet Dev* **21**: 286-294
- Vijayaraj P, Kröger C, Reuter U, Windoffer R, Leube RE, Magin TM (2009) Keratins regulate protein biosynthesis through localization of GLUT1 and -3 upstream of AMP kinase and Raptor *J Cell Biol* **187**: 175-184
- Villalonga P, Guasch RM, Riento K, and Ridley AJ (2004) RhoE inhibits cell cycle progression and Ras-induced transformation *Mol Cell Biol* **24**: 7829–7840.
- Virata ML, Wagner RM, Parry DA, Green KJ (1992) Molecular structure of the human desmoplakin I and II amino terminus *Proc Natl Acad Sci USA* **89**: 544-548
- Walko G (2007) Functions of plectin and its isoforms assessed in mouse stratified epithelia and keratinocyte cell cultures. PhD thesis. University of Vienna.
- Walko G, Vukasinovic N, Gross K, Fischer I, Sibitz S, Fuchs P, Reipert S, Jungwirth U, Berger W, Salzer U, Carugo O, Castañón MJ, Wiche G (2011) Targeted proteolysis of plectin isoform 1a accounts for hemidesmosome dysfunction in mice mimicking the dominant skin blistering disease EBS-Ogna *PLoS Genet* e1002396
- Watanabe T, Noritake J, Kaibuchi K (2005) Regulation of microtubules in cell migration *Trends Cell Biol* **15**: 76-83
- Waterman-Storer CM, Salmon ED (1997) Actomyosin-based retrograde flow of microtubules in the lamella of migrating epithelial cells influences microtubule dynamic instability and turnover and is associated with microtubule breakage and treadmilling *J Cell Biol* **139**: 417-434
- Waterman-Storer CM, Worthylake RA, Liu BP, Burridge K, Salmon ED (1999) Microtubule

- growth activates Rac1 to promote lamellipodial protrusion in fibroblasts *Nat Cell Biol* **1**: 45-50
- Wen Y, Eng CH, Schmoranzer J, Cabrera-Poch N, Morris EJS, Chen M, Wallar BJ, Alberts AS, Gundersen GG (2004) EB1 and APC bind to mDia to stabilize microtubules downstream of Rho and promote cell migration *Nat Cell Biol* **6**: 820-830
- Wiche G (1989) High-Mr microtubule-associated proteins: properties and functions *Biochem J* **259**: 1-12
- Wiche G (1998) Role of plectin in cytoskeleton organization and dynamics *J Cell Sci* **111**: 2477-2486
- Wiche G, Becker B, Lubert K, Weitzer G, Castañón MJ, Hauptmann R, Stratowa C, Stewart M (1991) Cloning and sequencing of rat plectin indicates a 488-kD polypeptide chain with a three-domain structure based on a central alpha-helical coiled coil *J Cell Biol* **114**: 83-99
- Wiche G, Briones E, Koszka C, Artlieb U, Krepler R (1984) Widespread occurrence of polypeptides related to neurotubule-associated proteins (MAP-1 and MAP-2) in non-neuronal cells and tissues *EMBO J* **3**: 991-998
- Wiche G, Winter L (2011) Plectin isoforms as organizers of intermediate filament cytoarchitecture *BioArchitecture* **1**: 14-20
- Wickstead B, Gull K (2011) The evolution of the cytoskeleton *J Cell Biol* **194**: 513-525
- Winter L, Abrahamsberg C, Wiche G (2008) Plectin isoform 1b mediates mitochondrion–intermediate filament network linkage and controls organelle shape *J Cell Biol* **181**: 903-911
- Winter L, Schröder R, Wiche G (2012) Plectinopathies *ISN Neuropathology Muscle Book* (in press)

- Wu X, Kodama A, Fuchs E (2008) ACF7 regulates cytoskeletal-focal adhesion dynamics and migration and has ATPase activity *Cell* **135**: 137-148
- Wu XS, Tsan GL, Hammer JA 3rd (2005) Melanophilin and myosin Va track the microtubule plus end on EB1 *J Cell Biol* **171**: 201–207
- Yamada K, Nakata M, Horimoto N, Saito M, Matsuoka H, Inagaki N (2000) Measurement of glucose uptake and intracellular calcium concentration in single, living pancreatic β -cells *J Biol Chem* **275**: 22278-22283
- Yang Y, Bauer C, Strasser G, Wollman R, Julien JP, Fuchs E (1999) Integrators of the cytoskeleton that stabilize microtubules *Cell* **98**: 229-238
- Yousuf A, Klinger F, Schicker K, Boehm S (2011) Nucleotides control the excitability of sensory neurons via two P2Y receptors and a bifurcated signaling cascade *Pain* **152**: 1899-1908
- Yu W, Qiang L, Solowska JM, Karabay A, Korulu S, Baas PW (2008) The microtubule-severing proteins spastin and katanin participate differently in the formation of axonal branches *Mol Biol Cell* **19**: 1485-1498
- Yuan A, Kumar A, Peterhoff C, Duff K, Nixon RA (2008) Axonal transport rates in vivo are unaffected by tau deletion or overexpression in mice *J Neurosci* **28**: 1682–1687
- Zeitelhofer M, Vessey JP, Xie Y, Tübing F, Thomas S, Kiebler M, Dahm R (2007) High-efficiency transfection of mammalian neurons via nucleofection *Nat Protoc* **2**: 1692–1704
- Zhang D, Rogers GC, Buster DW, Sharp DJ (2007) Three microtubule severing enzymes contribute to the ‘Pacman-flux’ machinery that moves chromosomes *J Cell Biol* **177**: 231–242
- Zaid H, Antonescu CN, Randhawa VK, Klip A (2008) Insulin action on glucose transporters through molecular switches, tracks and tethers *Biochem J* **413**: 201-215

Zörer M (2002) Analyse des murinen Plectin-Gens und seiner Transkrypte sowie Inaktivierung der neuronalen Plectin Isoform (Plectin 1c). PhD thesis. University of Vienna.

CURRICULUM VITAE

Personal Information

Name: Rocío García de la Cruz Valencia
Date of birth: October 31, 1983
Nationality: Spanish
Work Address: Max F. Perutz Laboratories
University of Vienna
Department of Biochemistry and Cell Biology
Dr. Bohr-gasse 9
A-1030 Vienna
Austria
Tel: +43 1 4277 52861
Email: rocio.garcia-de-la-cruz-valencia@univie.ac.at



Education

09/2008-06/2012 PhD studies (Molecular Biology) at the University of Vienna (Austria).
09/2001-07/2007 Master of Science in Biochemistry at the Universidad Autónoma de Madrid (Spain)
06/2001 University entrance exam (Madrid, Spain)

Fellowships

01/2010-03/2011 Grant Holder: PhD student under the DOC-fFORTE program funded by Austrian Academy of Science
09/2011 Award: SEBBM bursary (SEBBM meeting: Barcelona 2011)
06/2010 Award: Boehringer Ingelheim Travel Grant
01/2008-07/2008 Grant holder: Leonardo Da Vinci Contract under the Lifelong Learning Program of the European Union (Training grant: Methods in Cell Biology)
09/2005-07/2006 Erasmus student at the University of Vienna

Courses

02/2011-11/2011	University expert in biotechnology and law at the U.N.E.D (Spain)
04/2011	Biometrics: Statistical tests and survival analysis in medical research (Max F. Perutz Laboratories)
02/2011	Biometrics: Describing and visualizing medical data (Max F. Perutz Laboratories)
01/2011	Project management (Max F. Perutz Laboratories, Pentalog®)
06/2010	3D Microscopy of living cells course and 3D image processing course at the University of British Columbia, Vancouver (Canada)
01/2010-09/2010	University expert in Human Rights and Bioethics in Clinical Research at the U.N.E.D (Spain)

Posters

Valencia RG, Walko G, Janda L, Mihailovska E, Wiche G. Beyond networking: Microtubule destabilization via Plectin, an intermediate filament-associated cytolinker. "SEBBM Meeting-2011". Barcelona, Spain, September 5-8, 2011.

Teaching activities

2009-2010	Assignments as a tutor for molecular biology and biochemical courses for biologist and chemist at the University of Vienna
-----------	--

Software skills

Image deconvolution and processing tools: (SVI 3D Huygens Deconvolution Software and Image J)

Graphic design applications (Photoshop, Illustrator)

Microsoft Office tools (Word, Excel and Power Point)

Language skills

Spanish (Native), English (Fluent), German (Intermediate), and French (Basic)